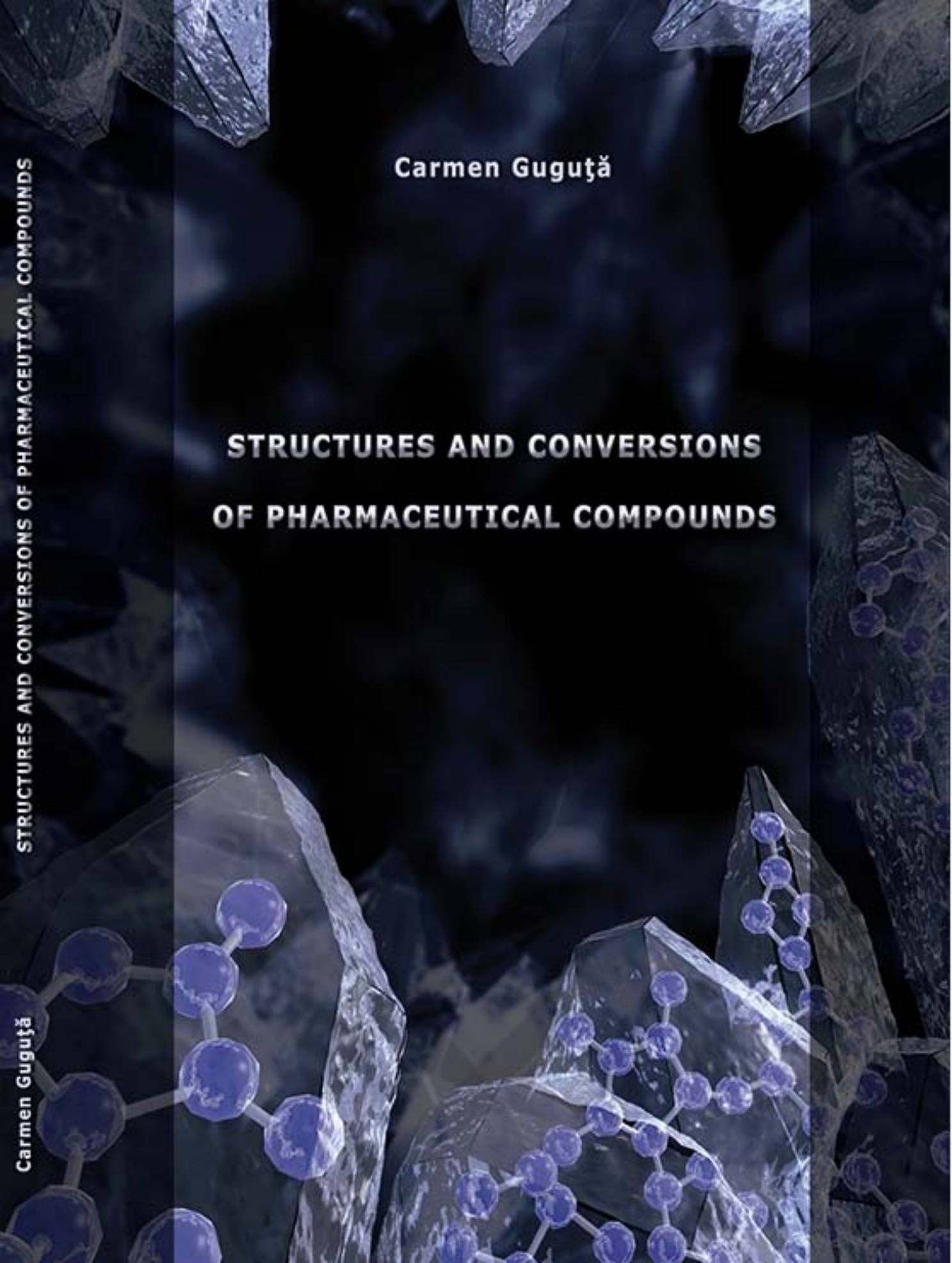


STRUCTURES AND CONVERSIONS OF PHARMACEUTICAL COMPOUNDS

Carmen Guguță

**STRUCTURES AND CONVERSIONS
OF PHARMACEUTICAL COMPOUNDS**

Carmen Guguță



**STRUCTURES AND CONVERSIONS
OF PHARMACEUTICAL COMPOUNDS**

Carmen Guguță

STRUCTURES AND CONVERSIONS OF PHARMACEUTICAL COMPOUNDS

An academic essay in Natural Science, Mathematics and Computing Science

Doctoral thesis

to obtain the degree of doctor
from Radboud University Nijmegen
on the authority of the Rector Magnificus, prof. dr. S.C.J.J. Kortmann,
according to the decision of the Council of Deans
to be defended in public on Monday, 6th April 2009
at 13.30 hours

by

Carmen Guguță

born in Constanța, Romania
on August 6th, 1979

Supervisor:

Prof. dr. E. Vlieg

Co-supervisor:

Dr. R. de Gelder

Doctoral Thesis Committee:


Prof. dr. S. Wijmenga

Dr. R. Peschar (University of Amsterdam)

Dr. P.J.C.M. van Hoof (Schering-Plough Organon, Oss)

Guguță, Carmen

PhD Thesis, Radboud University Nijmegen, The Netherlands

 This research was financially supported by the Dutch Technology Foundation STW (06216).

ISBN: 978-90-9024114-2

Copyright © 2009 by Carmen Guguță

Cover by Cosmin Genete

Printed by PrintPartners Ipskamp

STRUCTURES AND CONVERSIONS OF PHARMACEUTICAL COMPOUNDS

Een wetenschappelijke proeve op het gebied
van de Natuurwetenschappen, Wiskunde en Informatica

Proefschrift

ter verkrijging van de graad van doctor
aan de Radboud Universiteit Nijmegen
op gezag van de rector magnificus prof. mr. S.C.J.J. Kortmann,
volgens besluit van het College van Decanen
in het openbaar te verdedigen op maandag 6 april 2009
om 13.30 uur precies

door

Carmen Guguță

geboren op 6 augustus 1979
te Constanța, Roemenië

Promotor:

Prof. dr. E. Vlieg

Copromotor:

Dr. R. de Gelder

Manuscriptcommissie:


Prof. dr. S. Wijmenga

Dr. R. Peschar (University of Amsterdam)

Dr. P.J.C.M. van Hoof (Schering-Plough Organon, Oss)

Guguță, Carmen

PhD Thesis, Radboud University Nijmegen, The Netherlands

 This research was financially supported by the Dutch Technology Foundation STW (06216).

ISBN: 978-90-9024114-2

Copyright © 2009 by Carmen Guguță

Cover by Cosmin Genete

Printed by PrintPartners Ipskamp

To my parents

Table of Contents

Chapter 1. General introduction: Structure determination and solid-state analysis of pharmaceutical compounds	1
Why this thesis?.....	3
1.1. Pharmaceutical solids.....	5
1.2. Solid-state analysis.....	7
1.3. Crystalline materials.....	8
1.4. Polymorphs and solvates.....	11
1.5. Crystal structure determination from powder diffraction data.....	13
1.6. Scope of the thesis.....	15
Chapter 2. Crystal structure of aspartame anhydrate from powder diffraction data. Structural aspects of the dehydration process of aspartame	19
2.1. Introduction.....	21
2.2. Experimental.....	25
2.2.1. Preparation of the anhydrate form.....	25
2.2.2. Solid-state NMR spectroscopy.....	26
2.2.3. X-ray powder diffraction.....	26
2.2.4. Data analysis.....	27
2.3. Results and discussion.....	28
2.3.1. Dehydration of aspartame hemi-hydrate.....	28
2.3.2. Indexing, Pawley refinement and simulated annealing.....	29
2.3.3. Rietveld refinement.....	35
2.3.4. Comparison between the four pseudo-polymorphs of aspartame.....	36
2.4. Conclusions.....	42
Chapter 3. The hydration/dehydration behavior of aspartame revisited	43
3.1. Introduction.....	45
3.2. Experimental.....	50
3.2.1. Preparation of the four forms of aspartame.....	50

3.2.2.	Hot-humidity stage X-ray powder diffraction.....	52
3.2.3.	Differential scanning calorimetry	53
3.2.4.	Thermogravimetric analysis.....	53
3.2.5.	Molecular mechanics modelling.....	53
3.3.	Results and discussion.....	53
3.3.1.	Hot-humidity stage X-ray powder diffraction.....	53
3.3.2.	Thermal analysis.....	57
3.3.3.	Differential Scanning Calorimetry.....	57
3.3.4.	Thermogravimetric analysis.....	60
3.3.5.	Molecular mechanics modeling.....	62
3.4.	Conclusions.....	64
Chapter 4. Structural diversity of ethinyl estradiol solvates		67
4.1.	Introduction.....	69
4.2.	Experimental.....	72
4.2.1.	Materials.....	72
4.2.2.	Preparation of the solvates.....	72
4.2.3.	Single-crystal X-ray diffraction.....	73
4.2.4.	Hot-humidity stage X-ray powder diffraction.....	73
4.2.5.	Differential scanning calorimetry.....	74
4.3.	Results and discussion.....	74
4.3.1.	(Pseudo)polymorphism screening.....	74
4.3.2.	Structural details of the solvates.....	76
4.3.3.	Hot-humidity stage and DSC studies.....	87
4.4.	Conclusions.....	91
Chapter 5. Structural investigations of hydrate, anhydrate, free base and hydrochloride forms of morphine and naloxone		95
5.1.	Introduction.....	97
5.2.	Experimental.....	101
5.2.1.	Materials.....	101
5.2.2.	Preparation of morphine hydrochloride anhydrate.....	102

5.2.3.	Preparation of morphine anhydrate.....	102
5.2.4.	Preparation of naloxone hydrochloride di-hydrate.....	102
5.2.5.	Preparation of naloxone hydrochloride anhydrate.....	102
5.2.6.	Preparation of naloxone monohydrate.....	103
5.2.7.	Preparation of naloxone anhydrate.....	103
5.2.8.	X-ray powder diffraction.....	103
5.2.9.	Data analysis for crystal structure determination.....	104
5.2.10.	Solid-state NMR spectroscopy.....	105
5.3.	Results	105
5.3.1.	Crystal structure determination of the four anhydrate forms.....	105
5.3.2.	Rietveld refinement.....	109
5.4.	Discussion.....	111
5.5.	Conclusions.....	120

Chapter 6. Structural insight into the dehydration and hydration behavior of naltrexone and naloxone hydrochloride. Dehydration induced expansion vs. contraction **123**

6.1.	Introduction.....	126
6.2.	Experimental.....	129
6.2.1.	Materials.....	129
6.2.2.	Preparation of naltrexone hydrochloride tetra-hydrate.....	129
6.2.3.	Preparation of naltrexone hydrochloride anhydrate.....	129
6.2.4.	Preparation of naloxone hydrochloride di-hydrate.....	130
6.2.5.	Preparation of naloxone hydrochloride anhydrate.....	130
6.2.6.	Analytical methodology.....	130
6.3.	Results and discussion.....	134
6.3.1.	Crystal structure determination of naltrexone hydrochloride anhydrate.....	134
6.3.2.	Hot-humidity stage X-ray powder diffraction.....	139
6.3.3.	Microscopy.....	142
6.3.4.	Differential scanning calorimetry.....	144
6.3.5.	Thermal gravimetric analysis.....	146

6.3.6.	Solid-state NMR spectroscopy.....	148
6.3.7.	Structural aspects of hydration and dehydration.....	151
6.4.	Conclusions.....	158

Chapter 7. Fiddle. Simultaneous Indexing and Structure Solution from Powder Diffraction Data **163**

7.1.	Introduction.....	166
7.2.	Computational methodology.....	169
7.2.1.	Program description.....	166
7.2.2.	The genetic algorithm.....	171
7.2.3.	Comparison of powder diffraction patterns in <i>FIDDLE</i> : the fitness function.....	173
7.3.	Experimental.....	174
7.4.	Tests applied to calculated powder diffraction data (A).....	177
7.5.	Test applied to calculated powder diffraction data (B).....	180
7.6.	Tests applied to experimental data.....	182
7.7.	Application to unknown crystal structures.....	183
7.8.	Conclusions.....	189

References **191**

Summary (English version) **203**

Summary (Dutch version) **211**

Acknowledgements **219**

Curriculum vitae

List of publications



Chapter I

INTRODUCTION

Why this thesis?

Pharmaceutical compounds often have the tendency to crystallize in various polymorphs, solvates or hydrates as a function of the crystallization medium, temperature and humidity. This can cause many practical problems, including changes in stability, dissolution rates, bioavailability, morphology, vapor pressure, and packaging; the key factors for the development of appropriate dosage forms. The possibility to understand polymorphism and solvate or hydrate formation at the molecular level is very appealing. It critically depends, however, on the availability of powerful structure elucidation methods and other methods for solid-state analysis.

The first part of this thesis deals with application of different solid-state techniques in combination with crystal structure determination for the study of solvate and hydrate formation of pharmaceutical compounds and excipients. The second part presents a new strategy for crystal structure determination from powder diffraction data that circumvents the difficulties associated with separate indexing, nowadays one of the major bottlenecks in structure determination from powder diffraction data.

1.1 PHARMACEUTICAL SOLIDS

Pharmaceutical solids have the tendency to crystallize in multiple crystal forms and the significance of this phenomenon, polymorphism, has been demonstrated through the years (Vippagunta *et al.*, 2001). This can cause many practical problems, including changes in stability, dissolution rates, bioavailability, morphology and packaging. The physico-chemical properties of active pharmaceutical ingredients are key factors to the development of appropriate dosage forms.

Like polymorphs (solid crystalline phases of a compound, which have at least two different arrangements of the molecules in solid state), solvates (crystalline solids with solvent molecules as part of the structure) or hydrates (crystalline solids with water molecules as part of the structure) of an active pharmaceutical ingredient or of an excipient may differ in key properties such as solubility, dissolution rate, stability, and particle habit. Unlike polymorphs, solvates/hydrates represent different chemical entities as defined by the stoichiometry of solvent/water with respect to the active compound. Depending upon the nature of the solvate/hydrate, the solvent/water content may change over time with ambient humidity, temperature, or other processing conditions.

Pharmaceutical formulations contain the active ingredient(s) as well as excipients that serve a variety of purposes: fillers, stabilizers, coatings, drying agents, etc. As solid materials excipients exhibit varying degrees of crystallinity, from highly crystalline to nearly amorphous.

Another issue regarding pharmaceutical solids is the difficulty that is often encountered in the process of scaling up from laboratory quantities and procedures, through the pilot plant and into full production. Equipment changes, differences between the quality of laboratory scale and bulk chemicals, variation in heating/cooling rates, stirring procedures, seeding, can all influence the result of a crystallization procedure and the polymorph obtained (Morris *et al.*, 2001).

As a result, the need to identify and evaluate the solid-state interconversions that may take place at the molecular level for an active pharmaceutical ingredient or an excipient is as great as the need to assess polymorphism.

Figure 1.1 depicts the central role that solid-state research plays in pharmaceutical industry.

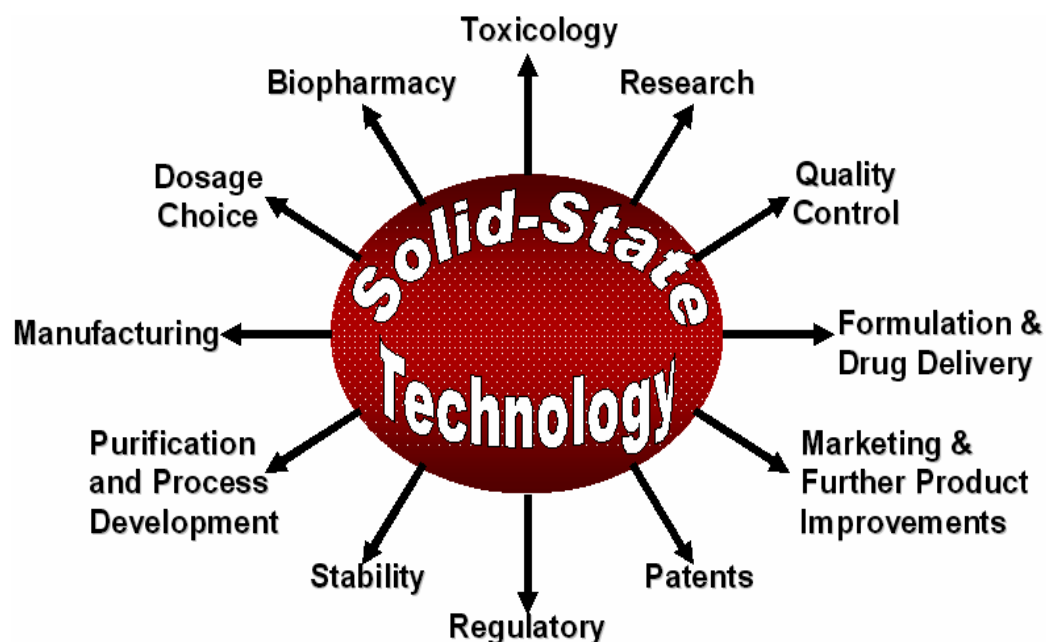


Figure 1.1. The role of solid-state technology in pharmaceutical industry

1.2 SOLID-STATE ANALYSIS

Several solid-state techniques are currently used for the study of polymorphism and solvate/hydrate formation such as: microscopy (scanning electron microscopy, hot stage optical microscopy), thermal methods (differential scanning calorimetry, thermogravimetric analysis), dynamic vapour sorption, Karl Fisher titrimetry, FT-IR spectroscopy, Raman spectroscopy, Solid-state NMR and X-ray diffraction (single-crystal diffraction, powder X-ray diffraction, hot-humidity stage X-ray powder diffraction).

The potential application of chemical and physical techniques for the study of polymorphs is virtually limitless. The combination of solid-state techniques into a single apparatus in order to extract the maximum information from an experiment and a sample is particularly applicable to polymorphic systems. The drawback in combining techniques is that the capabilities and versatility of each individual technique may be compromised. Nevertheless, the versatility of the new technologies combining together different solid-state methods allows for the use of the same sample providing valuable and more reliable information. Nowadays, there are several examples combining visual methods with spectroscopic and calorimetric measurements, mass spectroscopy or FT-IR with thermal analysis, Raman and FT-IR (Timken *et al.* 1990; Williams *et al.* 1994; Webster *et al.* 1998). The combination of X-ray powder diffraction and climate chambers with controlled temperature and humidity is very promising in research of hydrated forms of active ingredients (Loisel *et al.* 1998; Guguta *et al.* 2008). Structure determination from combined data obtained with solid-state NMR and X-ray powder diffraction is one of the new trends in solid-state drug

industry (Levitt *et al.* 2005; Reutzel-Edens 2007; Clawson *et al.* 2008; Brouwer 2008).

Structure analysis at the molecular level is an essential step in the understanding of chemical and physical properties and in the evaluation of polymorphism and solvate/hydrate formation. Combining the information obtained from different solid-state techniques with structural data, a detailed insight into the polymorphic or hydration/dehydration behaviour of pharmaceutical compounds can be obtained, even at the molecular level. Therefore, crystal structure determination is a key technique for understanding solid-state properties.

1.3 Crystalline materials

Crystalline material exists of structural units, unit cells, which are repeated regularly and indefinitely in three dimensions, thereby forming a so-called crystal lattice (see Fig. 1.2). In case of amorphous material such a long-range order is not present.

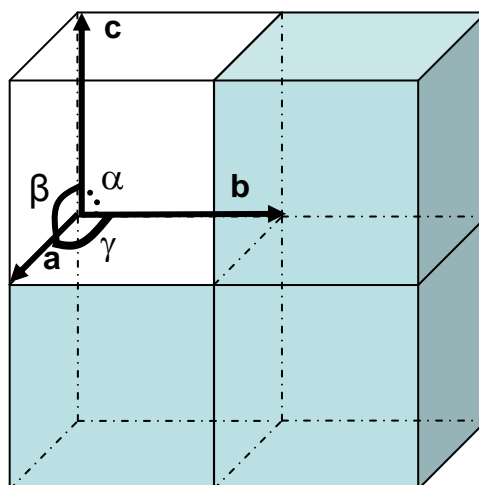


Figure 1.2. Regularly repeated unit cells in crystals

The dimensions of a unit cell are characterized by six quantities; three axial lengths (a , b , c) and three interaxial angles (α , β , γ). Therefore, the unit cell has a definite volume, V , that contains the atoms and molecules necessary for generating the crystal. Each unit cell contains at least one molecule and can be classified by one of the seven crystal systems: triclinic, monoclinic, orthorhombic, hexagonal, rhombohedral, tetragonal and cubic (see Table 1.1).

Table 1.1. The seven crystal systems

<i>Cubic</i>	$a = b = c; \alpha = \beta = \gamma = 90^\circ$
<i>Tetragonal</i>	$a = b \neq c; \alpha = \beta = \gamma = 90^\circ$
<i>Orthorhombic</i>	$a \neq b \neq c; \alpha = \beta = \gamma = 90^\circ$
<i>Hexagonal</i>	$a = b \neq c; \alpha = \beta = 90^\circ; \gamma = 120^\circ$
<i>Trigonal</i>	$a = b = c; \alpha = \beta = \gamma \neq 90^\circ$
<i>Monoclinic</i>	$a \neq b \neq c; \alpha = \gamma = 90^\circ; \beta \neq 90^\circ$
<i>Triclinic</i>	$a \neq b \neq c; \alpha \neq \beta \neq \gamma \neq 90^\circ$

Bravais discovered that there are 14 crystal lattices, consisting of seven primitive and seven non-primitive ones that conform to the seven crystal systems (Fig. 1.3).

Each of the crystal systems can have, in addition, one or more symmetry elements that describe the internal symmetry of the unit cell. The different finite symmetry elements are rotation, inversion, reflection and roto-inversion (simultaneous rotation and inversion) operations. There are 32 possible unique

combinations of the 10 possible finite crystallographic symmetry elements, each defined by a point group. The combination of 32 crystallographic point groups with the 14 Bravais lattices leads to 230 unique arrangements of "points" in space, termed space groups (Brittain *et al.* 1999).

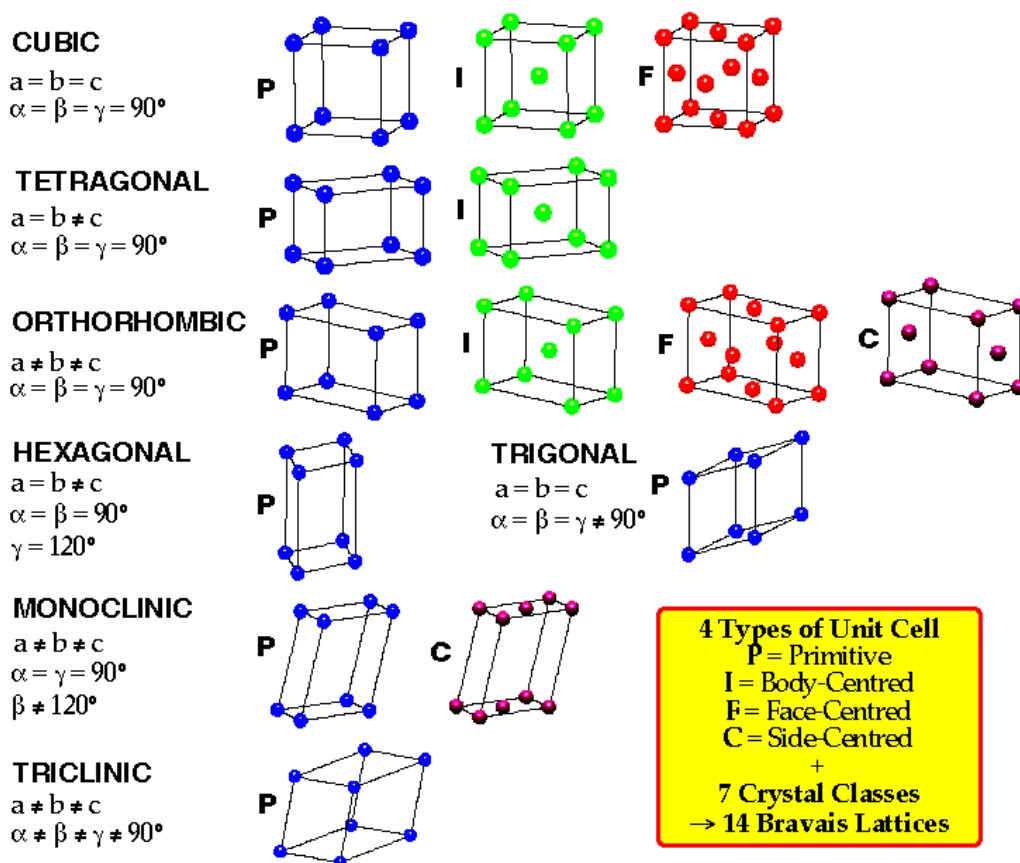


Figure 1.3. The 14 Bravais lattices

Certain space groups occur more frequently than others. About 79% of all organic and organometallic compounds crystallize in 5 space groups: $P2_1/c$, $P-1$, $P2_12_12_1$, $C2/c$ and $P2_1$ (Allen, 2002). The molecules in an organic crystal may be chiral or achiral. Chiral molecules (non-superimposable on their mirror images) crystallize in chiral space groups. A chiral space group is one without an inversion centre, mirror or glide plane. This limits the number of space

groups in which chiral molecules can crystallize to a total of 65. For crystal structure determination from X-ray powder diffraction data, the chirality of a compound is an important factor to take into account since it reduces the possible space groups thereby reducing computing time.

1.4 POLYMORPHS AND SOLVATES

The best known definition of a polymorphic form is still the one formulated by McCrone (1965), who defined a polymorph as ‘a solid crystalline phase of a given compound resulting from the possibility of at least two different arrangements of the molecules of that compound in the solid state’. A schematic representation of different solid forms of a (pharmaceutical) compound are shown in Fig. 1.4. In Figure 1.4 polymorph 1 and 2 differ in molecular packing while polymorph 1 and 3 differ in molecular conformation (conformational polymorphism).

Solvates are crystalline forms with solvent molecules as an integral part of the structure. When the solvent is water, the crystalline forms are called hydrates. The term of pseudopolymorphism is also used in connection with solvate and hydrate formation. Although the term was and is debated within the scientific world due to its ambiguous meaning, it is still used in pharmaceutical industry. The desolvation of a solvate can lead to a low-density structure, an isomorphic desolvate, which maintains the initial solvate crystal symmetry, or forms a desolvate/anhydrate (when the solvent is water) with a totally different crystal structure (see Fig. 1.4).

The formation of crystalline organic hydrates is a phenomenon that is frequently encountered during the isolation of active materials in the pharmaceutical and chemical industries. Because of its small size and multidirectional hydrogen bonding capability, a water molecule can often be easily incorporated into a crystal structure.

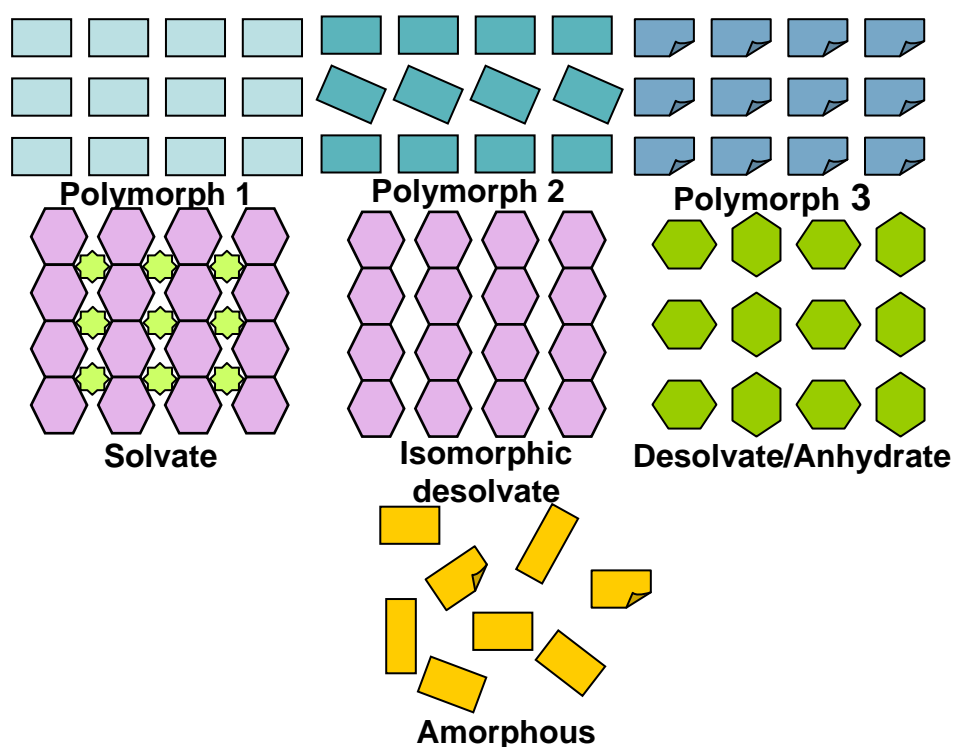


Figure 1.4. Different solid forms of a (pharmaceutical) compound

A search in the November 2007 release of the Cambridge Structural Database (~423 752 entries) yields 226 hits for the qualifier ‘form’, 2 757 hits for the qualifier ‘phase’, 14 076 hits for the qualifier ‘polymorph’, 137 hits for the qualifier ‘modification’, 66 689 hits for the qualifier ‘solvate’, 45 853 hits for the qualifier ‘hydrate’ and 2 hits for the qualifier ‘anhydrate’. The qualifiers ‘form’, ‘phase’ and ‘modification’ are denominating either a crystalline form of a solid compound, which might be a polymorphic form, or a solvate/hydrate

form. The frequency of polymorphs/solvates/hydrates, however, is obviously underestimated, since many crystal structures of polymorphic/solvate/hydrate systems are reported without making note of that fact.

An *amorphous* solid material is random in molecular conformation and/or molecular packing. Amorphous materials generally have a higher energy than crystalline materials and therefore tend to have higher solubilities and rates of dissolution.

1.5 CRYSTAL STRUCTURE DETERMINATION FROM POWDER DIFFRACTION DATA

Nowadays, single-crystal X-ray diffraction is the most common method for the determination of molecular structures and for the elucidation of intra and intermolecular interactions in various materials. Often, however, suitable crystals for single-crystal X-ray diffraction cannot be obtained. Compounds that show polymorphism or solvate/hydrate formation frequently cause difficulties in the crystallization of one of the modifications. In addition, recrystallization of unstable compounds that are initially obtained as microcrystalline powders is often not feasible. A possible route for the structure analysis of these "problematic" compounds is to make optimal use of powder diffraction data. Powder diffraction data contains less information than single-crystal diffraction data, but an optimal use of the data can lead to successful results. Every year the number of crystal structures determined from X-ray powder diffraction data is increasing.

The complexity of crystal structures determined from powder diffraction data has steadily increased through further development of "traditional" methods for structure determination in reciprocal space and application of global optimization algorithms in direct space (Harris *et al.*, 2001; David *et al.*, 2002; Altomare *et al.*, 2004; Tremayne, 2004). The currently available powder methods rely on high quality powder data. High quality data can only be obtained when the intrinsic properties of the powder and the underlying crystal structure are rather favorable, when frontline instrumentation (preferably synchrotron facilities) is used and only by careful sample preparation.

Figure 1.5 summarizes the possible routes to determine a structure from diffraction data. It shows that structure determination fails when no suitable single crystals can be grown, when only low or moderate quality powder patterns can be obtained and when crystal structure prediction methods cannot be applied.

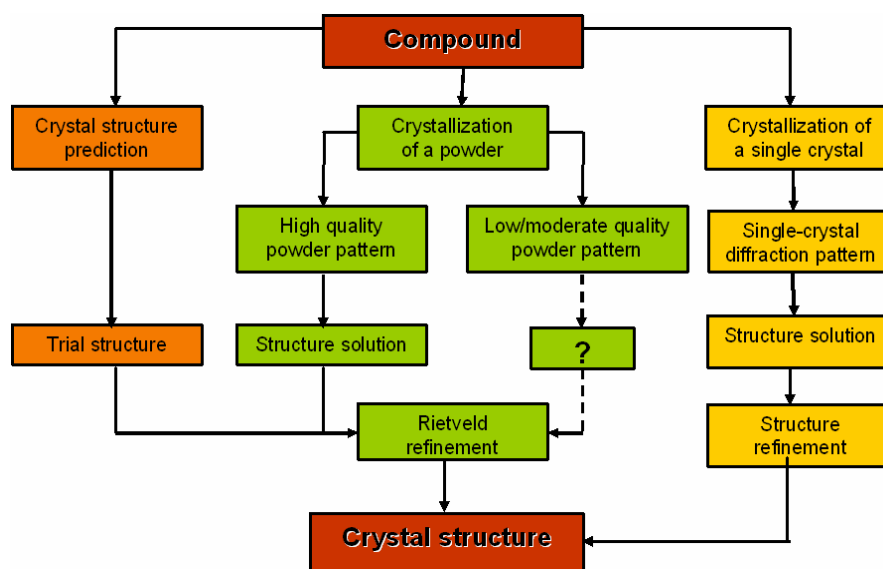


Figure 1.5. The possible routes to determine a structure from diffraction data

The usual process for structure determination from powder diffraction data consists of the following interdependent steps:

1. indexing of the powder pattern (determination of unit cell parameters $a, b, c, \alpha, \beta, \gamma$)
2. space group determination
3. structure solution (determination of an initial model)
4. structure refinement (leading to a final, accurate model)

Nowadays, steps (2) and (4) can be performed reasonably successful: the rules for space group determination are known, while for refinement the Rietveld method is used, which is available via many computer programs (McCusker *et al.*, 1999; Young, 2002). Recent developments with respect to step (3) are rather spectacular through the further development of direct-method techniques (Favre-Nicolin *et al.*, 2002; David and Shankland, 2008; Altomare *et al.*, 2004) and search methods that use prior information on molecular geometry, the so-called direct space methods (Harris, 2004; Shankland *et al.*, 2004; David, 2004; Padgett *et al.*, 2007). The lack of success in step (1) has now become one of the major bottlenecks.

1.6 SCOPE OF THE THESIS

The first part of this thesis deals with application of different solid-state techniques in combination with structure determination for the study of solvate and hydrate formation of a number of pharmaceutical compounds and excipients. The second part presents a new strategy for structure determination

from powder diffraction data that circumvents the difficulties associated with separate indexing.

Part one consists of five chapters that describe aspartame, a sweetener and excipient in drug formulation, ethinyl estradiol, a well-known steroid used in most of the anticonceptive pills, and three opioids, agonist and antagonist ones used for pain relief and treatment of drug and/or alcohol addiction. Chapter 2 and Chapter 3 provide the unknown crystal structure of aspartame anhydrate and a complete insight into the hydration and dehydration behavior of aspartame. Chapter 4 presents the crystal structures of four new ethinyl estradiol solvates together with a structural study of H-bond formation and isostructurality. In Chapter 5 the crystal structures of the naloxone monohydrate and four new anhydrate forms of morphine, naloxone, and their hydrochloride salts, determined from X-ray powder diffraction data, are presented. The role of water and the effect of the chloride counter-ion on structural properties of morphine and naloxone in the solid-state is revealed. Chapter 6 is showing how the different substituents in naltrexone and naloxone are influencing the hydration and dehydration behavior of these antagonists, also on the molecular scale.

The second part of this thesis consists of Chapter 7, where a new methodology, called *FIDDLE*, for structure determination from non-indexable powder patterns is proposed. Structure determination from powder diffraction data can be seen as a process of global optimization of all model parameters, including the unit cell parameters. This strategy is applied in the *FIDDLE* program. For the simultaneous optimization of the parameters that describe a

crystal structure a genetic algorithm together with a pattern matching technique based on auto and cross correlation functions is used. This "one-pot" strategy for indexing and structure determination was successfully used for determining the unknown crystal structures of ethinyl estradiol anhydrate, naloxone monohydrate and creatine anhydrate, cases for which indexing was problematic.

Chapter 2

CRYSTAL STRUCTURE OF ASPARTAME ANHYDRATE FROM POWDER DIFFRACTION DATA. STRUCTURAL ASPECTS OF THE DEHYDRATION PROCESS OF ASPARTAME

This chapter is based on:

**C. Guguta
H. Meekes
R. de Gelder**

2006

Crystal Growth & Design

6 (12), 2686 - 2692

ACKNOWLEDGMENTS

This research was supported by the Technology Foundation STW, applied science division of NWO and the technology programme of the Ministry of Economic Affairs. C.G. would like to acknowledge Dr. R. F. P. Grimbergen and Dr. Peter Vonk for supplying aspartame. Jacco van de Streek is gratefully acknowledged for his fruitful discussions. Also J. T. H. van Eupen is acknowledged for his useful support. Ineke Eeuwijk is acknowledged for performing the solid state NMR measurement.

Aspartame has three pseudo-polymorphic forms, two hydrates and a hemi-hydrate, for which crystal structures were determined from single-crystal diffraction data. This paper presents the crystal structure of the anhydrate, which was obtained by dehydrating the hemi-hydrate. The crystal structure of aspartame anhydrate, L-aspartyl-L-phenylalanine methyl ester, was determined from X-ray powder diffraction data. Aspartame anhydrate crystallizes in the monoclinic system with space group $P2_1$ and cell parameters: $a=19.4078(10)$ Å, $b=4.9605(2)$ Å, $c=15.6547(9)$ Å, $\beta=94.876(2)^\circ$, $V=1501.65(14)$ Å³. Final Rietveld refinement ended up with $R_{wp}=2.26$ and a GOF of 2.30. Comparison with the hydrates of aspartame and using molecular modeling provides a complete and clear picture of the dehydration behavior of aspartame at the molecular level.

2.1 INTRODUCTION

The tendency of many pharmaceutical solids and their excipients to crystallize in multiple crystal forms and the significance of this phenomenon, polymorphism, has been demonstrated through the years. The systematic analysis of the polymorphic, solvate or anhydrous forms of a drug or of its

excipients is nowadays an essential step in drug development as polymorphism can affect the final chemical, biological and pharmaceutical properties.

Aspartame, L-aspartyl-L-phenylalanine methyl ester, is a dipeptide sweetener increasingly used in pharmaceuticals, food and beverages. It is known to have different pseudo-polymorphic forms, each one containing a different amount of water (Leung *et al.*, 1998). The molecular structure of aspartame is presented in Fig. 2.1.

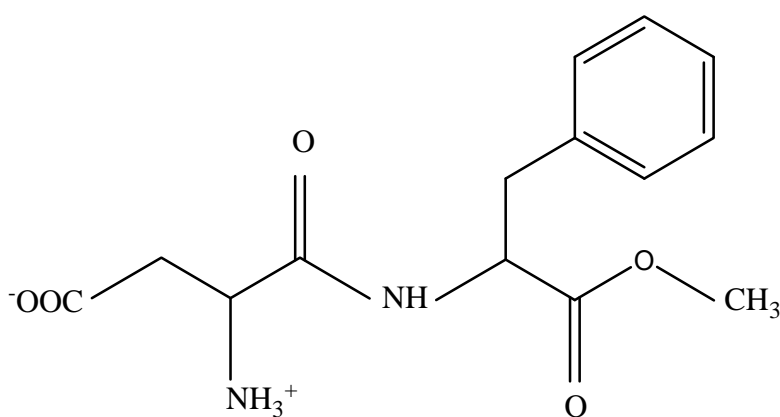


Figure 2.1. The molecular structure of aspartame

Most papers report the existence of four crystal forms of aspartame, hence forth called IA, IB, IIA and IIB, and just three of them are described in literature and available from the CSD database: IA (refcode EFIFOO01), IB (refcode ODOBAK) and IIA (refcode DAWGOX). The anhydrate form was described by S.S. Leung *et al.* in 1998, but without any details related to the crystal structure. The crystal structure of the water richest form IA was described recently in 2005 (H. M. Cuppen *et al.*, 2005). It crystallizes in the monoclinic system with space group $P2_1$ and cell parameters: $a=25.450(2)$ Å, $b=4.8795(9)$ Å, $c=23.749(2)$ Å, $\beta=116.468(8)^\circ$, $V=2640.12$ Å³. The second hydrate of aspartame, form IB, was determined in 2000 (T. Meguro *et al.*,

2000). IB also crystallizes in the monoclinic system with space group $P2_1$ and cell parameters: $a=22.96(2)$ Å, $b=4.964(5)$ Å, $c=23.50(2)$ Å, $\beta=123.2(1)^\circ$, $V=2241.17$ Å³ and the structure shows remarkable similarities with the structure of IA. Aspartame hemi-hydrate (IIA) crystallizes in the tetragonal system with space group $P4_1$ and cell parameters: $a=17.685(5)$ Å, $b=17.685(5)$ Å, $c=4.919(2)$ Å, $\alpha=\beta=\gamma=90^\circ$, $V=1538.46$ Å³ (M. Hatada *et al.*, 1985). The three known structures of aspartame were determined from single-crystal diffraction data and are presented in Fig. 2.2. The recently solved structure of the IA form shed light on the dehydration process between aspartames pseudo-polymorphs IA and IB. It appears that during dehydration of the water richest form (14% hydration water), IA, the principal packing does not change, but instead, the hydrate channels become smaller. The hydrate form IB contains a much smaller amount of hydration water (3.9%) and accordingly the ratio V/Z (cell volume/number of molecules in the cell) is significantly smaller for the IB form (373.528 Å³) than for the IA form (440.02 Å³).

In this paper the structure of aspartame anhydrate (from now on called IIB) is described and compared to the other known forms. The structure was determined from powder diffraction data using the DASH software (David *et al.*, 2004) and final Rietveld refinement was performed using the Topas software (Bruker AXS, 2003). It was a challenge to determine the crystal structure of this anhydrate form for several reasons. Aspartame anhydrate is extremely hygroscopic, crystallizes in tiny, thin needles, and due to these, no successful single-crystal X-ray diffraction experiment could be performed.

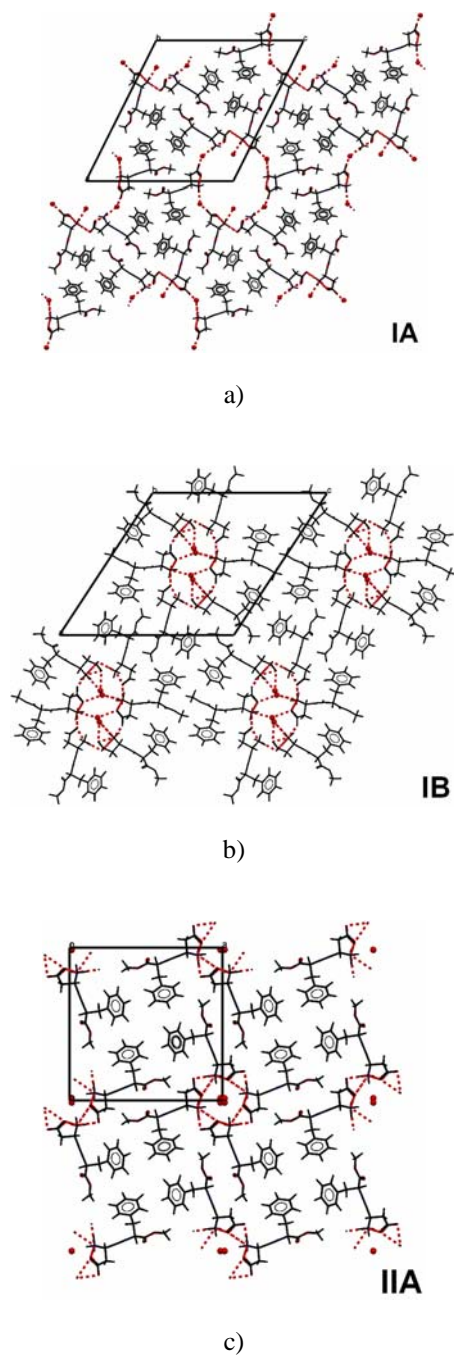


Figure 2.2. Projections along the short axis of the unit cell for (water molecules are indicated in gray): a) hydrate form IA (EFIFOO01); b) hydrate form IB (ODOBAK); c) hemi-hydrate form IIA (DAWGOX)

Other problems are related to experimental factors like preferred orientation and the quality of the microcrystalline powder that is usually obtained for the

anhydrate. Solution of the crystal structure of the anhydrate form using the DASH software, was hampered by the large amount of torsion angles present in the molecule in combination with the number of molecules in the asymmetric unit, $Z' = 2$. As it would complete the dehydration picture on the molecular level for all known pseudo-polymorphic forms of aspartame, determination of the structure of the anhydrate was very appealing.

2.2 EXPERIMENTAL

2.2.1 Preparation of the anhydrate form

Aspartame anhydrate was obtained by dehydrating hemi-hydrate form IIA. Hemi-hydrate form IIA was prepared at room temperature from a saturated solution of commercially available aspartame in water, mixed in equal volume with a solution made of 20% acetone, 20% ethanol, 10% dimethyl sulfoxide, 50% water (Hatada *et al.*, 1985). The mixture was kept at room temperature for four days after which a layer of needle shaped crystals was formed. To determine the dehydration temperature, a hemi-hydrate sample was placed in a Setaram calorimeter C80 II and heated from 20°C to 300°C at a rate of 0.01°C/minute. The scan indicated the formation of the anhydrate at 90°C. Therefore, aspartame anhydrate was finally prepared in the calorimeter at 90°C in air for 24 hours starting from pure hemi-hydrate. Before and after the experiment, argon gas was flushed into the calorimeter to avoid hydration. The sample was stored in a glove box under nitrogen atmosphere. Attempts to grow crystals suitable for single-crystal diffraction failed.

2.2.2 Solid-state NMR spectroscopy

100.6 MHz solid-state ^{13}C cross-polarization/magic angle spinning (CP/MAS) spectra were obtained using a Bruker AXS 400MHz spectrometer. The samples were packed into a 4 mm rotor and spun with a rate of 12 kHz. The ^{13}C spectra were collected using decay with 90° excitation pulse, 6.5 ms relaxation delay and 2.5ms cross polarization time.

2.2.3 X-ray powder diffraction

X-ray powder diffraction measurements were performed on the anhydrate sample using a Bruker D8 AXS Advance X-ray Diffractometer. The D8 was equipped with a Johansson type monochromator with a focusing curved Ge 111 crystal. A VÅNTEC-1 detector was used with an effective angular region of 2° . The data was collected in transmission capillary geometry using monochromatic $\text{Cu K}_{\alpha 1}$ radiation. The most important instrumental and data collection parameters are presented in Table 2.1.

The anhydrate sample was lightly ground, using an agate mortar with pestle and mounted in a 0.5 mm glass capillary tube in order to reduce preferred orientation effects (Howard *et al.*, 2000). The capillary tube was filled with the material and sealed in a glove box under nitrogen atmosphere. The capillary tube was spun at 15 rpm during data collection to minimize instrumental and sample packing aberrations (Dollase *et al.*, 1986).

Table 2.1. Instrumental and data collection parameters

<i>Typical instrument settings</i>	
<i>System</i>	Bruker D8 AXS Advance $\theta/2\theta$
<i>Generator</i>	40 kV, 40 mA
<i>Measuring circle (mm)</i>	435
<i>Radiation (Å)</i>	Cu $K_{\alpha 1}$, $\lambda=1.54056\text{Å}$
<i>Monochromator</i>	Primary, focusing curved Ge 111
<i>Geometry</i>	Transmission capillary configuration
<i>Sample holder</i>	0.5 mm glass capillary tube
<i>Detector</i>	VÅNTEC-1

<i>Typical measuring conditions</i>	
<i>Range (° 2θ)</i>	4-50
<i>Step size (° 2θ)</i>	0.0084696
<i>Step time (s)</i>	50
<i>Total data collection time (h)</i>	ca 74
<i>Spinning (rpm)</i>	15

2.2.4 Data analysis

The diffraction pattern was indexed using DICVOL91 (Boultif & Louër, 1991) to obtain lattice parameters that were subsequently refined in a Pawley fit (Pawley, 1981). Z-matrices describing the molecular topology of the fragments in the compound were generated automatically by DASH (David et al., 2004) from the structural data of hydrate form IB. Twenty runs with 107 SA (simulated annealing) moves per run were performed for structure solution. A final Rietveld refinement was performed using Topas (Cheary et al., 1992).

For molecular mechanics modeling, Cerius2 (Accelrys Inc., 2002) with the Dreiding force field was used. The electrostatic and van der Waals interactions were calculated using Ewald summation and Gasteiger point charges.

2.3 RESULTS AND DISCUSSION

2.3.1 Dehydration of aspartame hemi-hydrate

The calorimeter scan performed on the hemi-hydrate sample in a temperature range from 20°C to 300°C indicated an endothermic peak around 90°C, the decomposition of aspartame in diketopiperazine and release of methanol at 152°C and finally the melting point of diketopiperazine at 216°C, in accordance with the data reported by Leung *et al.* in 1997 (Fig. 2.3). The first endothermic peak was interpreted as resulting from the loss of the water in the hemi-hydrate form IIA. This was confirmed by the absence of water in the final crystal structure of the samples, which were dehydrated at 90°C.

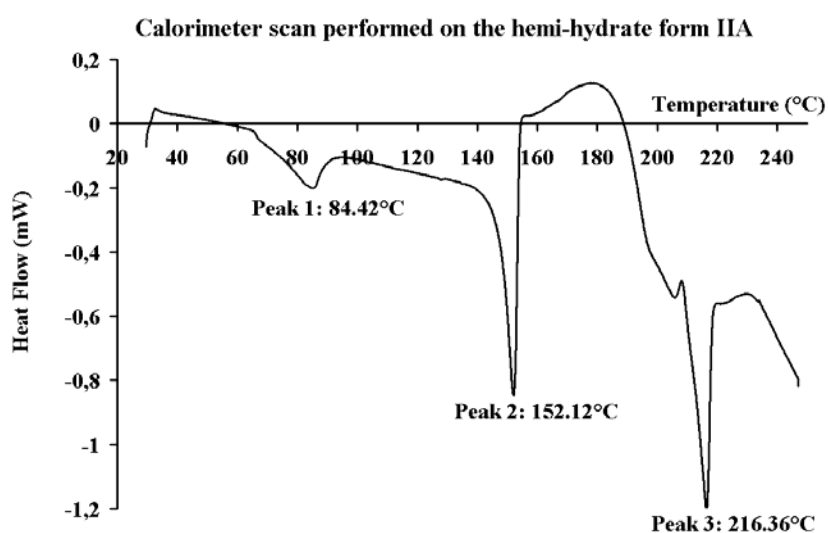


Figure 2.3. The calorimeter scan performed on the hemi-hydrate form IIA

2.3.2 Indexing, Pawley refinement and simulated annealing

The X-ray powder diffraction data collected in transmission capillary geometry for the anhydrate had a spatial resolution of 1.8230 Å in a range from 4-50° 2θ.

Twenty reflections with low and high intensity were introduced into DICVOL91 and a monoclinic cell with a volume of 1488.21 Å³ was found. Space group determination in DASH resulted in $P2_1$. The volume and space group $P2_1$ correspond to $Z' = 2$ (molecules per asymmetric unit). ¹³C solid-state NMR confirmed the number of molecules per asymmetric unit to be equal to two (Fig. 2.4).

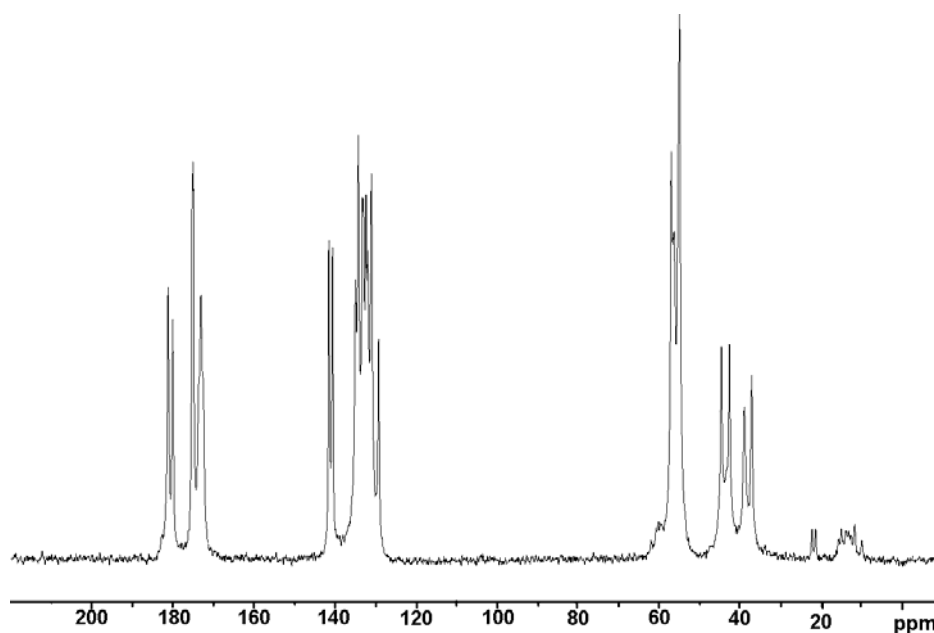


Figure 2.4. Solid-state 100.6 MHz ¹³C CP/MAS NMR spectra of anhydrate form IIB

The lattice parameters obtained after indexing were subsequently refined along with background, zero point, peak shape parameters and reflection

intensities in a Pawley fit. The characteristic parameters of the monoclinic cell obtained after the Pawley fit are presented in Table 2.2.

Table 2.2. Lattice parameters and Pawley fit results

<i>Lattice parameters</i>	
<i>System</i>	Monoclinic
<i>Space group</i>	$P2_1$
a (Å)	19.404
b (Å)	4.960
c (Å)	15.654
α (°)	90
β (°)	94.87
γ (°)	90
V (Å ³)	1501.24
<i>Zero point correction</i>	0.046
<i>Pawley fit results</i>	
<i>Number of reflections</i>	327
<i>Data points</i>	5408
R_{wp}	9.45
R_{exp}	5.28
<i>Pawley χ^2</i>	3.20

The peak shape is implemented in DASH as a convolution of Gaussian, Lorentzian and axial divergence terms (asymmetry). Actually, the X-ray line shape is a full Voigt function, which uses two parameters σ_1 and σ_2 to describe the angle-dependent Gaussian component:

$$\sigma^2 = \sigma_1^2 \sec^2 \theta + \sigma_2^2 \tan^2 \theta$$

and two parameters γ_1 and γ_2 to describe the angle-dependent Lorentzian component:

$$\gamma = \gamma_1 \sec \theta + \gamma_2 \tan \theta$$

The two other asymmetry parameters are fully defined by the peak fitting procedure and cannot be refined by Pawley fitting. The sample gave sharp diffraction lines with a mean FWHM = 0.110° and a minimum value FWHM = 0.104° for the first nine fitted peaks.

The profile Pawley χ^2 is described in DASH as:

$$\chi^2 = \left\{ \sum_i^N w_i [y_i(\text{obs}) - y_i(\text{calc})]^2 \right\} / (N - P + C),$$

where $y_i(\text{obs})$ is the observed intensity at the i^{th} step in the powder diffraction pattern; $y_i(\text{calc})$ is the associated calculated intensity; $w_i = 1/\sigma_i^2$, where σ_i is the standard deviation of the observed intensity at that point. The summation is performed over all N data points, where N is the number of data points, P the number of parameters and C the number of parameter constraints. The profile χ^2 for the Pawley fit had a final value of 3.20.

Two molecular conformations of the Z-matrices describing the molecular geometry are shown in Fig. 2.5.

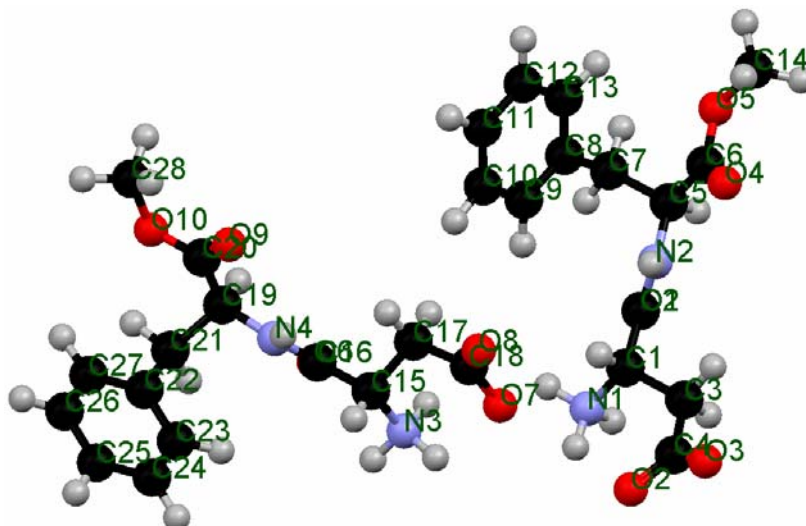


Figure 2.5. The two molecular conformations used for the Z-matrices

By superimposing the molecular conformations of the three known pseudo-polymorphs, a high degree of similarity between the molecular conformations of the IA, IB and IIA forms can be noticed (see Fig. 2.6).

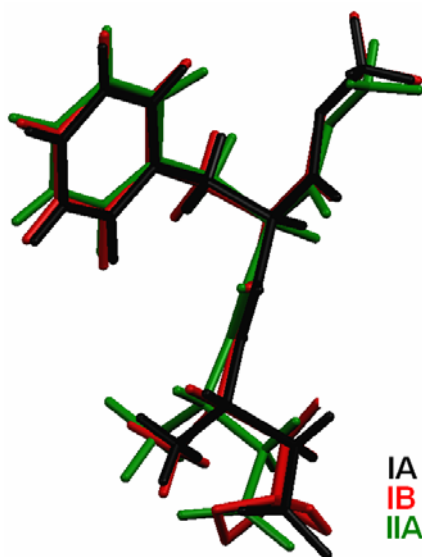


Figure 2.6. Molecular conformations of the three pseudo-polymorphs of aspartame

It is known that the two hydrates, IA and IB, have each three molecules in the asymmetric unit and the hemi-hydrate, IIA, has just one molecule in the

asymmetric unit. So, the total number of independent molecular conformations is seven. Measuring the values of the nine flexible torsion angles in the seven molecular conformations, all torsion angles, except one, exist in a narrow range of values. Therefore, two different simulated annealing processes were carried out. For one of the processes most, in principle optimisable, torsion angles in the anhydrate form were fixed. Only two torsion angles corresponding to each molecule used for the Z-matrices were optimized: O2:C4:C3:C1 and C4:C3:C1:C2, respectively O7:C18:C17:C15 and C18:C17:C15:C16. For the other simulated annealing process, all nine torsion angles had 60° of freedom.

Both simulated annealing processes ended up with the same crystal structure for the solutions, having low profile χ^2 values. A superposition of the two molecular conformations resulting from the two simulated annealing processes is presented in Fig. 2.7a.

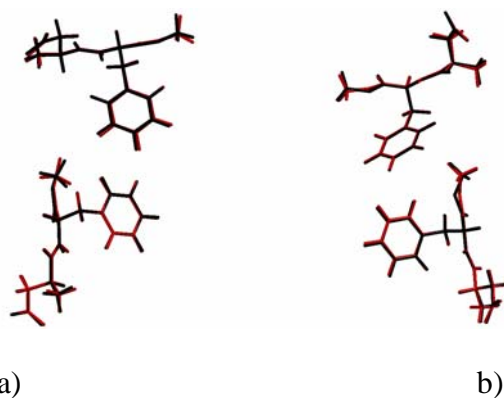


Figure 2.7. Superposition of the two molecular conformations resulting from: a) the two simulated annealing runs (black: fixed torsion angles; gray: 60° freedom in torsion angles); b) simulated annealing with 60° freedom in torsion angles (black) and the one after Rietveld refinement (gray)

The structure of the best solution had a profile χ^2 of 8.16. The fit of the observed and calculated diffraction data for this solution is shown in Fig. 2.8.

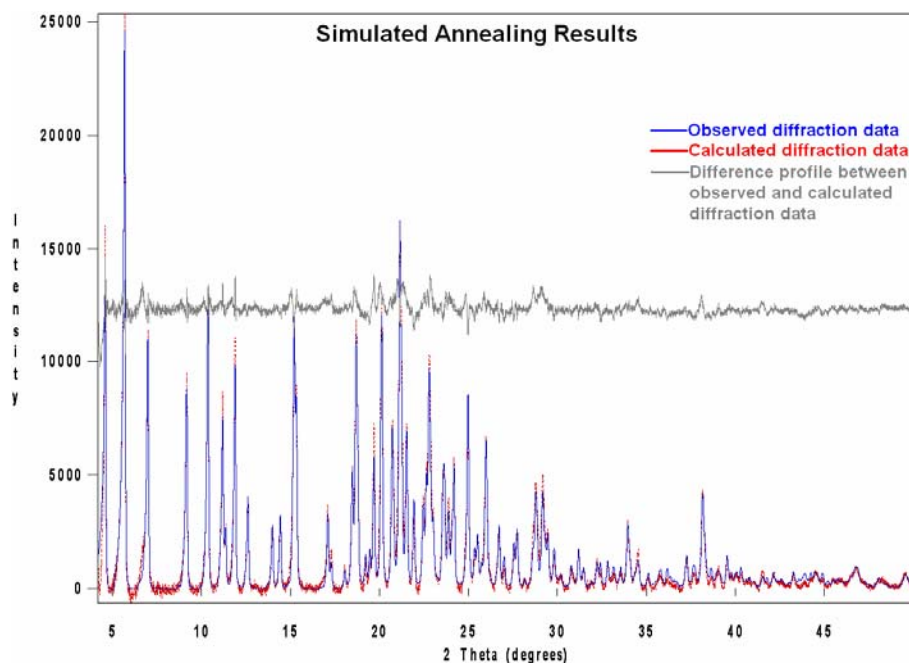


Figure 2.8. The fit to the diffraction data returned by the SA process

2.3.3 Rietveld refinement

A final Rietveld refinement (Young, 1996) of the best solution returned by the SA process gave a final profile $R_{wp}=2.26$, $R_p=1.71$ and a GOOF of 2.30. The fit of the final calculated diffraction data to the observed data is shown in Fig. 2.9.

A comparison between the rough structure initially determined by simulated annealing (SA) and the one after Rietveld refinement is presented in Fig. 2.7b.

All coordinates of the non-hydrogen atoms were freely refined, but soft restraints on bond lengths and angles were introduced in order to reduce the number of free parameters. The final crystal structure of aspartame anhydrate is presented in Fig. 2.10.

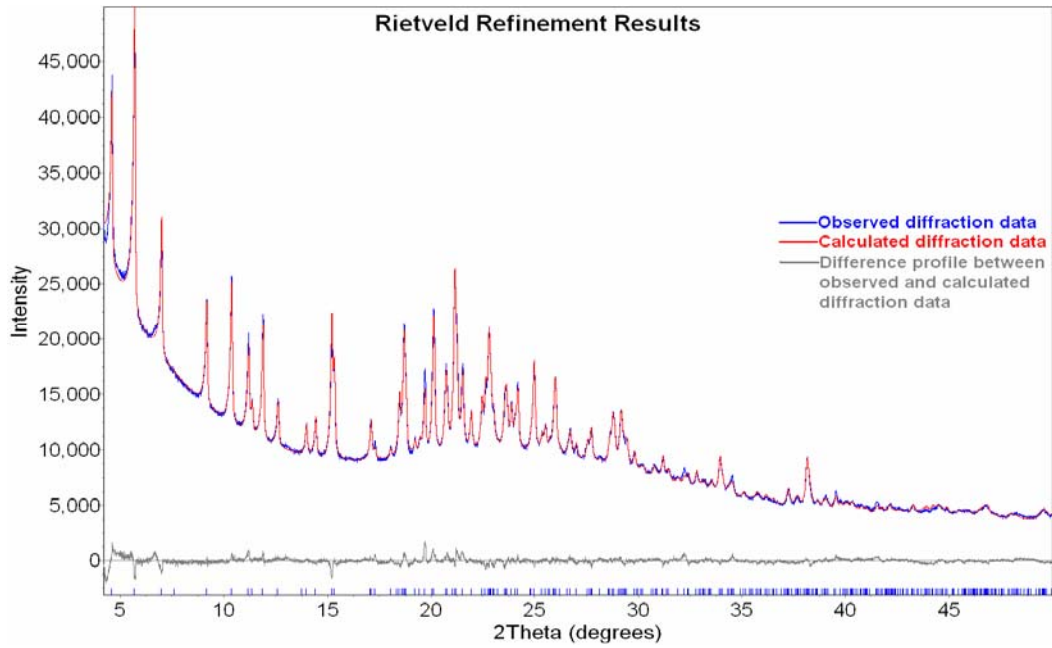


Figure 2.9. The fit after Rietveld refinement

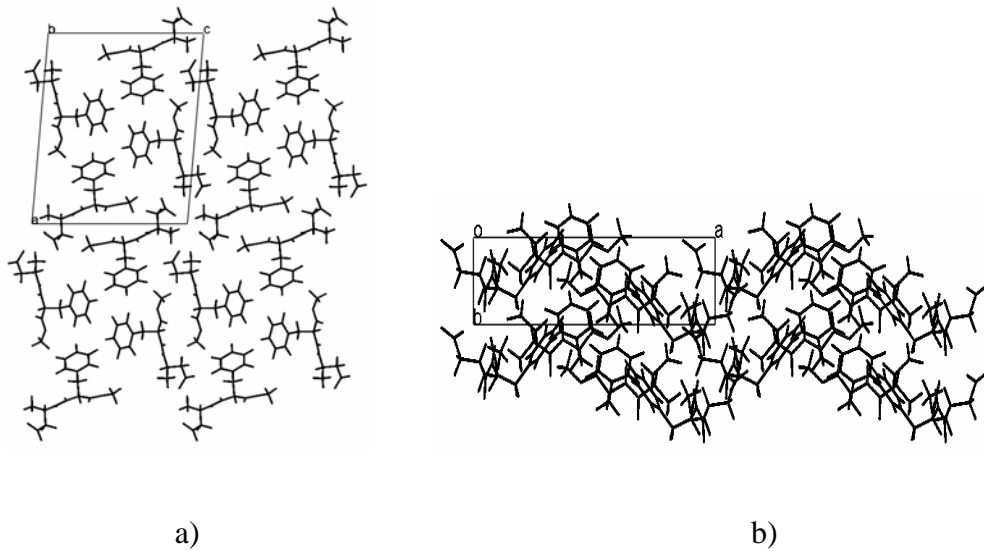


Figure 2.10. Crystal structure of aspartame anhydrate: a) **b**-projection of four unit cells, b) **c**-projection of four unit cells

2.3.4 Comparison between the four pseudo-polymorphs of aspartame

A comparison between the crystal structure of hemi-hydrate form IIA and the anhydrate form is presented in Fig. 2.11 a.

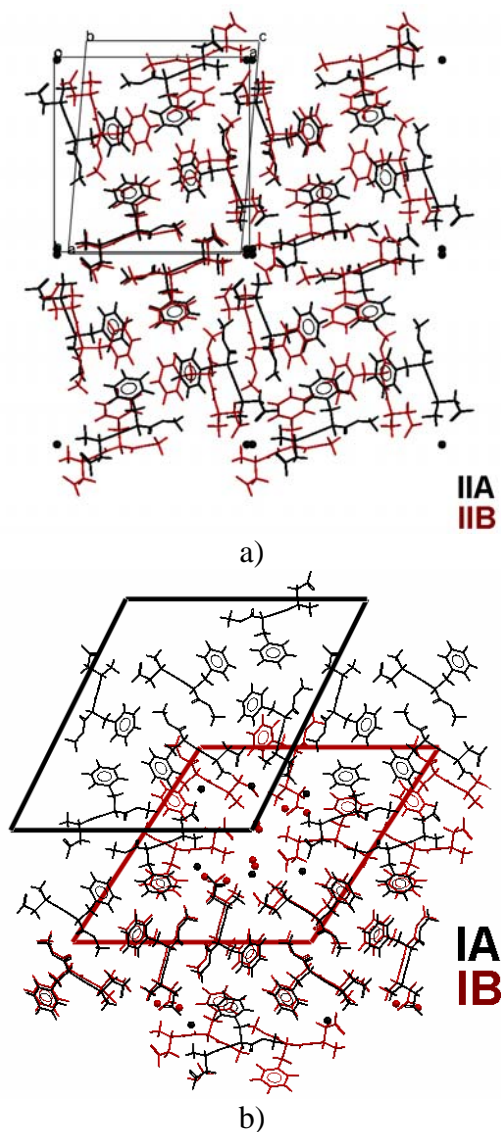


Figure 2.11. The crystal structures of: a) hemi-hydrate form IIA (black) and anhydrate IIB (gray) and b) hydrate form IA (black) and hydrate form IB (gray)

A high degree of similarity between the structural models can be observed. Apparently, by dehydrating the hemi-hydrate (tetragonal system), the water disappears from the channels, the structure collapses slightly and the tetragonal

symmetry breaks to give a monoclinic one. The resulting volume of the unit cell of the anhydrate form is obviously smaller. H. M. Cuppen *et al.* discussed in 2004 whether the water molecules do or do not play an important role in stabilizing the crystal structure of hemi-hydrate form IIA.

Now, after determining the crystal structure of the anhydrate form, it is clear that the water molecules do play a role in stabilizing the tetragonal structure of the hemi-hydrate since dehydration leads to a loss of the tetragonal symmetry and the disappearance of the channels initially occupied by water. To shed more light on the role of the water molecules in form IIA and to possibly mimic the conversion of form IIA to IIB by dehydration, a number of energy minimization experiments were carried out in analogy with the experiments performed earlier by Cuppen *et al.*, this time however with a different approach and final goal. For that, the same software and force field settings were used. The most obvious strategy to mimic dehydration of IIA is the removal of all water molecules from the channels and the minimization of the resulting structure. Cuppen already showed that such a minimization in $P4_1$ hardly changes the structure and it is clear that such a minimization cannot lead to the experimental anhydrate structure in $P2_1$. Redoing this minimization after removing all water molecules and reducing the space group symmetry of the structure to $P1$, which opens the possibility for symmetry breaking, yields a result that is very similar to the one obtained by Cuppen for $P4_1$. Clearly, only removing the water molecules is not sufficient to simulate the conversion from IIA to IIB. It is important to realize that the $P4_1$ structure IIA contains disordered water channels and that the presence of merely two molecules per four molecules of aspartame on the average leads to the conclusion that locally the water

molecules must be arranged according to a $P2_1$ symmetry. By converting the DAWGOX structure of IIA, that contains one water molecule per aspartame molecule, to $P1$ and by removing half of the water molecules per channel, an ordered hemi-hydrate structure can be built which has an ideal $P2_1$ symmetry and which shows no disordered channels. Minimizing this structure in $P1$ imposes no specific symmetry on the system and might result, in principle, in a structure with other or lower symmetry than $P2_1$. Remarkably, minimizing this structure leads to a hemi-hydrate structure that is virtually identical to the anhydrate structure with respect to the packing of aspartame molecules (see Fig. 2.12).

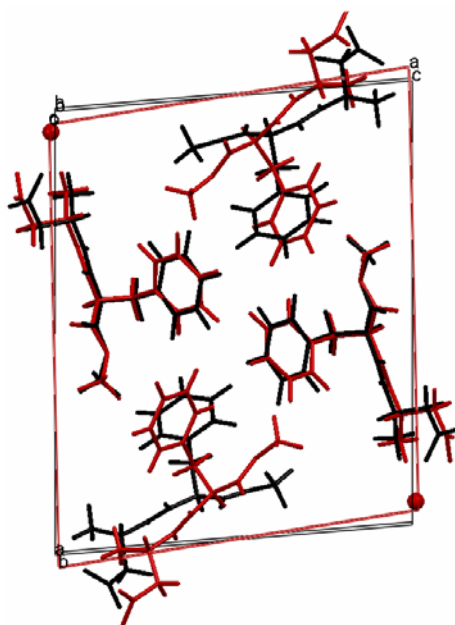


Figure 2.12. Comparison between the crystal structures of anhydrate form IIB (black) and ordered hemi-hydrate minimized after removing half of water molecules per channel (gray)

Subsequent removal of the remaining water molecules from this minimized hemi-hydrate structure, which shows almost ideal $P2_1$ symmetry, results in a

structure that shows a slightly better match with the anhydrate structure but this last step is clearly less important than the ordering step (see Fig. 2.13).

These results suggest that during dehydration of IIA, which takes place at elevated temperatures, the essential first step for conversion of the $P4_1$ structure to the $P2_1$ structure is an ordering of the water molecules inside the channels, prior to the final removal of the water molecules. The effect of a temperature raise might be a widening of the channels in IIA just enough to allow the water molecules, which are locked at lower temperatures as a result of the narrow channels, and stabilize the tetragonal structure by being disordered, to become ordered according to the $P2_1$ symmetry. This also suggests that there might be another polymorph of the hemi-hydrate, which is an ordered form of IIA, having $P2_1$ symmetry and having a structure very similar to the anhydrate IIB. The existence of this new polymorph is the subject of subsequent research. Minimization experiments suggest that the crystal structure after removing once all water molecules is a more stable structure with energy difference 0.92 kcal/mol lower in comparison with the structure for which the water molecules were removed in subsequent steps. However, this energy difference is on the edges of the accuracy of the force field calculations.

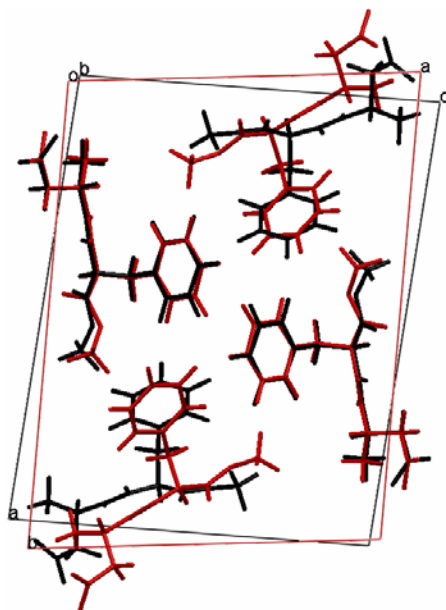


Figure 2.13. Comparison between the crystal structures of anhydrate form IIB (black) and ordered hemi-hydrate minimized after removing also the remaining water molecules (gray)

Minimization experiments can also be performed on the IIA structure described in *P1* in which the ratio aspartame to water is 4:1 instead of 2:1, followed by a minimization of the resulting structure in which all water molecules are removed. This would mimic partly dehydration of the IIA structure and could show an alternative pathway for the dehydration process. In this case, however, such minimizations never lead to a structure with a symmetry and packing close to the experimental anhydrate structure, but rather closer to the tetragonal packing.

A different relation was noticed between the crystal packing of the water richest hydrate form IA and hydrate form IB. During dehydration of IA, the principal packing also does not change and the hydrate channels only shrink (see Fig. 2.11b). However, the monoclinic symmetry is maintained during the transition. In Table 2.3 the crystallographic data for all pseudo-polymorphic

forms of aspartame is presented to illustrate the structural differences and similarities between the aspartame forms.

Table 2.3. Crystallographic data of the aspartame pseudo-polymorphs

<i>Unit cell</i>	IA (<i>EFIFOO01</i>)	IB (<i>ODOBAK</i>)	IIA (<i>DAWGOX</i>)	IIB (<i>Anhydrate</i>)
<i>System</i>	Monoclinic-b	Monoclinic-b	Tetragonal-c	Monoclinic-b
<i>Space group</i>	<i>P2₁</i>	<i>P2₁</i>	<i>P4₁</i>	<i>P2₁</i>
<i>a</i> (Å)	25.450(2)	22.96(2)	17.685(2)	19.4078(10)
<i>b</i> (Å)	4.8795(9)	4.964(5)	17.685(5)	4.9605(2)
<i>c</i> (Å)	23.749(2)	23.50(2)	4.919(5)	15.6547(9)
α (°)	90	90	90	90
β (°)	116.468(8)	123.2(1)	90	94.876(2)
γ (°)	90	90	90	90
<i>V/Z</i> (Å ³)	440.02	373.528	384.615	375.412
<i>% H₂O</i>	14	3.9	3	0

Moreover, in the case of hydrate form IA, the hydrophilic channel is made up of both water and aspartame molecules. Inside the channels, the remaining water molecules are disordered as they are much more loosely bound to the skeleton (H. M. Cuppen *et al*, 2005). Hydrate form IB has the hydrophilic channels made up only of aspartame molecules and the water molecules can be found only inside these channel. As for the case of the hemi-hydrate and anhydrate forms, the crystal packing of the two hydrates IA and IB are still very comparable. The hydrogen-bonding scheme formed by the polar amino and carboxyl groups of the aspartame molecules is similar. The hydrophobic sides of aspartame, the phenyl rings, are grouped in triples for the hydrate forms IA and IB, and for the hemi-hydrate and anhydrate forms in quadruples. Obviously, there is a relation between the crystal structures of IA, IB, IIA and IIB, and the possible conversions that take place between the four forms. A

detailed study of the possible transitions between the four forms of aspartame is described in Chapter 3.

2.4 CONCLUSIONS

The crystal structure of aspartame anhydrate was determined successfully by collecting X-ray powder diffraction data in transmission capillary geometry and using the DASH software for structure determination.

Comparison of the structures of the hydrates and the anhydrate reveals a remarkable similarity between the structures of IA and IB on the one hand and between IIA and IIB on the other hand. Minimization experiments suggest that another hemi-hydrate polymorph exists and that the ordering of the water molecules inside the channels is an essential step in the dehydration mechanism of the hemi-hydrate.

Chapter 3

THE HYDRATION/ DEHYDRATION BEHAVIOR OF ASPARTAME REVISITED

This chapter is based on:

**C. Guguta
H. Meekes
R. de Gelder**

2008

*Journal of Pharmaceutical
and Biomedical Analysis*

46, 617 - 624

ACKNOWLEDGMENTS

This research was supported by the Technology Foundation STW, applied science division of NWO and the technology programme of the Ministry of Economic Affairs. I. Eeuwijk is also acknowledged for performing TGA measurements.

Aspartame, L-aspartyl-L-phenylalanine methyl ester, has two hydrates (IA and IB), a hemi-hydrate (IIA) and an anhydrate (IIB). The hydration/dehydration behavior of aspartame was investigated using hot-humidity stage X-ray powder diffraction (XRPD) and molecular mechanics modeling in combination with differential scanning calorimetry (DSC) and thermogravimetric analysis (TGA). The results of this study are compared to earlier studies on aspartame as described in literature. It is shown that earlier transition studies were hampered by incomplete conversions and wrong assignment of the forms. The combination of the techniques applied in this study now shows consistent results for aspartame and yields a clear conversion scheme for the hydration/dehydration behavior of the four forms.

3.1 INTRODUCTION

Pharmaceutical solids have the tendency to crystallize in multiple crystal forms and the significance of this phenomenon, polymorphism, has been demonstrated through the years (Cui, 2007). Like polymorphs, the hydrates of an active pharmaceutical ingredient or of an excipient may differ in key properties such as solubility, dissolution rate, stability, and particle habit. Unlike polymorphs, hydrates represent different chemical entities as defined by the stoichiometry of water with respect to the active compound. Depending upon the nature of the hydrate, the water content may change over time with ambient humidity, temperature, or other processing conditions. A well-known example in industry is the "caking" phenomenon attributed to (re)crystallization

of a form during storage, often induced by humidity. As a result, the need to identify and evaluate the hydration states available to an active pharmaceutical ingredient or an excipient is as great as the need to assess polymorphism.

Aspartame, L-aspartyl-L-phenylalanine methyl ester, is a dipeptide sweetener increasingly used in pharmaceuticals, food and beverages. The molecular structure of aspartame (APM) is presented in Fig. 3.1.

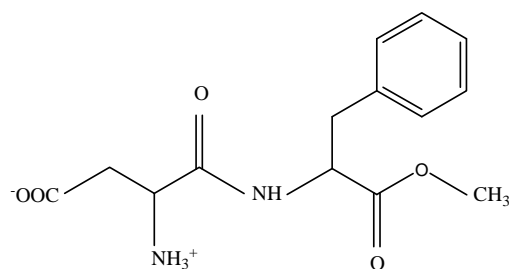


Figure 3.1. The molecular structure of aspartame

In 1983, Chauvet *et al.* reported on the kinetics of desolvation and decomposition of aspartame (Chauvet *et al.*, 1983). Two years later, in 1985, the crystal structure of aspartame hemi-hydrate form IIA was described by Hatada *et al.* (Hatada *et al.*, 1985). Aspartame hemi-hydrate (IIA) crystallizes in the tetragonal system with space group $P4_1$ and cell parameters: $a=17.685(5)$ Å, $c=4.919(2)$ Å, $V/Z=384.615$ Å³. Kishimoto *et al.* reported in 1988 on the morphology and process development of aspartame, demonstrating that the large-scale crystallization process is technically and economically possible (Kishimoto *et al.*, 1988). Almost nine years later, in 1997, Leung *et al.* presented stability studies of aspartame and aspartylphenylalanine, showing that such model dipeptides undergo solid-state intra-molecular aminolysis by the elimination of methanol (Leung *et al.*, 1997). In the case of aspartame, this

process leads to the cyclic compound diketopiperazine (DKP) as the exclusive solid product.

In 1998, Leung *et al.* described the existence of two polymorphs of aspartame hemi-hydrate, pointing actually to hydrate form IB and hemi-hydrate form IIA (Leung *et al.*, 1998). In the same year, the authors described the hydration and dehydration process for the hemi-hydrate form IIA and the existence of four forms for aspartame (Leung *et al.*, 1998). They also provided a conversion scheme for the four (hydrate) forms of aspartame, based on differential scanning calorimetry (DSC), hot-stage X-ray powder diffraction (XRPD) and humidity experiments. Meguro *et al.* reported in 2000 on the crystal structure of the "low-humidity" form IB determined from single-crystal X-ray diffraction data (Meguro *et al.*, 2000). The hydrate form IB crystallizes in the monoclinic system with space group $P2_1$ and cell parameters: $a=22.96(2)$ Å, $b=4.964(5)$ Å, $c=23.50(2)$ Å, $\beta=123.2(1)^\circ$, $V/Z=373.528$ Å³. In the same year, Rastogi *et al.* presented a study of the decomposition behavior of the hemi-hydrate form IIA using real-time hot-stage XRPD (Rastogi *et al.*, 2001). The authors also discussed the decomposition of aspartame, concluding that the amount of the reaction product increases with increasing temperature. In 2004, Cuppen *et al.* described the needle-like morphology of aspartame crystals by means of Monte Carlo simulations (Cuppen *et al.*, 2004).

One year later, Cuppen *et al.* reported on the crystal structure of the hydrate form IA and the morphology prediction for this form (Cuppen *et al.*, 2005). The water richest hydrate form IA crystallizes in the monoclinic system with space

group $P2_1$ and cell parameters: $a=25.450(2)$ Å, $b=4.8795(9)$ Å, $c=23.749(2)$ Å, $\beta=116.468(8)^\circ$, $V/Z=440.02$ Å³.

The crystal structure of the anhydrate form of aspartame (IIB) was recently described by Guguta *et al.* (Guguta *et al.*, 2006). The anhydrate form IIB crystallizes in the monoclinic system with space group $P2_1$ and cell parameters: $a=19.4078(10)$ Å, $b=4.9605(2)$ Å, $c=15.6547(9)$ Å, $\beta=94.876(2)^\circ$, $V/Z=375.412$ Å³. An overview of the crystal structures of the four forms of aspartame is presented in Fig. 3.2 (Spek, 1990).

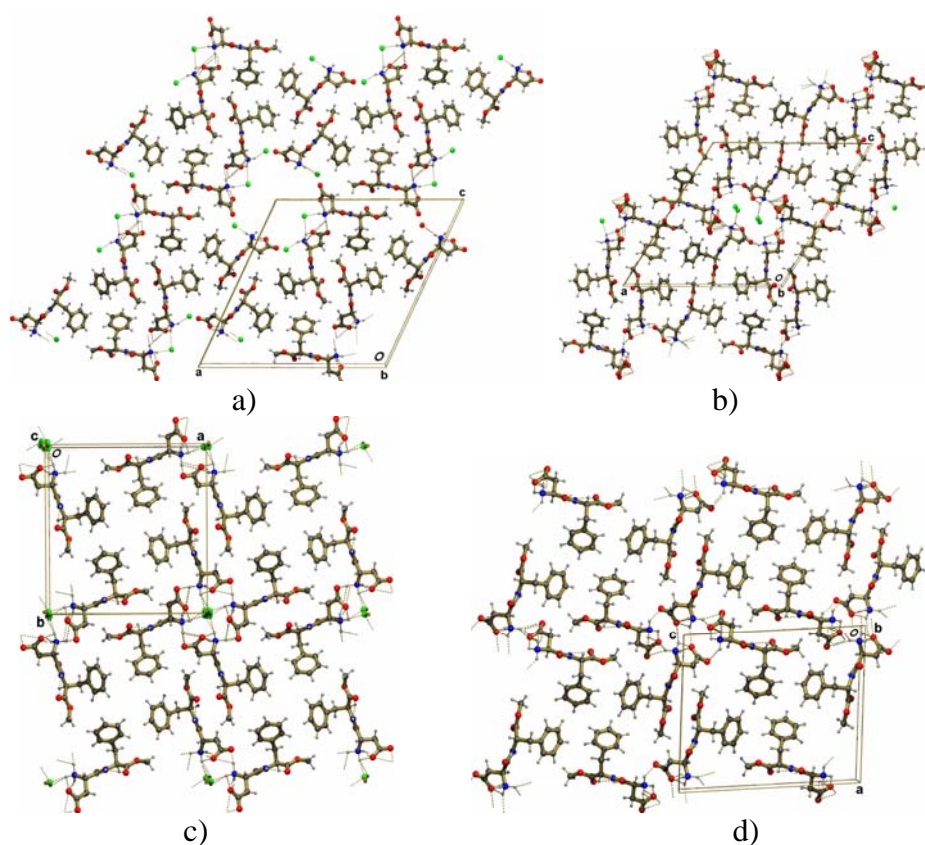


Figure 3.2. Projections along the short axis of the unit cell for: a) hydrate form IA (CSD refcode EFIFOO01); b) hydrate form IB (CSD refcode ODOBAK); c) hemi-hydrate form IIA (CSD refcode DAWGOX); d) anhydrate IIB (CSD refcode KETXIR); water molecules are indicated in gray

A high degree of similarity between the structures of hydrate form IA and form IB can be observed. In the case of form IA, the hydrophilic channel is made up of both water and aspartame molecules. Inside the channels, the remaining water molecules are disordered as they are loosely bound to the skeleton (Cuppen *et al.*, 2005). Hydrate form IB contains hydrophilic channels made up of only aspartame molecules and the water molecules can be found only inside these channels. The hydrophobic sides of aspartame, the phenyl rings, are grouped in triples for the hydrate forms IA and IB. During dehydration of the water richest form IA (14% hydration water corresponding to 2.6 molecules H₂O/molecule aspartame), the principal packing does not change, but instead, the hydrate channels become smaller. The hydrate form IB contains a smaller amount of hydration water (3.9% hydration water corresponding to 0.6 molecule H₂O/molecule aspartame) and accordingly the ratio V/Z (cell volume/number of aspartame molecules in the cell) is significantly smaller for the IB form (373.528 Å³) than for the IA form (440.02 Å³).

For the case of the hemi-hydrate and anhydrate forms, a different relation was noticed between the crystal structures (Guguta *et al.*, 2006). Both the hydrophobic and hydrophilic sides of aspartame are grouped in quadruples in these forms. Hemi-hydrate form IIA has hydrophilic channels made up of only aspartame molecules and the water molecules can be found only inside these channels. Apparently, by dehydrating the hemi-hydrate (3% hydration water corresponding to 0.5 molecule H₂O/molecule aspartame), the water disappears from the channels, the structure collapses slightly and the tetragonal symmetry breaks down to give a monoclinic one.

Altogether, aspartame is a well-studied and interesting system with respect to its hydration/dehydration behavior. However, combining all the information existent in the literature about conditions and possibilities for conversions and trying to match the recently available structural information of all forms IA, IB, IIA, and IIB with the forms identified and described in the literature, leads to confusing and contradictory results. The various assignments of pure forms seem to be hampered by incomplete conversions leading to different conditions for transitions.

Therefore, this study is aimed to provide a detailed insight into the hydration and dehydration behavior of aspartame, down to the molecular level, using hot-humidity stage X-ray powder diffraction and molecular mechanics modeling in combination with differential scanning calorimetry and thermogravimetric analysis.

3.2 EXPERIMENTAL

3.2.1 Preparation of the four forms of aspartame

Hydrate form IA was prepared from a saturated solution of commercially available aspartame in water (1.16g APM : 100mL H₂O) at room temperature. After a few hours small needle shaped crystals already formed. To avoid the dehydration of the sample before the measurements, the adhering water solution was not removed.

Hydrate form IB was obtained from a saturated solution of commercially available aspartame in water, heated to 50°C (2.6g APM : 100mL H₂O) and

allowed to cool to room temperature. After one week, the solvent solution was evaporated completely and a layer of needle shaped crystals was formed.

Hemi-hydrate form IIA was prepared at room temperature from a saturated solution of commercially available aspartame in water, by mixing it with an equal volume of a solution made of 20% acetone, 20% ethanol, 10% dimethyl sulfoxide and 50% water (Leung *et al.*, 1998). After four days, the solvent solution was evaporated completely and a layer of needle shaped crystals was formed.

The anhydrate form IIB can be obtained by dehydrating the hemi-hydrate form IIA at 90°C. Exposure to air of the anhydrate form IIB leads immediately to conversion to the hemi-hydrate form IIA and therefore IIB form was stored in a glove box under nitrogen atmosphere.

The purity of all four forms of aspartame was checked using X-ray powder diffraction (Fig. 3.3).

3.2.2 Hot-humidity stage X-ray Powder Diffraction (XRPD)

X-ray powder diffraction was performed on the investigated samples using a Bruker D8 AXS Advance X-ray Diffractometer with hot-humidity stage and VÅNTEC-1 detector. The diffractometer was equipped with a Johansson type monochromator. The detector was set at an effective angular region of 2°. The data were collected in reflection geometry using monochromatic $\text{CuK}_{\alpha 1}$ radiation. The most important instrumental and data collection parameters are presented in Table 3.1.

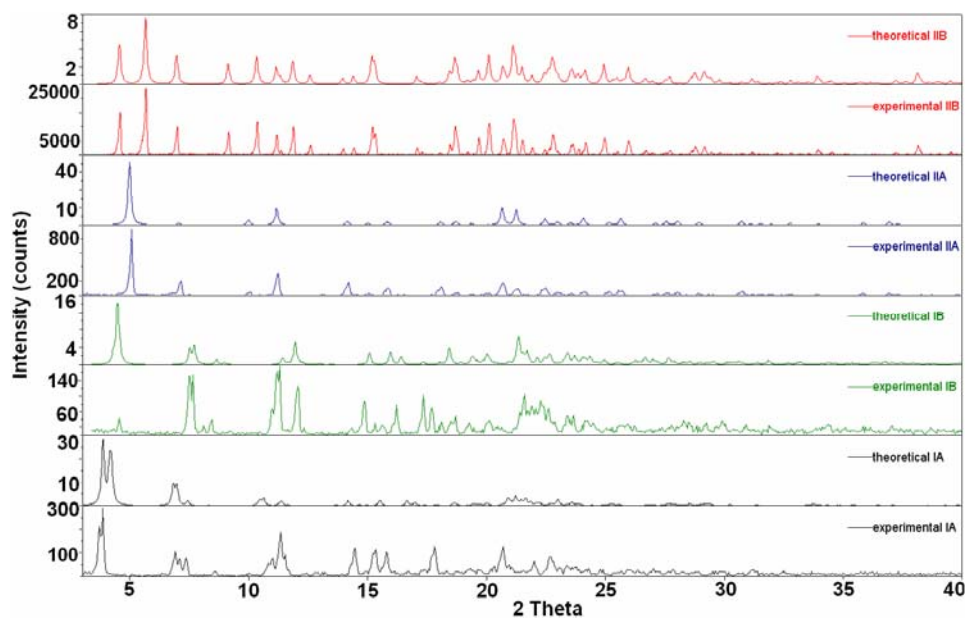


Figure 3.3. The experimental X-ray powder diffraction patterns of: hydrate form IA; hydrate form IB; hemi-hydrate form IIA; anhydrate form IIB together with the simulated patterns of the forms

Table 3.1. Instrumental and data collection parameters

Typical measuring conditions	
Range ($^{\circ} 2\theta$)	2 – 40
Step size ($^{\circ} 2\theta$)	0.05
Step time (s)	1
Relative Humidity (%RH)	0 – 80
Temperature range ($^{\circ}\text{C}$)	25 – 125
Heating rate ($^{\circ}\text{C}/\text{min}$)	1
Carrier gas	Nitrogen

3.2.3 Differential Scanning Calorimetry (DSC)

Differential scanning calorimetry curves were obtained using a Mettler Toledo 822 DSC with a TSO 801RO Sample Robot. The instrument was temperature calibrated using indium standards. The samples were scanned at 0.5°C/min or 1°C/min from 20 to 250°C under nitrogen purge at 40 mL/min in pierced aluminum pans.

3.2.4 Thermogravimetric Analysis (TGA)

Thermogravimetric analysis curves were generated using a TA Instruments Q500 TGA. The instrument was temperature calibrated using indium, tin and zinc standards. A weight calibration was performed using standard weights under nitrogen purge. The samples were scanned at 1°C/min from 20 to 250°C under nitrogen purge at 40 mL/min in pierced aluminum pans.

3.2.5 Molecular mechanics modeling

For molecular mechanics modeling, Cerius² with the Dreiding force field was used. The electrostatic and van der Waals interactions were calculated using Ewald summation and Gasteiger point charges (Cerius², 2002).

3.3 RESULTS AND DISCUSSION

3.3.1 Hot-humidity stage X-ray powder diffraction (XRPD)

The complete conversions recorded with hot-humidity stage X-ray powder diffraction for the hydrate forms IA and IB and hemi-hydrate form IIA are presented in Fig. 3.4.

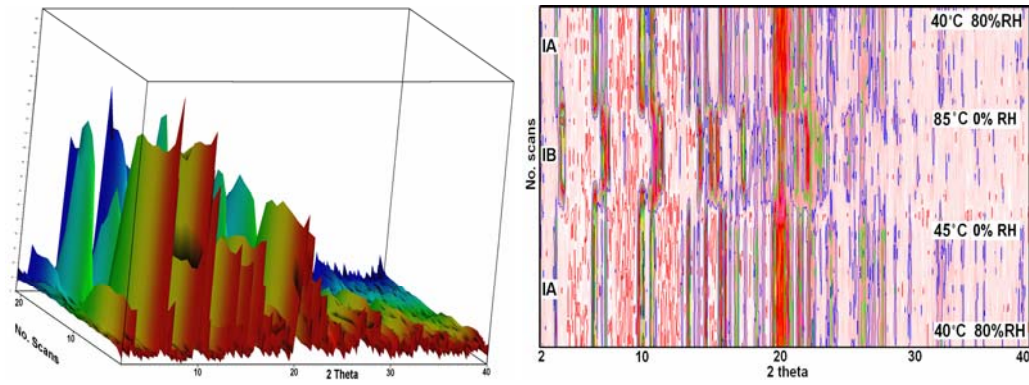
Hot-humidity stage X-ray powder diffraction was first performed on samples of the water richest form IA. During the hydration of form IA at 40°C and 80% RH for 12 hours, no other forms with a higher amount of hydration water were observed. After dehydrating form IA in a temperature range between 45 - 85°C at 0%RH, hydrate IB is formed. In order to study the reverse process, *i.e.* the conversion of the hydrate IB to form IA, form IB was hydrated at 40°C and 80% RH. After 30 min at 40°C and 80% RH a complete conversion to form IA was observed (Fig. 3.4a).

By dehydrating form IB in a temperature interval of 25 - 125°C at 0%RH, a complete conversion to the anhydrate form IIB was observed (Fig. 3.4b). No intermediate conversion to the hemi-hydrate form IIA was observed.

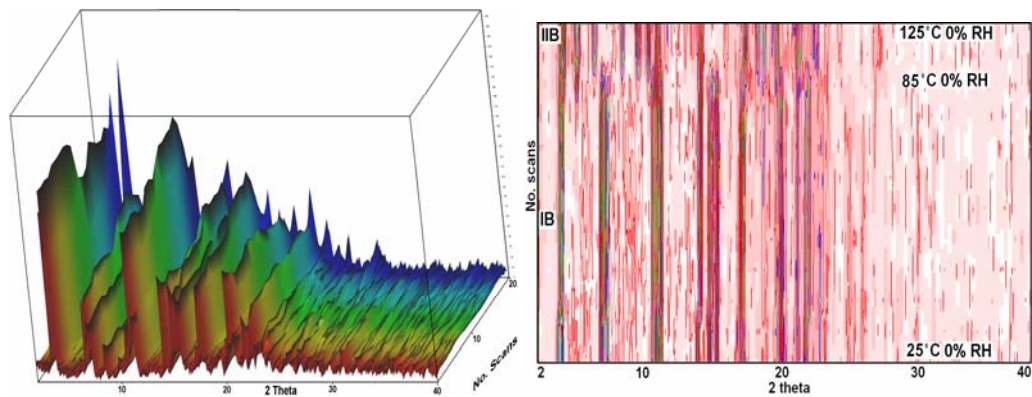
To study the dehydration of the hemi-hydrate form IIA, the crystallized form IIA was heated in a temperature range between 40 - 85°C at 0%RH. A complete conversion to the anhydrate form IIB was already observed at 40°C. Leaving the anhydrate form IIB at 40°C and 80% RH for 140 min resulted in the reverse formation of form IIA (Fig. 3.4c). Continued exposure of the hemi-hydrate form IIA to 80%RH and 40°C, did not lead to any further conversion.

If we compare our results with the conversion scheme reported by Leung *et al.* in 1997, we find significant differences. The X-ray powder diffraction patterns of the converted forms described by Leung *et al.* do not correspond to pure forms but to mixtures, as can be concluded from the crystal structures of the four forms now available. Leung *et al.* state that reversible conversions take place between aspartame "di-hemi-hydrate" and "hemi-hydrate form II". The dehydration of the "hemi-hydrate form II" leads to the anhydrate form. The

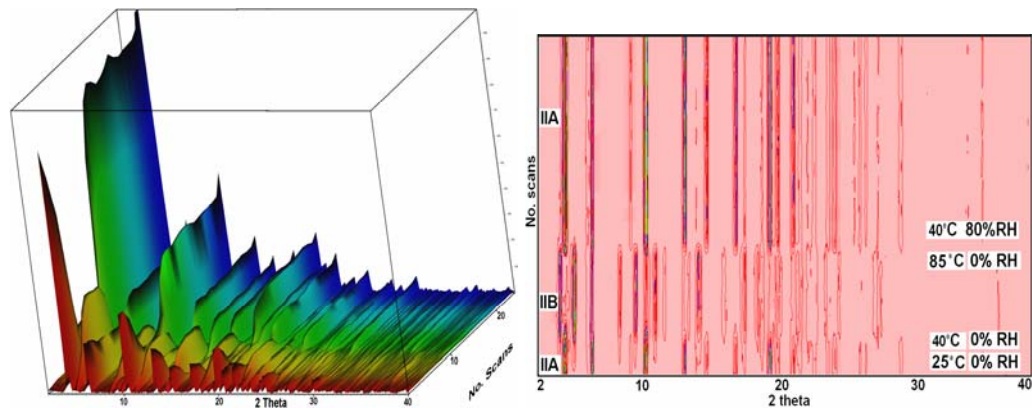
aspartame "hemi-hydrate form I" can be hydrated to the "di-hemi-hydrate". During the dehydration of the "hemi-hydrate form I", the anhydrate is formed. Leung *et al.* also states that dehydration of the "hemi-hydrate form II" leads to the "hemi-hydrate form I". We can now reinterpret the conversion scheme of Leung *et al.*. In terms of forms IA, IB, IIA and IIB, the scheme shows that their hemi-hydrate form II is in fact hydrate form IB and their "di-hemi-hydrate" is in fact the water richest hydrate form IA which contains considerably more water than the presumed monohydrate. Their hemi-hydrate form I corresponds to our hemi-hydrate form IIA and their anhydrate to our anhydrate form IIB. The main discrepancy between Leung *et al.* conversion scheme and ours is that we do not find a conversion from form IIA to form IA and also do not find a conversion from form IB to form IIA. In addition, Leung *et al.* attempted to investigate the susceptibility of aspartame "hemi-hydrate" to polymorphic transitions by ball-milling at elevated temperatures and compression. Pointing towards a "mechanical activation" of the solid fractions as a final result, the decreased crystallinity of the obtained forms unfortunately hampered the solid-state characterization of the investigated forms. On the other hand, we found that milled material when used as such for conversion experiments, often shows incomplete conversions. Our study shows that for all conversions pure forms, in principal, can be obtained. Therefore, we attribute this discrepancy between our results and those of Leung *et al.* to our use of crystalline material that was not ground before experiments and to the extreme hygroscopicity of the anhydrate form.



a)



b)



c)

Figure 3.4. 3D pictures (left) and top views (right) of the hot-humidity stage X-ray powder diffraction experiments: a) the conversion of hydrate form IA to form IB and back to hydrate form IA; b) the conversion of hydrate form IB to anhydrate form IIB; c) the conversion of hemi-hydrate form IIA to anhydrate form IIB and back to hemi-hydrate form IIA

3.3.2 Thermal Analysis

Thermal analysis can provide information on the nature of the hydrate and proof of the hydration level. Differential scanning calorimetry and thermogravimetric analysis were applied to both hydrates (IA and IB) and hemi-hydrate (IIA). As expected, each of the forms yielded unique DSC and TGA signatures.

3.3.3 Differential Scanning Calorimetry (DSC)

Differential scanning calorimetry curves of hydrates IA, IB and hemi-hydrate IIA at different heating rates are shown in Fig. 3.5.

In order to avoid the dehydration of the sample, the adhering water from the IA crystals was not removed before the measurement was carried out. Otherwise, the sample would already have partly converted into the hydrate form IB. The DSC measurement of hydrate form IA, applying a heating rate of 0.5°C/min, exhibits two endothermic events between 20 - 100°C due to solvent loss, corresponding to the formation of the hydrate form IB and respectively to the formation of the anhydrate form IIB (also suggested by the results obtained with hot-humidity stage X-ray powder diffraction). The first endothermic effect is remarkably large due to the removal of adsorbed water molecules and the water molecules incorporated in the crystal structure on one hand, and to the degradation of aspartame on the other hand (Fig. 3.5a). It is known that in aqueous solution, aspartame hydrolyses to form aspartylphenylalanine and phenylalanine methyl ester, competing with diketopiperazine formation (Leung *et al.*, 1997). Using a higher heating rate (1°C/min), the presence of the second endothermic event becomes uncertain but the hot-humidity stage X-ray powder

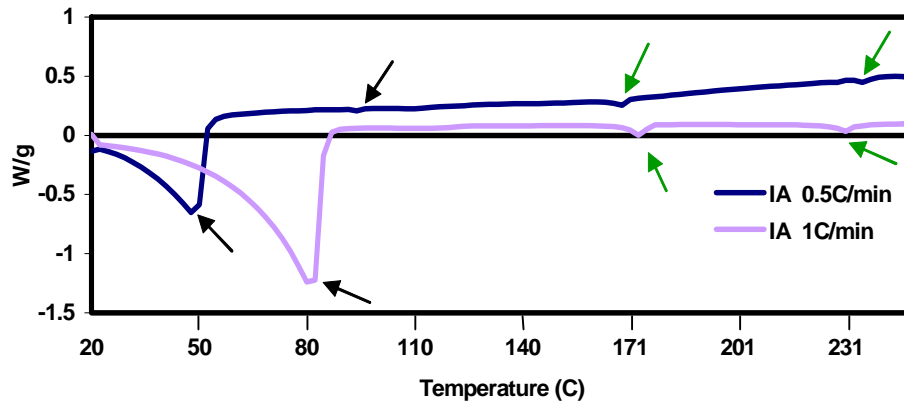
diffraction experiments at the same heating rate supports the presence of this event.

The DSC measurement of hydrate form IB (Fig. 3.5b) shows an endothermic event due to solvent loss at temperatures between 80 - 120°C confirming once again the results obtained with hot-humidity stage X-ray powder diffraction.

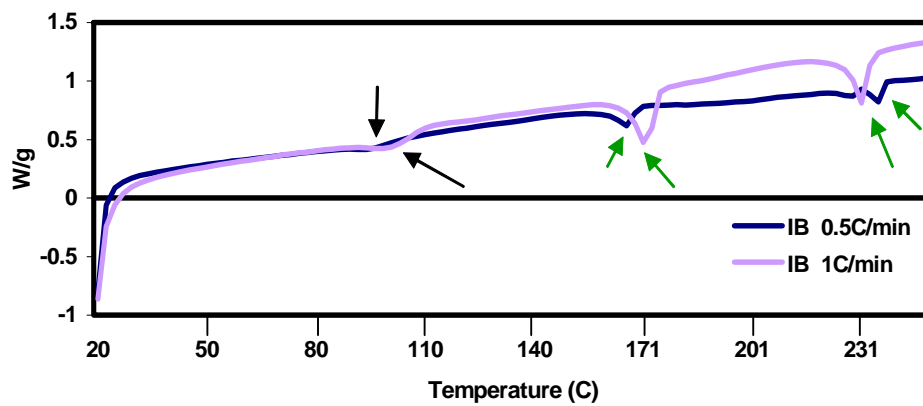
DSC analysis recorded for the sample of hemi-hydrate form IIA exhibits an endothermic event at temperatures between 20 - 50°C indicating the loss of solvent and the formation of the anhydrate IIB (Fig. 3.5c).

Both hydrates and the hemi-hydrate exhibit two endothermic events in the region from 160 to 250°C for a heating rate of 1°C/min. The endothermic event recorded around 160°C, corresponding to the decomposition of aspartame, is significantly smaller when starting with form IA compared to the results when starting with form IB or IIA, due to prior decomposition of the sample.

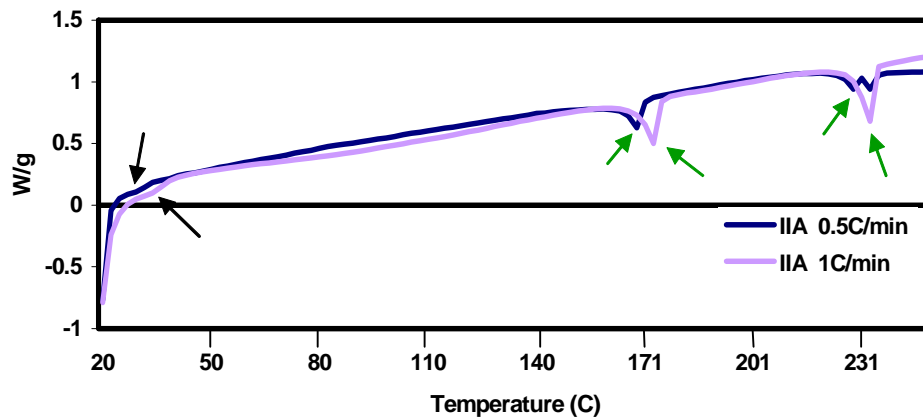
The endothermic event is attributed to a cyclization reaction, which involves an intra-molecular aminolysis with release of methanol to form the cyclic compound diketopiperazine (DKP), which is in a good agreement with the findings of Leung *et al* (Leung *et al.*, 1997). The second endothermic event observed at 230°C indicates the melting of the DKP. The DSC measurement recorded with 0.5°C/min for the hemi-hydrate form IIA exhibits an endothermic event at 230°C indicating the decomposition of DKP and another endothermic effect at 235°C, indicating the melting of the decomposition compound. The shifts recorded for all the investigated forms with 1°C/min in comparison with the ones observed at 0.5°C/min are attributed to the higher heating rate.



a)



b)



c)

Figure 3.5. DSC curves recorded for: a) hydrate IA; b) hydrate IB; c) hemi-hydrate IIA (the endothermic events are pointed out with arrows)

3.3.4 Thermogravimetric Analysis (TGA)

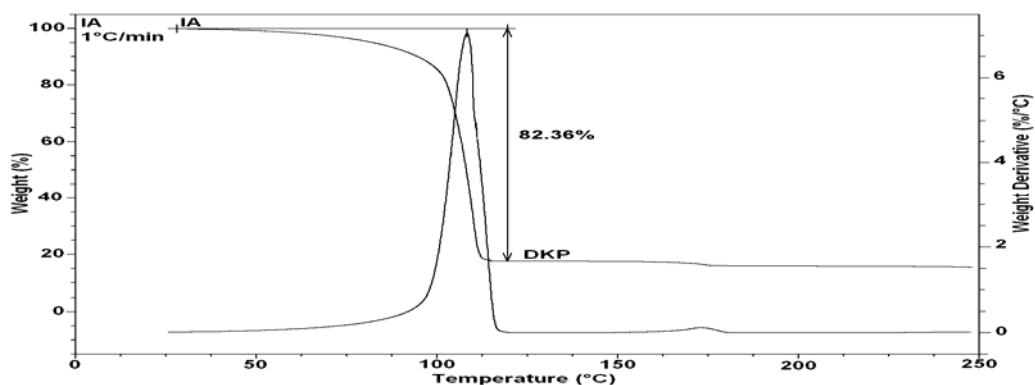
TGA curves and their derivatives of the investigated hydrates (IA and IB) and hemi-hydrate (IIA) are presented in Fig. 3.6.

Hydrate IA exhibited a remarkably high weight loss of 82.36% in a temperature range from 20 - 120°C. In order to avoid the dehydration of the sample into the hydrate form IB, the adhering water solution from the IA crystals was not removed. Taking also into account that aspartame readily degrades in an aqueous solution, it is impossible to distinguish between the loss of weight caused by the removal of adsorbed water molecules, the loss due to the removal of water molecules incorporated in the crystal structure and the one corresponding to the degradation process (Fig. 3.6a). It seems that like in aqueous solution, the presence of adhered water allows the hydrolysis of aspartame to form aspartylphenylalanine and phenylalanine methyl ester, to compete with diketopiperazine formation (Leung *et al.*, 1997). Determination of an exact temperature range corresponding to the formation of hydrate IB and anhydrate IIB from hydrate IA is impossible using TGA alone.

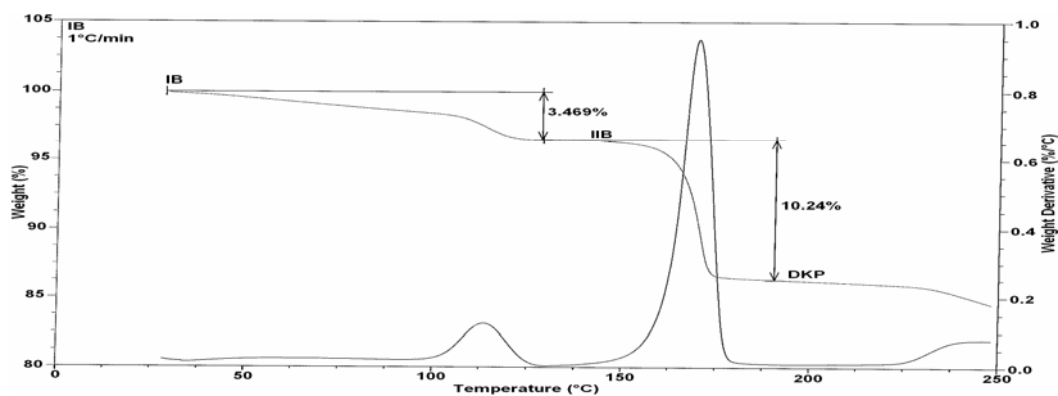
For hydrate form IB, the TGA curve shows a weight loss of 3.469% (0.59 molecule H₂O/molecule aspartame) in a temperature range from 20 - 130°C, which can be associated with the formation of the anhydrate IIB (Fig. 3.6b). In this case, the data obtained from TGA are in accordance with the data obtained from hot-humidity stage X-ray powder diffraction and DSC.

In a temperature range from 20 - 130°C, the TGA curve of the hemi-hydrate IIA exhibits a two-step weight loss corresponding to 0.38 molecule H₂O/molecule aspartame in total (Fig. 3.6c). This might be an indication that

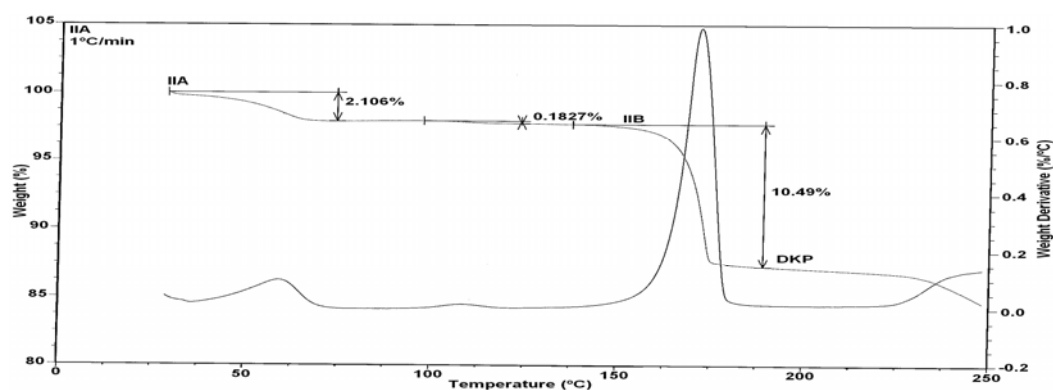
the hemi-hydrate IIA can convert upon heating to another form and finally to the anhydrate form. This could, however, not be confirmed by DSC or hot-humidity stage X-ray powder diffraction.



a)



b)



c)

Figure 3.6. TGA and derivative curves (1°C/min) for: a) hydrate form IA; b) hydrate form IB; c) hemi-hydrate form IIA

All investigated forms of aspartame decomposed at 170°C and the decomposition product DKP melted at temperatures between 230 - 250°C. As found in the DSC measurements, the weight loss recorded at 170°C, corresponding to the decomposition of aspartame is significantly smaller when starting with form IA as compared to the results when starting with form IB or IIA, due to prior decomposition of the sample. The decomposition of aspartame results in the release of methanol with a theoretical weight loss of 10.55% close to the observed weight loss of 10.24% for the hydrate form IB and respectively 10.49% for the hemi-hydrate form IIA. This shows that almost all aspartame is decomposed.

3.3.5 Molecular mechanics modeling

To shed more light on the role of the water molecules in form IA and to mimic the conversion of form IA to IB by dehydration, a number of energy minimization experiments were carried out in analogy with the experiments successfully performed earlier for the dehydration of form IIA (Guguta *et al.*, 2006). The most obvious strategy to mimic dehydration of the IA form is the removal of some water molecules from the channels in $P2_1$ and the minimization of the resulting structure. The inconvenience in this case is that the water molecules inside the channels are disordered and loosely bound to the skeleton, whereas the water molecules making up the channels are relatively strongly bonded to the aspartame architecture. The second problem is that not all water molecules inside the channels were well determined by single-crystal X-ray diffraction. Nevertheless, partial removal of water molecules, by removing two of the water molecules making up the channel and placing the

other two water molecules at an arbitrary position inside the channel followed by minimization of the energy, leads to a packing similar to the hydrate form IB minimized (Fig. 3.7a). Removing all water molecules existent in hydrate form IA and minimizing the structure again, also leads to such a structure (Fig. 3.7b). In Table 2, the unit cell parameters of the structures of hydrate IB, minimized hydrate IB, hydrate IA minimized in $P2_1$ after partial removal of the water molecules and hydrate IA minimized in $P2_1$ after removal of all water molecules are presented.

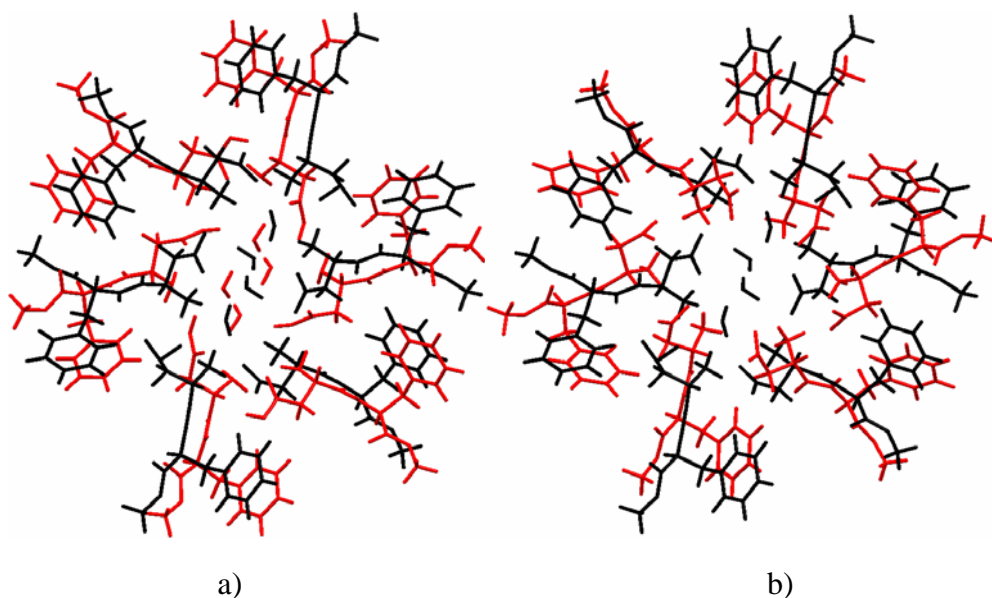


Figure 3.7. Comparison between the crystal structures of: a) the minimized hydrate IB (black) and hydrate IA minimized in $P2_1$ after partial removal of two water molecules (gray); b) the minimized hydrate IB (black) and hydrate IA minimized in $P2_1$ after removing all water molecules (gray)

Repeating the minimization experiments with partial removal of water molecules but now reducing the space group symmetry of the structure to $P1$, which opens the possibility for symmetry breaking, yields a result that is almost similar to the one obtained before. Minimizing this structure in $P1$ imposes no

specific symmetry on the system and might result, in principle, in a structure with other or lower symmetry than $P2_1$. Apparently, in the case of aspartame forms IA and IB the water molecules do not play an important role in maintaining the monoclinic symmetry. This might have been expected for the water molecules inside the channels, but surprisingly even holds for the water molecules that make up the channels of form IA.

Table 3.2. Comparison between the hydrate IB and the minimized IA structures

Unit cell parameters	IB (CSD refcode ODOBAK)	Minimized IB	Minimized IA after partial removal of water molecules	Minimized IA after removal of all water molecules
a (Å)	22.96(2)	23.062	23.03	23.356
b (Å)	4.964(5)	5.061	4.953	5.293
c (Å)	23.50(2)	23.784	23.922	23.438
β (°)	123.2(1)	118.88	117.06	123.80
V (Å ³)	2241.17	2430.6	2429.22	2408.07

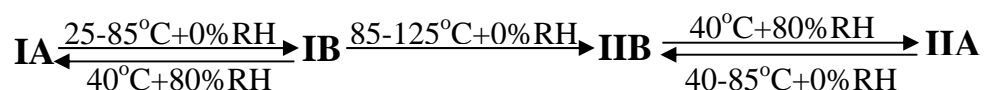
3.4 CONCLUSIONS

The hydration/dehydration behavior of aspartame was investigated using hot-humidity stage X-ray powder diffraction (XRPD) and molecular mechanics modeling in combination with differential scanning calorimetry (DSC) and thermogravimetric analysis (TGA).

The combination of the applied techniques shows consistent results for aspartame and yields a clear conversion scheme for the four forms. It also

indicates that application of hot-humidity stage X-ray powder diffraction gives more detailed information.

Hot-humidity stage X-ray powder diffraction showed reversible and complete conversions between the two hydrates IA and IB, and between the hemi-hydrate IIA and anhydrate IIB. Using the same technique, the irreversible conversion upon heating between hydrate form IB and anhydrate IIB was also observed. The conversions can be summarized in the following scheme:



Hot-humidity stage X-ray powder diffraction offers a convenient way to follow both hydration and dehydration with respect to time, showing in particular the completeness of the conversions.

Comparison of the two hydrates IA and IB revealed a remarkable similarity between the crystal structures. Molecular modeling experiments for the conversion of form IA to form IB suggest that the water molecules do not play an important role in maintaining the overall structure and the monoclinic symmetry of form IA. On removal of the water molecules in various ways and to various extents the packing of the aspartame molecules around the channels attains a similar motif. The major structural change is a shrinkage of the channel diameter.

Comparing our experimental results with the structural information of the four forms of aspartame shows that a number of forms described in literature

are wrongly assigned or correspond to mixtures. The systematic study on aspartame as presented in this paper may be of importance for a further understanding of the formation of hydrates and shows that the availability of crystal structures together with analytical data provides a detailed insight into the hydration/dehydration behavior of compounds.

Chapter 4

STRUCTURAL DIVERSITY OF ETHINYL ESTRADIOL SOLVATES

This chapter is based on:

**C. Guguta
I. Eeuwijk
J. M. M. Smits
R. de Gelder**

2008

Crystal Growth & Design

8 (3), 823 - 831

ACKNOWLEDGMENT

This research was supported by the Technology Foundation STW, applied science division of NWO and the technology program of the Ministry of Economic Affairs. Organon is acknowledged for supplying the ethinyl estradiol compound.

The (pseudo)polymorphism of ethinyl estradiol was investigated via extensive crystallization experiments. Four new crystal structures of ethinyl estradiol solvates that resulted from this study are presented, containing dioxane, nitromethane, ethanolate or DMF. The crystal structures of the hemihydrate, methanolate and acetonitrile solvates were redetermined to obtain accurate hydrogen atom positions. The structural details of the different solvates of ethinyl estradiol were investigated in order to understand the scope of solvate formation of ethinyl estradiol. Ethinyl estradiol forms many solvates, mostly with solvents having H-bond accepting or both accepting and donating propensity. Despite our rather comprehensive study no true polymorph of ethinyl estradiol anhydrate was found.

4.1 INTRODUCTION

Many drugs on the market are available in crystalline form owing to reasons of stability and ease of handling during the various stages of drug development. Crystalline solids can exist in pure form, as solvates or hydrates and, moreover, often show polymorphism. Phase transitions such as polymorph interconversion, desolvation, formation of hydrates and conversion of crystalline to amorphous forms may occur during various pharmaceutical processes, which may alter the dissolution rate and transport characteristics of a

drug. Hence it is desirable to choose the most suitable and stable form of a drug in the initial stages of its development.

The success rate of discovering new polymorphs by crystallization from solution may be increased if solvents with diverse properties are used during initial polymorph screening. Over the last years, several solvent classifications were made to provide guidelines for the judicious choice of solvents with diverse properties for polymorph screening. In 1994 Gu *et al.* reported a cluster analysis of different solvent properties. The authors separated 96 solvents into 15 solvent groups taking into account eight solvent parameters, including hydrogen bond acceptor propensity, hydrogen bond donor propensity, polarity/dipolarity, dipole moment, dielectric constant, viscosity, surface tension and cohesive energy density which is equal to the square of the solubility parameter. Since the current understanding of the influence of solvent properties on the occurrence of polymorphs is limited, it is difficult to choose the set of solvents that represents each group most appropriately. Therefore, Gu *et al.* recommended combining the solvents routinely used for polymorph screening, such as methanol and water, with other solvents from the same cluster. The authors also suggested that if a polymorph is discovered from a particular solvent, the corresponding solvent cluster might assist the choice of solvents for process optimization.

In 1999 Nangia and Desiraju analyzed the relative solvate-forming properties of fifty common solvents, and highlighted the need for systematic studies on the formation and crystal structure determination of solvates. We have been engaged in such a study, focusing on ethinyl estradiol, an estrogen analogue

which shows remarkable solvate forming abilities, as was found from a detailed investigation of the pseudo-polymorphism of this compound.

Estrogens are the essential hormones for the development of primary and secondary female sex characteristics and have a common steroid ring skeleton. Since the molecular conformation of steroids is related to their biological activity, several estrogen analogues have been investigated. Ethinyl estradiol is the most widely used estrogenic component in low dose oral contraceptives and is at least twenty times as potent in oral doses as the natural estradiol hormone. The molecular structure of ethinyl estradiol is presented in Fig. 4.1.

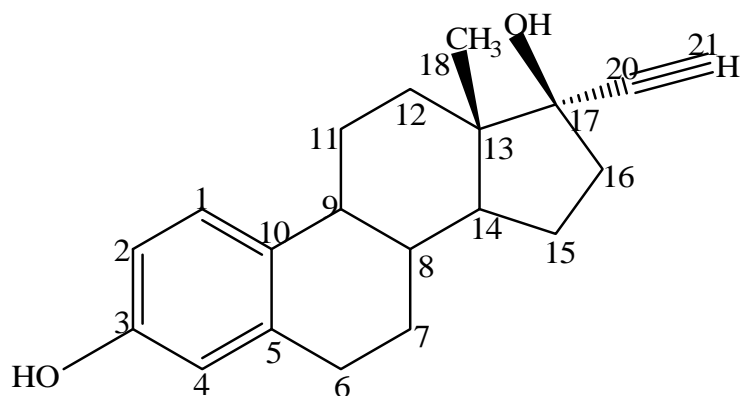


Figure 4.1. The molecular structure of ethinyl estradiol

Ethinyl estradiol, (17 α)-19-norpregna-1,3,5-(10)-trien-20-yne-3,17-diol is known to have different pseudo-polymorphic forms. Crystal structures of three of them are described in literature and the hemihydrate structure is available from the CSD database. In 1987 van Geerestein reported the crystal structure of the hemihydrate form (CSD refcode FISWIN). It crystallizes in the monoclinic system with space group *C*2 and cell parameters: $a=20.99(1)$ Å, $b=6.647(7)$ Å,

$c=12.124(2)$ Å, $\beta=90.51^\circ$, $V=1691.4(8)$ Å³. In 1989, Ishida *et al.* redetermined the hemihydrate structure and also determined the structures of the methanolate and the acetonitrile solvates. The methanolate crystallizes in the monoclinic system with space group $P2_1$ and cell parameters: $a=6.685(2)$ Å, $b=16.631(6)$ Å, $c=8.665(3)$ Å, $\beta=106.27(5)^\circ$, $V=924.8(6)$ Å³. The acetonitrile solvate crystallizes in the orthorhombic system with space group $P2_12_12_1$ and cell parameters: $a=20.531(9)$ Å, $b=7.283(2)$ Å, $c=23.815(9)$ Å, $V=3561(2)$ Å³.

Here we are presenting the crystal structures of four new ethinyl estradiol solvates (the dioxane, nitromethane, ethanolate and *N,N*-dimethylformamide solvates), redeterminations of the hemihydrate, the methanol and acetonitrile solvates and an attempt to characterize an unstable solvate formed from toluene. In order to understand the diversity in solvate formation of ethinyl estradiol, structural details like H-bond formation and isostructurality were investigated.

4.2 EXPERIMENTAL

4.2.1 Material

Ethinyl estradiol was obtained from Organon commercial supply. The preparation of the individual pseudo-polymorphic forms of ethinyl estradiol is described below.

4.2.2 Preparation of the solvates

A large number of solvates was used for possible solvate formation, but just a few of them gave solvate crystals or the already known hemihydrate form. All obtained solvates were prepared from saturated solutions of the commercially available ethinyl estradiol in the corresponding solvents (methanol, acetonitrile,

dioxane, nitromethane, *N,N*-dimethylformamide (DMF), ethanol and toluene) that were heated to temperatures about 10°C below the boiling points, followed by cooling to room temperature.

4.2.3 Single-crystal X-ray diffraction

Crystals were mounted on glass needles (Table 4.2). Intensity data were collected at -65°C on a Nonius Kappa CCD single-crystal diffractometer, using Mo-K α radiation and applying φ and ω scan modes. The intensity data were corrected for Lorentz and polarization effects. A semi-empirical multi-scan absorption correction was applied (SADABS, Sheldrick, 1996). Direct methods (CRUNCH, de Gelder *et al.*, 1993) and Patterson search methods (DIRDIF, Beurskens *et al.*, 1999) were applied for structure determination. The structures were refined with standard methods (refinement against F^2 of all reflections with SHELXL97) with anisotropic displacement parameters for the non-hydrogen atoms (Sheldrick, 1997). When possible, the hydrogen atoms were obtained from a difference Fourier map and refined independently. In other cases they were placed at calculated positions and refined riding on the parent atoms.

4.2.4 Hot-humidity stage X-ray powder diffraction (XRPD)

X-ray powder diffraction employed for investigating the dehydration/desolvation behavior of the pseudo-polymorphs was performed with a Bruker D8 AXS Advance X-ray diffractometer configured with a hot-humidity stage, controlled by an Ansyco humidity and temperature control unit. The samples were scanned at 25 to 150°C in a 2θ range from 5° to 40°, with

0.01° step size and a counting time of 0.1s per step. Several measurements were done with the same characteristics using a Panalytical X'Pert Pro Diffractometer and an Anton Paar TTK 450 cell.

4.2.5 Differential Scanning Calorimetry (DSC)

Differential scanning calorimetry curves were obtained using a Mettler Toledo 822 DSC with a TSO 801RO Sample Robot. The temperature axis and the cell constant were calibrated using indium. The samples were scanned with 5°C/min starting from 20°C to 245°C under nitrogen purge at 50 mL/min in punched aluminum pans.

4.3 RESULTS AND DISCUSSION

4.3.1 (Pseudo)polymorphism screening

It is an endless task to try every solvent in the hope to find new (pseudo)polymorphic forms, therefore a selection of solvents has to be made. Every selection contains the risk of overlooking a new form. A solvent classification based on cluster analysis looks very promising; however, it is not guaranteed that solvents from the same group show comparable behavior. In Table 4.1, the solvents used for (pseudo)polymorph screening are presented, ordered according to their hydrogen bond accepting and/or donating capabilities.

The choice of solvents depended mainly on their availability. Those with both hydrogen bond accepting and donating propensity have either an amine group or an alcohol group. The solvents that yielded crystalline material are shown in colors, blue meaning known solvate formation, red meaning new

solvate formation and green meaning hemihydrate formation although an excess of another solvate was used. The crystals from solvents in the first two columns could be used for single-crystal X-ray diffraction and appeared to include the corresponding solvent. For the solvents with no hydrogen bond accepting or donating capability, crystals could only be obtained from benzene, chloroform, 1,2-dichloroethane and toluene. Except for toluene those crystals appeared to be the hemihydrate, although in the literature a solvate of chloroform is described (Ishida *et al.*, 1989). For all other solvents (black) no (micro) crystalline material was obtained. Ethinyl estradiol did not show any true polymorphism as was concluded from our crystallization experiments.

Table 4.1. Overview of solvents used

H-bond accepting and donating propensity	Only H-bond accepting propensity	No H-bond accepting and donating propensity
Water	Acetonitrile	Toluene
Methanol	<i>N,N</i> -Dimethylformamide	Benzene
Ethanol	1,4-Dioxane	Chloroform
Aniline	Nitromethane	1,2-Dichloroethane
Di-isopropylamine	Acetone	Benzylchloride
Dimethylamine	Butyl Acetate	Chlorobenzene
Methylamine	Diethylether	Cyclohexane
Propanol	Dimethylsulfoxide	Dichlorobenzene
	Ethyl Acetate	Hexane
	Ethylsulfide	Methylenechloride
	Nitroethane	Pentane
	Propionitrile	Tetrachloromethane
	Propyl Acetate	<i>o</i> -Xylene
	Pyridine	
	Tetrahydrofuran	
	Triethylamine	

4.3.2 Structural details of the solvates

It has been estimated that approximately one-third of the pharmaceutically active substances are capable of forming crystalline hydrates (Morris *et al.*, 1993). The water molecule, because of its small size, can easily fill structural voids and because of its multidirectional hydrogen bonding capability, is also ideal for linking a majority of drug molecules into stable crystal structures (Byrn *et al.*, 1999). Solvates behave in a similar way as hydrates do. Solvent molecules have four different functions in crystal lattices: participants in hydrogen-bonding networks, space fillers with no strong interactions between solvent and solute molecules, bridges between polar and apolar regions and/or ligands completing the coordination around a metal ion. The last function will not be discussed here, because it is not relevant for ethinyl estradiol.

The crystal structures of the four new solvates obtained from dioxane, nitromethane, ethanol and *N,N*-dimethylformamide were determined from single-crystal X-ray diffraction data. The most important crystal data for the new solvates together with three redeterminations are given in Table 4.2.

In 1989 Ishida *et al.* reported the existence of four pseudo-polymorphs of ethinyl estradiol: the hemihydrate, the methanolate, the acetonitrile and the chloroform solvates and the crystal structures of the hemihydrate, methanolate and acetonitrile crystal structures could be determined. The hemihydrate form was already reported by van Geerestein two years earlier. We redetermined the crystal structures of the hemihydrate, the methanolate and the acetonitrile forms at -65°C , resulting in lower final R factors (0.0509 for the hemihydrate, 0.0412 for the methanolate and 0.0514 for the acetonitrile *vs.* the values obtained by

Ishida *et al.*: 0.057, 0.082 and 0.084 respectively). The main reason behind these redeterminations was, however, the wish to obtain the positions of the hydrogen atoms.

Table 4.2. Crystal data for the investigated pseudo-polymorphs

	<i>Hemihydrate</i>	<i>Methanolate</i>	<i>Acetonitrile</i>	<i>Dioxane</i>	<i>Nitromethane</i>	<i>Ethanolate</i>	<i>DMF</i>
System	Monoclinic	Monoclinic	Orthorhombic	Orthorhombic	Monoclinic	Monoclinic	Monoclinic
Space group	<i>C2</i>	<i>P2₁</i>	<i>P2₁2₁2₁</i>	<i>P2₁2₁2₁</i>	<i>P2₁</i>	<i>P2₁</i>	<i>P2₁</i>
a (Å)	21.0163(7)	6.6449(7)	7.2604(5)	6.7531(9)	12.2381(5)	7.7250(4)	7.0732(3)
b (Å)	6.5877(5)	16.5425(14)	20.4231(17)	12.2300(14)	6.7999(7)	14.6810(13)	11.2715(6)
c (Å)	12.0946(5)	8.6480(4)	23.6356(16)	50.824(7)	21.4221(14)	23.9456(16)	30.645(2)
β (°)	91.099(3)	106.090(7)	90	90	94.878(4)	94.327(4)	94.895(6)
V (Å ³)	1674.18(16)	913.38(13)	3504.6(8)	4197.5(8)	1776.2(2)	2708.0(3)	2434.2(8)
Z'	1	1	2	2	2	3	2
Density (mg/m ³)	1.212	1.1942(2)	1.2013(1)	1.2168(3)	1.2225(1)	1.1868(1)	1.2076(1)
F(000)	660	356	1368	1664	704	1048.6	960
Final R	0.0509	0.0412	0.0514	0.0565	0.0588	0.0643	0.1306
Crystal dimensions (mm ³)	0.55x0.15x0.1	0.2x0.29x0.3	0.45x0.35x0.4	0.16x0.23x0.3	0.55x0.5x0.25	0.3x0.5x0.06	0.3x0.3x0.4

Structure determinations of the ethinyl estradiol solvates showed a remarkable variety of structures with varying propensity of hydrogen bonding between the ethinyl estradiol and solvent guest molecules. Ethinyl estradiol forms different types of hydrogen bonds, such as: O-H...O, N-H...O, and C-H...O. In all investigated solvates (except the toluate) hydrogen bonds involving the –OH groups attached to the C(3) and/or C(17) of ethinyl estradiol and the corresponding solvent molecules are found. Another type of hydrogen bond appears between different ethinyl estradiol molecules, namely between the –OH groups attached to the C(3) and those attached to C(17). These hydrogen

bonds are comparable to those found in the hemihydrate form. The crystal structure of the hemihydrate form is presented in Fig. 4.2.

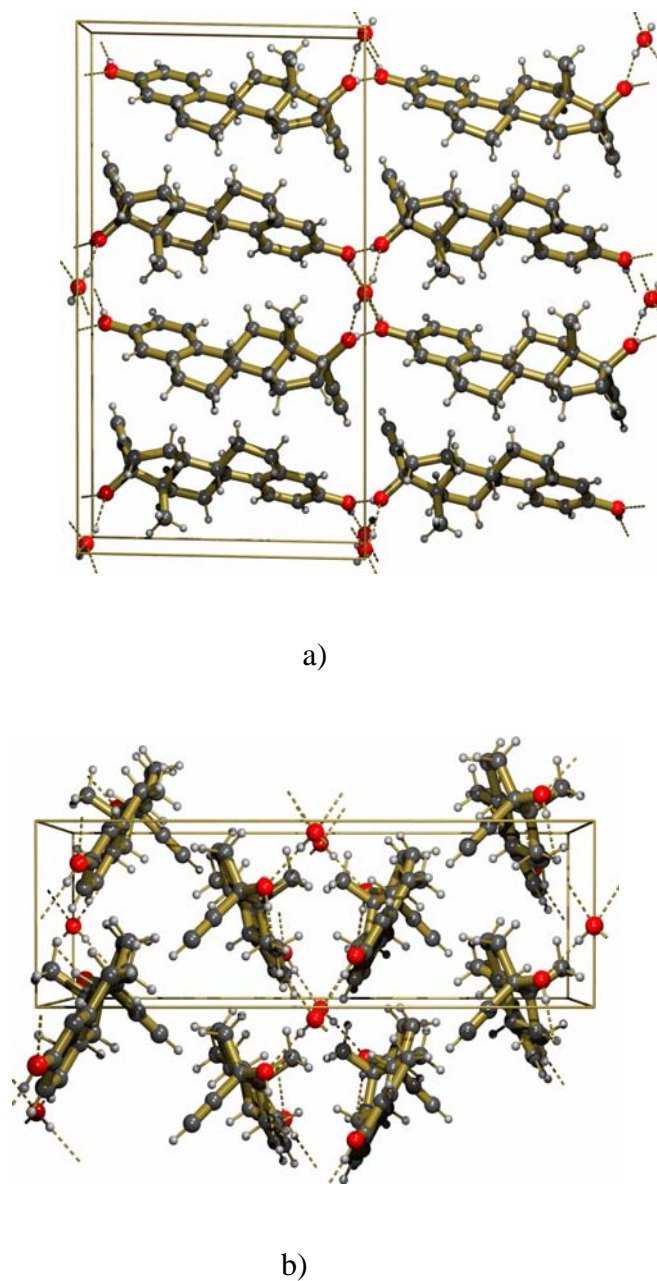


Figure 4.2. Projection of the hemihydrate form along: a) *b*-axis, b) *c*-axis

The water molecules in the hemihydrate structure form hydrogen bonds with four ethinyl estradiol molecules. For the methanolate form this is obviously

impossible. The molecules of ethinyl estradiol in the methanolate form are hydrogen bonded in a head-to-tail-to-methanol fashion forming a two-dimensional network (Fig. 4.3).

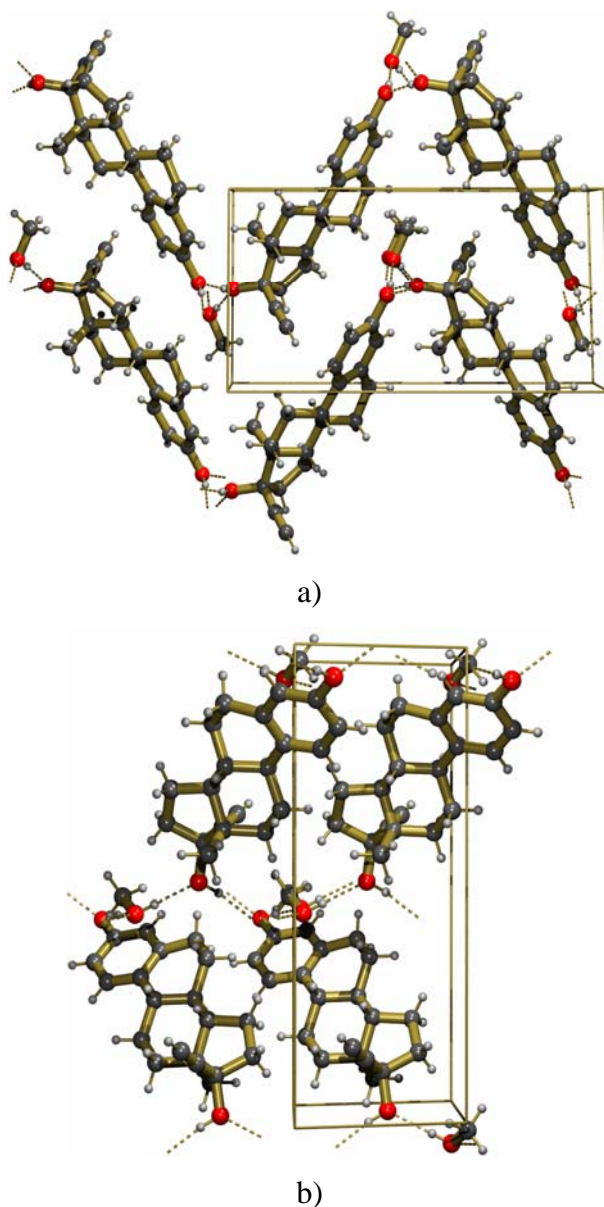


Figure 4.3. Projection of the methanol form along: a) *a*-axis, b) *c*-axis

In the acetonitrile solvate, the molecules of ethinyl estradiol are hydrogen bonded in a head-to-head-to-tail fashion forming a two-dimensional network. The hydrogen bonds are between the -OH groups attached to C(3) from different ethinyl estradiol molecules, as well as between -OH groups attached

to C(17) and C(3). The solvent molecule forms a hydrogen bond between its N atom and the –OH group attached to C(17) of an ethinyl estradiol molecule (Fig. 4.4).

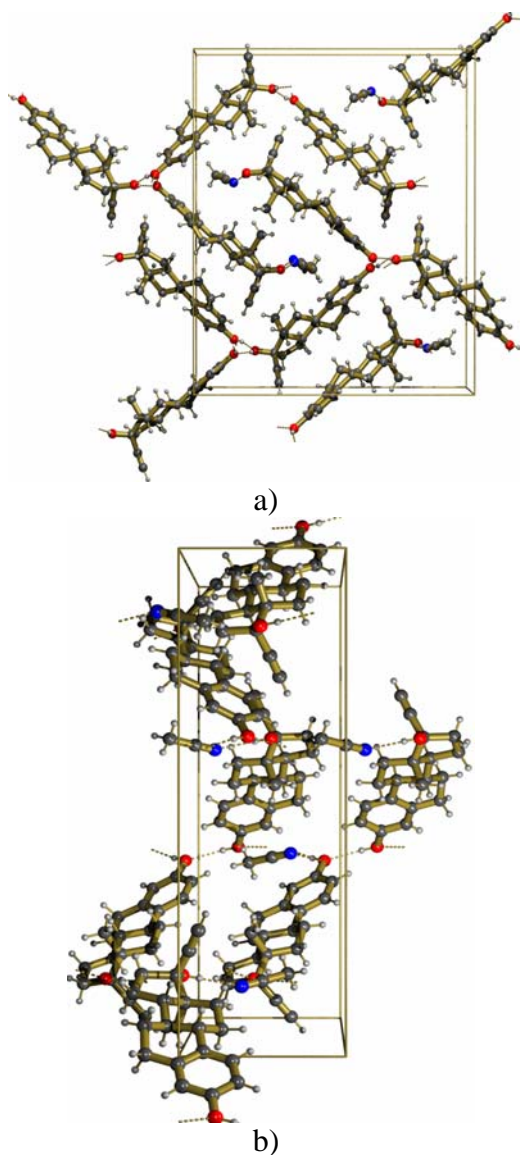


Figure 4.4. Projection of the acetonitrile form along: a) *a*-axis, b) *b*-axis

The dioxane solvate forms chains of ethinyl estradiol molecules in a head-to-tail fashion, with another molecule of ethinyl estradiol perpendicularly bonded to the chain (Fig. 4.5). The space between neighboring chains of ethinyl estradiol molecules that are related by a twofold screw axis are occupied by molecules of dioxane. One of those solvent molecules forms hydrogen bonds

with the –OH group attached to C(17). The second dioxane solvent molecule forms hydrogen bonds with the ethynyl group of the ethinyl estradiol molecules (O...H-C(51)). As Nangia and Desiraju concluded in 1999, in most dioxane solvates the acceptor O atom of the dioxane molecule is found in the neighborhood of a hydrogen donor.

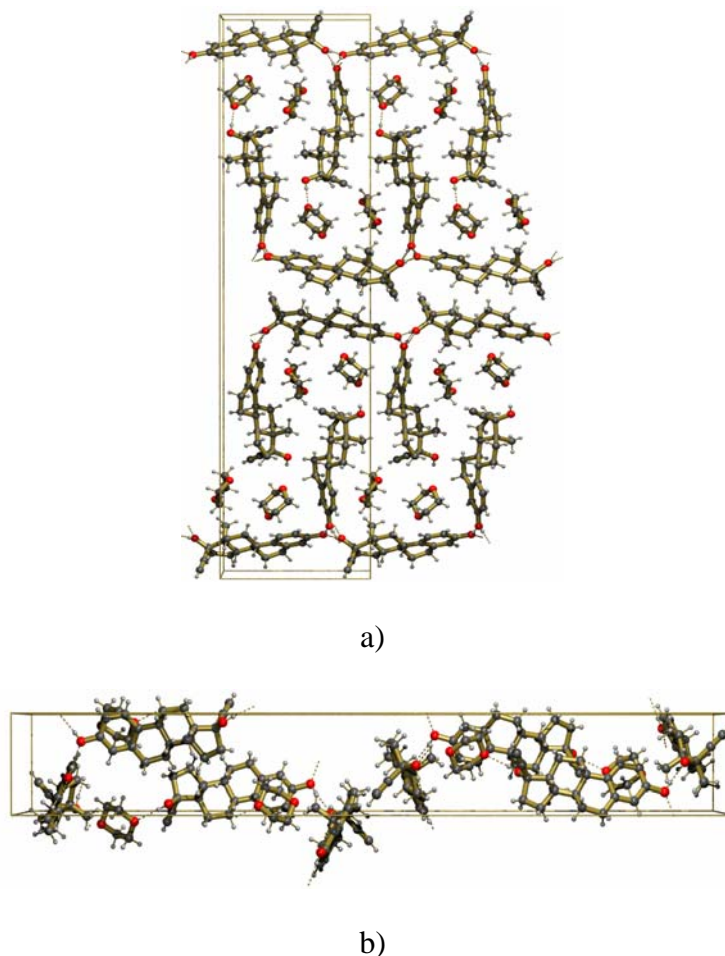


Figure 4.5. Projection of the dioxane form along: a) *a*-axis, b) *b*-axis

Making a comparison with the dioxane solvate, the nitromethane solvate shows similar chains of ethinyl estradiol molecules, and once again other molecules of ethinyl estradiol are perpendicularly bonded to the chain (Fig. 4.6). However, now only one molecule of nitromethane occupies the space between neighboring chains. Nitromethane shows the same type of hydrogen

bonding to the –OH group of the ethinyl estradiol as dioxane, but the ethinyl group is now involved in a hydrogen bond between two ethinyl estradiol molecules, resulting in a two-dimensional hydrogen bonding network.

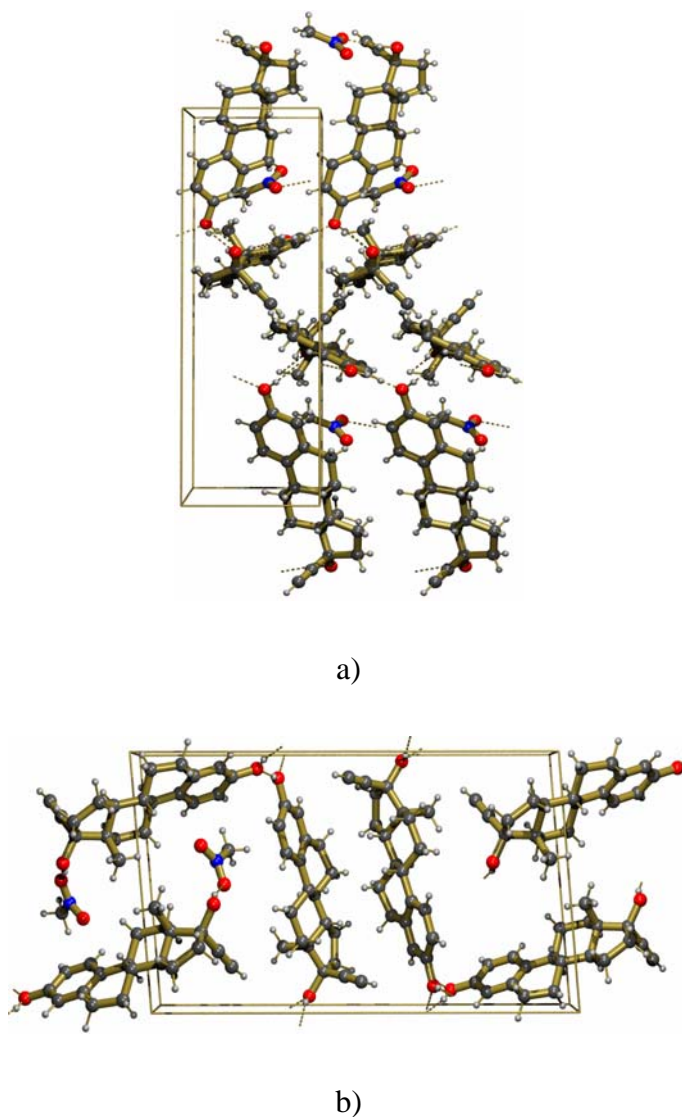


Figure 4.6. Projection of the nitromethane form along: a) *a*-axis, b) *b*-axis

The ethinyl estradiol molecules in the DMF solvate are oriented anti-parallel and are shifted by half a unit cell edge with respect to each other. Remarkably in this solvate no hydrogen bonds are formed between ethinyl estradiol molecules (Fig. 4.7). Hydrogen bonding is only present between ethinyl

estradiol and solvent molecules. Nangia and Desiraju concluded from their search in the Cambridge Structural Database that 13 entries out of 14 for –OH, 13 out of 16 for –NH and 29 out of 38 for –CH act as donors to DMF.

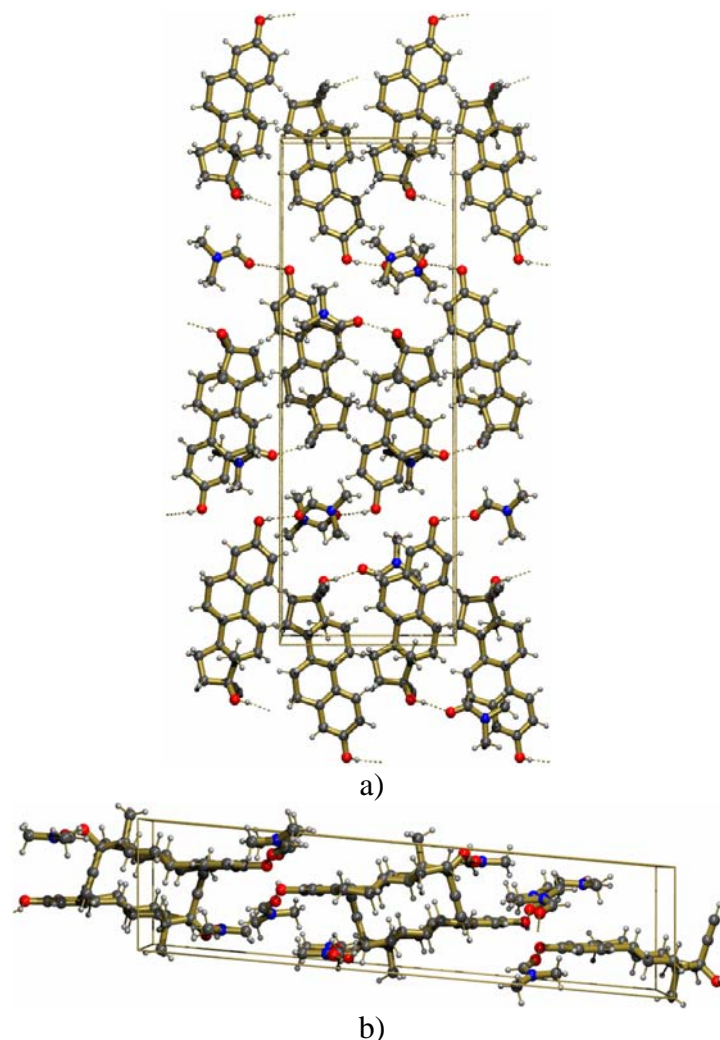
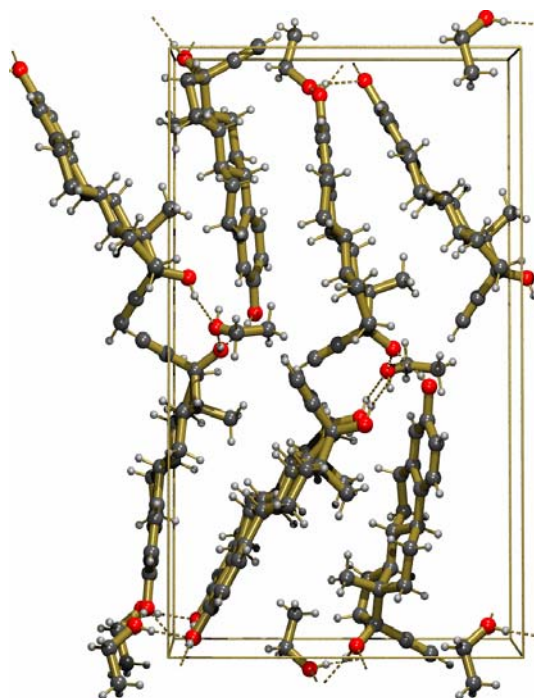


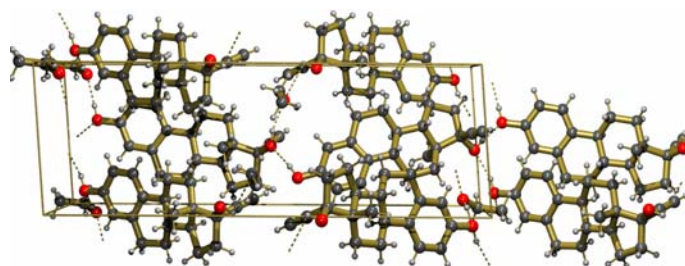
Figure 4.7. Projection of the DMF form along: a) *a*-axis, b) *b*-axis

Hydrogen bonding for the ethanolate solvate yields an infinite three-dimensional network. The molecules are ordered in a head-to-tail-to-ethanol-to-tail fashion (Fig. 4.8). The ethinyl groups of the ethinyl estradiol molecules are also involved in hydrogen bonding as was the case for the dioxane solvate.

The hydrogen bond distances and angles for all investigated solvates are presented in Appendix 4.1.



a)



b)

Figure 4.8. Projection of the ethanolate form along: a) a -axis, b) b -axis

The toluene solvate is a very unstable pseudo-polymorph converting to the hemihydrate form within minutes. Protecting the crystals with paraffin oil was not sufficient in order to collect enough data for a successful structure determination. Although the unit cell parameters and a $P42_12$ space group could be determined, a final refinement of the crystal structure was not successful. It seems that the ethinyl estradiol molecules form square type

channels with the -OH groups attached to the C(3) and C(17) atoms pointing to each other at the corners. Inside the square type channels, disordered toluene molecules are present.

In summary, a high degree of similarity between the packing of the nitromethane and dioxane solvates can be observed (Fig. 4.9). Despite these solvates crystallize in different space groups, the two solvates contain isostructural layers of ethinyl estradiol molecules.

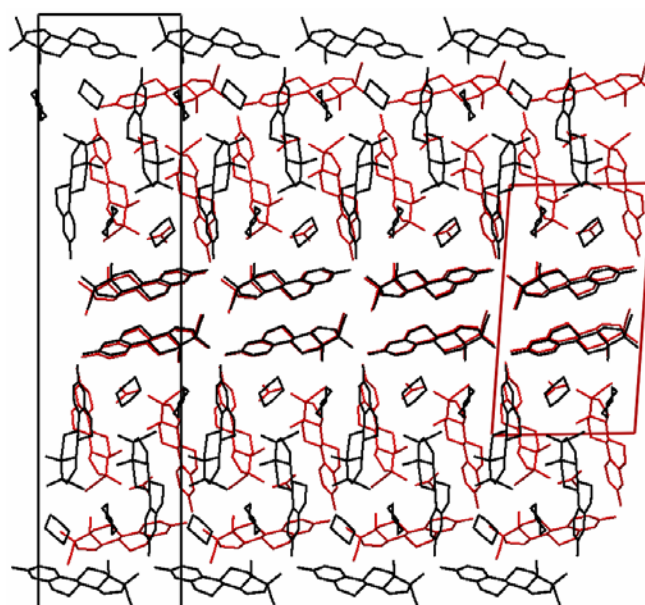


Figure 4.9. Comparison between the crystal structures of dioxane (black) and nitromethane (gray)

The crystal packing of the acetonitrile (ACN) solvate shows some similarities with the dioxane and nitromethane packing model. These solvents all have hydrogen bond accepting capabilities. Another solvent with only hydrogen bond accepting propensity and yielding a solvate is DMF. However this solvate showed a remarkable different packing.

Ethinyl estradiol can very easily form hydrogen bonds between the solvent molecules and the steroid molecule, and between the ethinyl estradiol molecules themselves. A solvent with either hydrogen bond accepting and donating propensity or only hydrogen bond accepting capability is necessary for the formation of stable solvates. Solvents with no hydrogen bond accepting or donating propensity occur as instable solvates (toluene and chloroform), as a hemihydrate or do not yield crystalline material at all. Clearly ethinyl estradiol has the flexibility of forming distinctly different hydrogen-bonding patterns and therefore it allows for the formation of a rather large and diverse series of pseudo-polymorphs. All investigated pseudo-polymorphs of ethinyl estradiol form hydrogen bonds between the –OH groups attached to the C(3) and/or C(17) and the corresponding solvent molecules, as well as hydrogen bonds between different ethinyl estradiol molecules in most of them.

Ethinyl estradiol forms solvates with acceptor molecules, like acetonitrile, DMF, dioxane and nitromethane, and with solvents, which are both acceptors and donors, like ethanol and methanol. Only with toluene, which does not exhibit any acceptor/donor propensity, an unstable solvate is formed. In Table 4.3 the structural data for all pseudo-polymorphic forms of ethinyl estradiol are presented to illustrate the structural differences and similarities between the ethinyl estradiol forms.

4.3.3 Hot-humidity and DSC studies

The investigated solvates are converting over time into the hemihydrate form. Therefore the hemihydrate form is apparently the most stable form under normal conditions. A representative thermal conversion analyzed with X-ray

powder diffraction of one of the ethinyl estradiol solvates is presented in Fig. 4.10. Due to fast scanning time and the climate chamber environment, the X-ray powder diffraction data showed poor resolution. However, the recorded data allowed us to conclude on the desolvation process of the ethinyl estradiol solvates. From the thermal measurements performed with hot-stage X-ray powder diffractometer, it is shown that during heating in the end at similar temperatures (100 - 110°C) all solvates transform into the anhydrate form (Fig. 4.10).

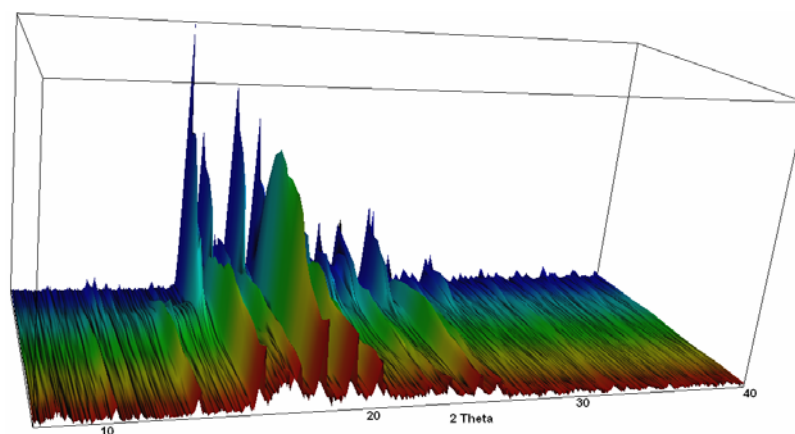


Figure 4.10. XRPD patterns of acetonitrile solvate conversions at different temperatures

There are some exceptions: the methanolate form changes via an intermediate form to the anhydrate form. The dioxane solvate shows a different behavior: the solvate melts and recrystallizes from the melt, despite DSC could not confirm these events.

All investigated pseudo-polymorphs of ethinyl estradiol yielded unique events in DSC, although some similarities could be noticed.

The dioxane solvate exhibits two gradually broad and small endothermic effects, prior to the endothermic melt event, which takes place at 100°C. The ethanolate solvate shows a different behavior: the solvate recrystallizes at 145°C after the two endothermic events (100-110°C, respectively 125-130°C), although this could not be confirmed with hot-stage X-ray powder diffraction experiments. The endothermic melting effect takes place at 184°C like for the other investigated pseudo-polymorphs. The hemihydrate form shows an endothermic effect at 130°C due to the loss of water, respectively the anhydrate formation. All the other investigated solvates showed a similar endothermic event at temperatures between 125-130°C. Despite the fact that in the DSC analysis the anhydrate formation takes place at a higher temperature than the one recorded with the hot-stage X-ray powder diffraction, this technique confirms that ethinyl estradiol solvates melt as the anhydrate form. The methanolate, acetonitrile and nitromethane solvates showed a unique endothermic effect at temperatures between 100-125°C, which is probably due to partial loss of solvent. Unfortunately, this event could not be reproduced by the hot-stage X-ray powder diffraction experiments. Despite the fact that DSC and hot-stage X-ray powder diffraction experiments show that ethinyl estradiol solvates melt as the anhydrate form, the DSC results do not match completely with the ones obtained from the hot-stage X-ray powder diffraction measurements.

The DSC data recorded for the investigated pseudo-polymorphs are presented in Fig. 4.11.

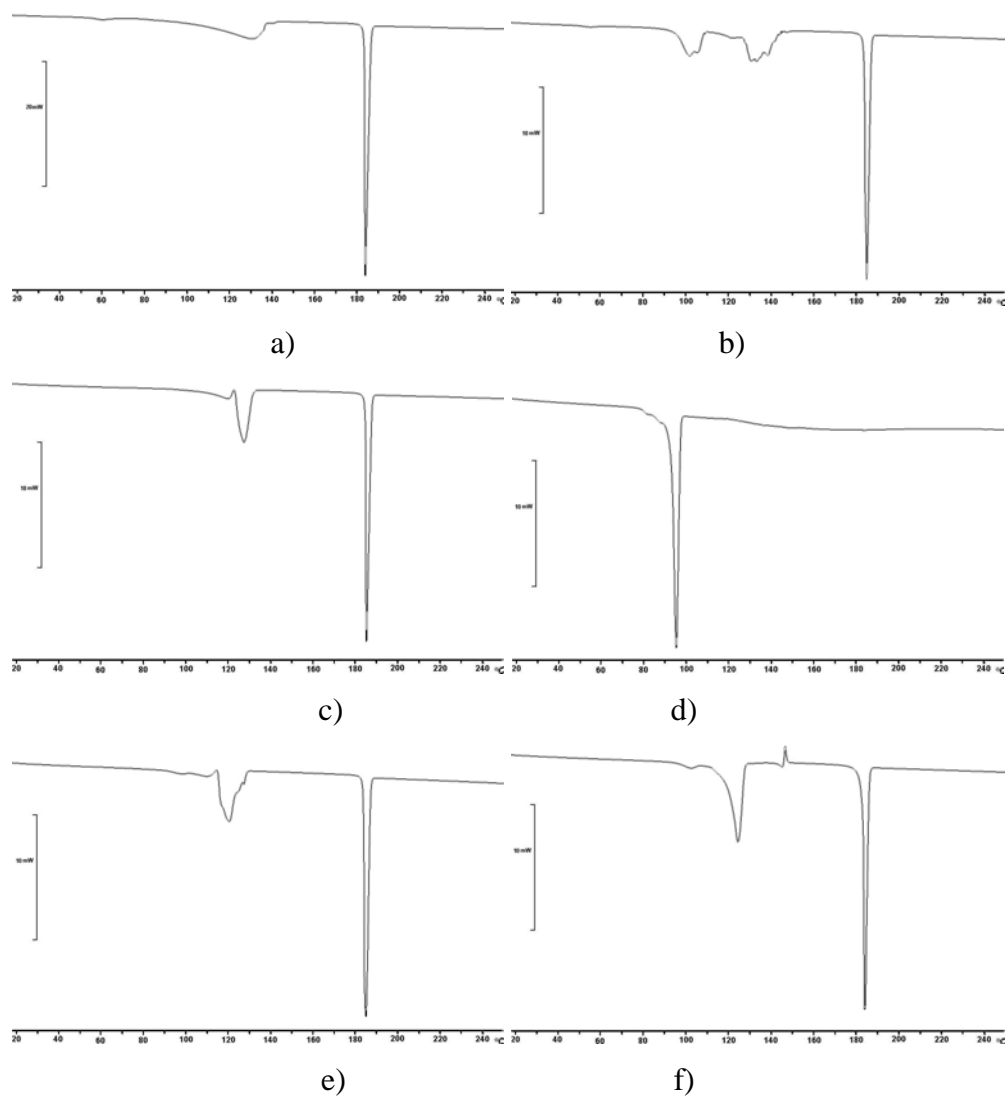


Figure 4.11. DSC results of ethinyl estradiol pseudo-polymorphs: a) hemihydrate, b) methanolate, c) acetonitrile, d) dioxane, e) nitromethane, f) ethanolate

Table 4.3. Structural data for all pseudo-polymorphic forms of ethinyl estradiol

Pseudo-polymorphs	Type of H-bond	Packing patterns of EE molecules	H-bond network	EE/solvent ratio	Donor/acceptor (D/A) propensity of the solvent molecules
Hemihydrate	C(3)-OH...§ C(17)-OH...§ C(3)...OH...C(17)	head-to-tail	2D	2/3	D/A
Methanolate	C(3)-OH...§ C(17)-OH...§ C(3)...OH...C(17)	head-to-tail-to-methanol	2D	1	D/A
Acetonitrile	C(3)-OH...§ C(17)-OH...§ C(3)...OH...C(17) C(3)...OH...C(33)	head-to-head-to-tail	2D	2	D/A
Dioxane	C(17)-OH...§ C(3)...OH...C(17) C(3)...OH...C(33) ethinyl...§	head-to-tail	1D	1	A
Nitromethane	C(17)-OH...§ C(3)...OH...C(17) C(3)...OH...C(33)	head-to-tail	2D	2	A
Ethanolate	C(3)-OH...§ C(17)-OH...§ C(3)...OH...C(17) ethinyl...O-C(33)	head-to-tail-to-ethanol-to-tail	3D	3/2	D/A
DMF	C(3)-OH...§ C(17)-OH...§ C(18)-H (18)...O(17) §...§	EE-to-DMF	0D	1/2	A

§ - from different solvent molecules

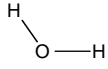
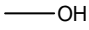
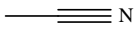
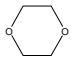
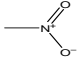
4.4 CONCLUSIONS

Ethinyl estradiol forms a fairly large number of pseudo-polymorphs but no true polymorph was found in this study. The crystal structures of four new ethinyl estradiol solvates (dioxane, nitromethane, ethanolate and DMF) were determined from single-crystal X-ray diffraction data. The crystal structures of the hemihydrate and the methanolate and ACN solvates were also redetermined from single-crystal X-ray diffraction data. An attempt to determine the crystal structure of the toluene solvate failed, owing to the instability of the crystallized material.

The characteristic H-bonds formed by the ethinyl estradiol pseudo-polymorphs are between the –OH groups attached to the C(3) and/or C(17) and the corresponding solvent molecules, as well as hydrogen bonds between different ethinyl estradiol molecules, namely between the –OH groups attached to the C(3) and those attached to C(17). Ethinyl estradiol forms pseudo-polymorphs mainly with solvents having H-bond accepting or both accepting and donating propensity and shows a remarkable flexibility in forming distinctly different hydrogen-bonding patterns, resulting in a diverse set of solvate structures. A high degree of similarity can be observed between the crystal packing of the nitromethane and dioxane solvates, forming isostructural sheets of ethinyl estradiol molecules arranged parallel in a head-to-tail fashion.

DSC and hot-stage X-ray powder diffraction measurements showed that upon heating all ethinyl estradiol pseudo-polymorphs convert to the anhydrate form before melting.

Appendix 4.1. Hydrogen bond distances and angles for all investigated solvates

Donor-H...Acceptor	D-H (Å)	H...A (Å)	D...A (Å)	D-H...A (°)
Hemihydrate 				
O(3) – H(3)...O(§)	0.80(3)	2.01(3)	2.804(3)	170
O(17) – H(17)...O(3)	0.79(3)	2.09(3)	2.864(3)	172
O(§) – H(§)...O(17)	0.82(3)	2.01(3)	2.805(3)	166
Methanol 				
O(3) – H(3)...O(§)	0.85(3)	1.80(3)	2.642(2)	171(3)
O(17) – H(17)...O(3)	0.86(3)	1.88(3)	2.7271(19)	169(2)
O(§) – H(§)...O(17)	0.82(3)	1.90(3)	2.725(2)	175(3)
Acetonitrile 				
O(3) – H(3)...O(17)	0.88(3)	1.90(3)	2.765(2)	167(2)
O(17) – H(17)...O(33)	0.85(3)	2.05(3)	2.8691(2)	160(3)
O(33) – H(33)...O(3)	0.84(3)	2.04(3)	2.868(2)	167(2)
O(47) – H(47)...N(§)	0.82(4)	2.12(4)	2.938(4)	171(3)
C(§) – H(§)...O(47)	0.97(4)	2.43(3)	3.375(4)	165(2)
Dioxane 				
O(3) – H(3)...O(33)	0.79(4)	1.93(4)	2.716(3)	179(5)
O(17) – H(17)...O(3)	0.93(3)	1.87(3)	2.795(3)	170(3)
O(33) – H(33)...O(17)	0.77(3)	1.94(3)	2.702(3)	175(3)
O(47) – H(47)...O(§)	0.83(4)	1.98(4)	2.808(3)	177(3)
C(48)–H(48)...O(47)	0.88(4)	2.44(3)	2.752(4)	101(3)
C(51)–H(51)...O(§)	0.87(3)	2.32(3)	3.161(4)	162(2)
Nitromethane 				
O(3) – H(3)...O(33)	0.85(5)	1.93(5)	2.761(4)	167(4)
O(17) – H(17)...O(3)	0.86(5)	2.02(4)	2.836(4)	158(4)

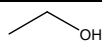
O(33) – H (33)...O(17)	0.81(5)	1.92(5)	2.712(4)	168(5)
O(47) – H(47)...O(§)	0.99(6)	2.03(6)	2.998(4)	165(4)
C(§) – H(§)...O(47)	0.93(5)	2.53(5)	3.362(5)	150(4)

***N,N*-Dimethylformamide (DMF)**



O(3) – H (3)...O(§)	0.83	2.14	2.720(8)	126
O(17) – H(17)...O(§)	0.83	1.86	2.673(8)	165
O(33) – H (33)...O(§)	0.83	1.97	2.718(9)	150
O(47) – H(47)...O(§)	0.83	1.88	2.702(8)	171
C(2)–H (2)...O(§)	0.94	2.55	3.218(9)	129
C(32)–H (32)...O(§)	0.94	2.54	3.231(8)	130
C(§)–H (§)...O(3)	0.97	2.53	3.347(9)	142
C(§)–H (§)...O(§)	0.97	2.33	2.737(13)	105
C(18)–H (18)...O(17)	0.97	2.26	2.812(7)	115

Ethanol



O(3) – H(3)...O(§)	0.83	1.84	2.674(4)	177
O(17) – H (17)...O(§)	0.83	1.81	2.613(9)	163
O(33) – H (33)...O(17)	0.83	1.94	2.745(6)	164
O(47) – H(47)...O(3)	0.83	1.91	2.736(3)	174
O(63) – H (63)...O(47)	0.83	1.87	2.685(3)	165
O(77) – H (77)...O(§)	0.83	2.47	2.795(8)	105
O(§) – H(§)...O(63)	0.83	1.99	2.813(4)	174
C(81)–H (81)...O(33)	0.94	2.32	3.260(7)	179
C(§)–H (§)...O(33)	0.98	2.31	3.162(10)	144
C(§)–H (§)...O(77)	0.98	2.58	3.156(12)	118

§ - from different solvent molecules

Chapter 5

STRUCTURAL INVESTIGATIONS OF HYDRATE, ANHYDRATE, FREE BASE AND HYDROCHLORIDE FORMS OF MORPHINE AND NALOXONE

This chapter is based on:

C. Guguta
Th. P. J. Peters
R. de Gelder

2008

Crystal Growth & Design

8 (11), 4150 - 4158

ACKNOWLEDGMENT

This research was supported by the Technology Foundation STW, applied science division of NWO and the technology program of the Ministry of Economic Affairs. Dr. Anja Stiewe is gratefully acknowledged for supplying naloxone hydrochloride and fruitful discussions. Dr. Ernst van Eck is acknowledged for performing the solid state NMR measurements.

For the structurally related agonist morphine and the antagonist naloxone, hydrates and anhydrides exist for both the free bases and the hydrochloride salts. We present five new crystal structures, determined from X-ray powder diffraction data, for morphine and naloxone: four anhydrides and one hydrate. These new structures, together with already known structures from the Cambridge Structural Database, enabled us to investigate the influence of the subtle molecular differences between these agonist and antagonist, the role of water and the effect of the chloride counter-ion on structural properties of morphine and naloxone in the solid state. These results suggest that the introduction of water or counter-ions like chlorine generate structures with higher dimensional hydrogen bonding networks than the corresponding anhydrate or free base structures.

5.1 INTRODUCTION

An agonist is a compound which binds to a specific receptor and triggers a response in the cell. An antagonist can compete with an agonist for a receptor site and can prevent an agonist from acting (Karle, 1974). Narcotic antagonists are 10 to 1000 times more potent enhancing receptor binding than their corresponding agonists (Pert *et al.*, 1973). The agonist *morphine*, (5 α ,6 α)-7,8-didehydro-4,5-epoxy-17-methylmorphinan-3,6-diol, a prototypical opioid, is a highly potent opiate analgesic drug and is one of the main active agents in opium. The chemical structure of morphine was established by Gates & Tschudi in 1952, who succeeded in synthesizing the complete molecule. In 1925, Gulland & Robinson had already proposed exactly the same structure but

were unable to confirm it. The molecular structure of morphine was finally determined and verified from two projections of hydroiodide di-hydrate by MacKay & Hodgkin in 1955 and therefore the chemical structure was verified. In Fig. 1 the molecular structure of morphine is presented. It has been observed that when a suitable substituent is introduced on the nitrogen atom of a nor-morphine derivative, the resulting compounds are not addicting and, are actually narcotic antagonists. The antagonist *naloxone* (NLX), (5 α)-17-(allyl)-4,5-epoxy-3,14-dihydroxymorphinan-6-one, is a drug used to counter the effects of opioid overdose, for example morphine or heroin. Although differing only slightly from narcotics, the antagonist naloxone can completely block the analgesic and euphoric effects of agonists, and currently it is used as emergency treatment for overdose of narcotics and/or alcohol.

Naloxone (NLX) is marketed as naloxone hydrochloride due to its solubility in water. The molecular structure of the naloxone is presented in Fig. 5.1.

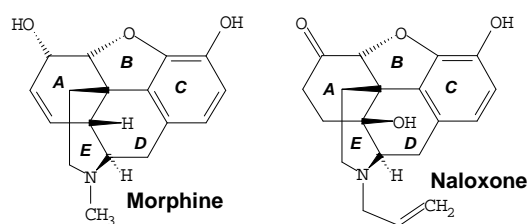


Figure 5.1. The molecular structures of morphine and naloxone

For the structurally related agonist morphine and the antagonist naloxone, hydrates and anhydrides exist for both the free bases and the hydrochloride salts. The hydrochloride tri-hydrate form of morphine (refcode MORPHC) was determined by Gylbert in 1973 and crystallizes in the orthorhombic space group $P2_12_12_1$ with cell parameters: $a=6.941 \text{ \AA}$, $b=13.019 \text{ \AA}$, $c=20.750 \text{ \AA}$,

$V=1875.071 \text{ \AA}^3$. The crystal structure of the hydrochloride anhydrate form is not described in literature. The crystal structure of the morphine monohydrate (refcode MORPHM01) was determined in 1976 by Bye. It crystallizes in the orthorhombic space group $P2_12_12_1$ with cell parameters: $a=7.438(1) \text{ \AA}$, $b=13.751(3) \text{ \AA}$, $c=14.901(3) \text{ \AA}$, $V=1524.073 \text{ \AA}^3$. The morphine anhydrate (refcode MORPIN) was determined for the first time by Duchamp, but 3D coordinates are not available in the CSD (Duchamp *et al.*, 1977). The authors reported that the morphine anhydrate crystallizes in the orthorhombic space group $P2_12_12_1$ with cell parameters: $a=7.408 \text{ \AA}$, $b=13.713 \text{ \AA}$, $c=14.781 \text{ \AA}$, $V=1501.541 \text{ \AA}^3$. Making a comparison between the unit cell parameters of the monohydrate and anhydrate forms of morphine, the values reported for the unit cell parameters are doubtful. The unit cell parameters of the morphine anhydrate are very close to the cell parameters of the morphine monohydrate. Therefore, it is unlikely that the reported unit cell is related to the crystal structure of the morphine anhydrate. Crystallographic data of the morphine hydroiodide di-hydrate (refcode MORPHI) and the morphine hydrobromide di-hydrate (refcode ZZZRHC) is also available from the CSD indicating that the two forms are isostructurally related, crystallizing in the orthorhombic system with space group $P2_12_12_1$ (Mackay *et al.*, 1955). The hydrobromide and hydroiodide forms of morphine are not subjected to the present study due to their toxic properties and are therefore less important for the pharmaceutical industry.

Naloxone hydrochloride exists in different crystal forms, but just one of them is described in literature and available from the CSD database: the di-hydrate form (refcode NALOXC02). The cell parameters were described for the first

time in 1974 (Karle *et al.*, 1974), but the crystal structure was determined later on, in 1975 and redetermined in 1987. It crystallizes in the orthorhombic space group $P2_12_12_1$ with cell parameters: $a=7.769(3)$ Å, $b=13.234(5)$ Å, $c=18.492(7)$ Å, $V=1901.254$ Å³ (Klein *et al.*, 1987). The monohydrate form of the naloxone crystallizes in the orthorhombic system with space group $P2_12_12_1$ and cell parameters: $a=13.903(5)$ Å, $b=7.257(7)$ Å, $c=16.641(1)$ Å, $V=1678.99$ Å³ (Guguta *et al.*, 2008).

Comparing the molecular conformation of the agonist (*i.e.* morphine) and the antagonist (*i.e.* naloxone) opioids the well-known T-shape is observed. The five-ring system forms two planes. The stock of the T-shape is formed by the B, C and D rings and the arms of the T by the A and E rings (Fig. 5.2). Furthermore, there are no remarkable differences in the bond lengths and angles. The B and D rings take an envelope conformation, while the E ring has a chair conformation and C is a flat ring. The A ring has a twisted boat conformation in the already known morphine forms while, within the known naloxone forms, the A ring has a twisted chair conformation.

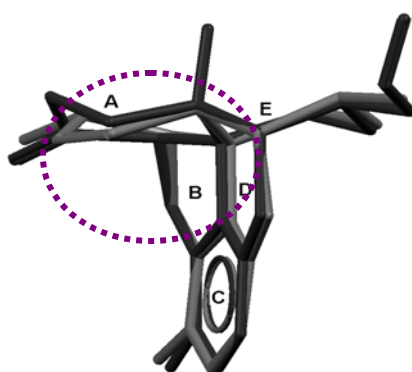


Figure 5.2. The T-shape five-ring system depicting with gray the molecule of morphine and with black the molecule of naloxone (the dashed circle points to the different A ring conformation)

The overall molecular conformation of the agonist and antagonist opioids shows minor differences although chemically they are quite different. The effects of the longer substituent on the nitrogen atom or the existence of a counter ion is not affecting in a dramatic way the molecular structure of the two opioids.

Comparing the existent structural data in the CSD shows that all morphine and naloxone forms crystallize in the orthorhombic space group $P2_12_12_1$. From a crystallographic point of view it is interesting to determine how substituents, water and counter ion are influencing the chemical crystallography of the agonist and antagonist under subject. In this study the crystal structures of the naloxone monohydrate and four new anhydrate forms of morphine, naloxone and their hydrochloride salts are determined from X-ray powder diffraction data. Knowledge of the structural crystallographic data enables us to investigate the influence of the subtle molecular differences between these agonist and antagonist, the role of water and the effect of the chloride counter-ion on structural properties of morphine and naloxone in the solid state.

5.2 EXPERIMENTAL

5.2.1 Material

Morphine hydrochloride and morphine were obtained from Campro Scientific commercial supply. Naloxone hydrochloride was obtained from Diosynth commercial supply. The preparation procedures of the individual hydrate/anhydrate forms for morphine hydrochloride, morphine, naloxone hydrochloride and naloxone, are described below.

5.2.2 Preparation of morphine hydrochloride anhydrate

Morphine hydrochloride anhydrate was obtained by dehydrating the tri-hydrate form at 140°C, under vacuum (10^{-2} mbar). Before and after the experiment, argon gas was flushed into the reaction vessel. The sample was stored in a glove box under nitrogen atmosphere.

5.2.3 Preparation of morphine anhydrate

Morphine anhydrate was obtained by dehydrating the monohydrate at 150°C, under vacuum (10^{-2} mbar). Before and after the experiment, argon gas was flushed into the reaction vessel. The sample was stored in a glove box under nitrogen atmosphere.

5.2.4 Preparation of naloxone hydrochloride di-hydrate

The di-hydrate form of naloxone hydrochloride was prepared from a diluted aqueous HCl solution of starting material at room temperature (1g NLX : 100mL H₂O). After the complete evaporation of the solvent, needle shaped crystals were obtained.

5.2.5 Preparation of naloxone hydrochloride anhydrate

Naloxone hydrochloride anhydrate was obtained by dehydrating the di-hydrate form at 140°C, under vacuum (10^{-2} mbar) and in presence of P₂O₅ drying agent. Before and after the experiment, argon gas was flushed into the reaction vessel. The sample was stored in a glove box under nitrogen atmosphere. Attempts to grow crystals suitable for single-crystal diffraction failed.

5.2.6 Preparation of naloxone monohydrate

A solution of sodium bicarbonate (0.25g NaHCO₃ :100 mL H₂O) was added to an aqueous solution of naloxone hydrochloride (1g naloxone hydrochloride: 100 mL H₂O). After complete addition, the reaction mixture was stirred for one hour at room temperature to stimulate CO₂ release. The formed naloxone free base was extracted from the NaCl solution with chloroform. After the total removal of the chloroform the monohydrate form of naloxone was obtained.

5.2.7 Preparation of naloxone anhydrate

The previously obtained white powder of naloxone monohydrate was heated at 140°C, under vacuum (10⁻²mbar). Before and after the experiment, argon gas was flushed into the reaction vessel. White needle shaped crystals of naloxone anhydrate sublimated on the reaction vessel. The sample was stored in a glove box under nitrogen atmosphere.

5.2.8 X-ray Powder Diffraction (XRPD)

X-ray powder diffraction measurements for crystal structure determination were performed using a Bruker AXS D8 Advance X-ray Diffractometer. The D8 was equipped with a Johansson type monochromator with a focusing curved Ge 111 crystal. A VÅNTEC-1 detector was used with an effective angular region of 2°. The data was collected in transmission capillary geometry using monochromatic Cu K_{α1} radiation. The anhydrate samples were lightly ground, using an agate mortar with pestle and mounted in 0.5 mm glass capillary tubes. The capillary tubes were filled with the materials and sealed in a glove box under nitrogen atmosphere. The capillary tubes were spun at 15 rpm during data

collection in order to reduce preferred orientation effects (Howard *et al.*, 2000) and to minimize instrumental and sample packing aberrations (Dollase *et al.*, 1986).

The most important instrumental and data collection parameters are presented in Table 5.1.

Table 5.1. Instrumental and data collection parameters

<i>Typical instrument settings</i>	
System	Bruker AXS D8 Advance $\theta/2\theta$
Generator	40 kV, 40 mA
Measuring circle (mm)	435
Radiation (Å)	Cu K $_{\alpha 1}$, $\lambda=1.54056\text{Å}$
Monochromator	Primary, focusing curved Ge 111
Geometry	Transmission capillary configuration
Sample holder	0.5 mm glass capillary tube
Detector	VÅNTEC-1
<i>Typical measuring conditions</i>	
Range ($^{\circ} 2\theta$)	5-50 (60)
Step size ($^{\circ} 2\theta$)	0.0084696
Step time (s)	50
Total data collection time (h)	ca 75 (92)
Spinning (rpm)	15

5.2.9 Data analysis for crystal structure determination

All diffraction patterns (except the one for naloxone monohydrate) were indexed using DICVOL91 (Boultif & Louër, 1991) to obtain lattice parameters that were subsequently refined in a Pawley fit (Pawley, 1981). Z-matrices describing the molecular topology of the fragments in the compound were

generated automatically by DASH (David *et al.*, 2004) from the structural data of the investigated compounds available in the CSD and twenty runs with 10^7 SA (simulated annealing) moves per run were performed for structure solution. To the best solution obtain after SA process, a final full Rietveld refinement was performed using Topas software (Cheary *et al.*, 1992).

The crystal structure of naloxone monohydrate was determined using the FIDDLE program (2008). A final full Rietveld refinement was performed on the naloxone monohydrate structure using the Topas software.

5.2.10 Solid-State NMR Spectroscopy (SSNMR)

100.6 MHz solid-state ^{13}C cross-polarization/magic angle spinning (CP/MAS) spectra were obtained using a Bruker AXS 400MHz spectrometer. The samples were packed into a 4 mm rotor and spun with a rate of 12 kHz. The ^{13}C spectra were collected using decay with 90° excitation pulse, 6.5 ms relaxation delay and 2.5ms cross polarization time.

5.3 RESULTS

5.3.1 Crystal structure determination of the four anhydrate forms

Indexing, Pawley refinement and simulated annealing process

The 2θ ranges used for indexing, Pawley refinement and simulated annealing were from $5-45^\circ$ for the anhydrate forms of morphine hydrochloride and naloxone hydrochloride with a spatial resolution of 2.0129 \AA , and from $5-60^\circ$ for the anhydrate forms of morphine and naloxone, with a spatial resolution of 1.5406 \AA .

Twenty reflections with low and high intensity were introduced into DICVOL91 and an orthorhombic cell was found for the anhydrates of morphine hydrochloride, morphine and naloxone hydrochloride. Naloxone anhydrate crystallizes in the monoclinic system. Space group determination in DASH resulted in $P2_12_12_1$ for morphine hydrochloride, morphine and naloxone hydrochloride, and $P2_1$ for the naloxone anhydrate. The volume and space group $P2_12_12_1$ respectively $P2_1$ correspond to $Z' = 1$ (molecules per asymmetric unit). ^{13}C solid-state NMR confirmed the number of molecules per asymmetric unit to be equal to one.

The lattice parameters obtained after indexing were subsequently refined along with background, zero point, peak shape parameters and reflection intensities using Pawley refinement. The characteristic parameters of the orthorhombic cells and the monoclinic one obtained after Pawley refinements are presented in Table 5.2.

The peak shape is implemented in DASH as a convolution of Gaussian, Lorentzian and axial divergence terms (asymmetry). Actually, the X-ray line shape is a full Voigt function, which uses two parameters σ_1 and σ_2 to describe the angle-dependent Gaussian component:

$$\sigma^2 = \sigma_1^2 \sec^2 \theta + \sigma_2^2 \tan^2 \theta$$

and two parameters γ_1 and γ_2 to describe the angle-dependent Lorentzian component:

$$\gamma = \gamma_1 \sec \theta + \gamma_2 \tan \theta$$

Table 5.2. Lattice parameters and Pawley refinement results

<i>Lattice parameters</i>	Morphine hydrochloride anhydrate	Morphine anhydrate	Naloxone hydrochloride anhydrate	Naloxone anhydrate
<i>System</i>	Orthorhombic	Orthorhombic	Orthorhombic	Monoclinic
<i>Space group</i>	$P2_12_12_1$	$P2_12_12_1$	$P2_12_12_1$	$P2_1$
<i>a</i> (Å)	16.179	13.861	17.453	8.540
<i>b</i> (Å)	12.816	12.770	14.684	12.679
<i>c</i> (Å)	7.430	7.690	7.978	7.652
<i>β</i> (°)	-	-	-	97.081
<i>V</i> (Å ³)	1540.882	1362.059	2044.816	822.330
<i>Zero point correction</i>	0.084	0.032	0.057	0.030
<i>Pawley refinement results</i>				
<i>Number of reflections</i>	134	249	173	254
<i>Data points</i>	4738	6862	4612	6515
<i>Pawley χ^2</i>	9.306	7.056	22.460	4.880

The two other asymmetry parameters are fully defined by the peak fitting procedure and cannot be refined by Pawley fitting. The investigated samples gave sharp diffraction lines, for the first eight fitted peaks, with a mean FWHM = 0.178° for morphine hydrochloride anhydrate, 0.085° for morphine anhydrate, 0.092° for naloxone hydrochloride anhydrate and 0.076° for naloxone anhydrate, and a minimum value FWHM = 0.131° for morphine hydrochloride anhydrate, 0.072° for morphine anhydrate, 0.078° for naloxone hydrochloride anhydrate and 0.0704° for naloxone anhydrate.

The profile Pawley χ^2 is described in DASH as:

$$\chi^2 = \left\{ \sum_i^N w_i [y_i(\text{obs}) - y_i(\text{calc})]^2 \right\} / (N - P + C),$$

where $y_i(\text{obs})$ is the observed intensity at the i^{th} step in the powder diffraction pattern; $y_i(\text{calc})$ is the associated calculated intensity; $w_i = 1/\sigma_i^2$, where σ_i is the standard deviation of the observed intensity at that point. The summation is performed over all N data points, where N is the number of data points, P the number of parameters and C the number of parameter constraints.

The molecular conformations of the Z-matrices describing the molecular geometry of the investigated forms are shown in Fig. 5.3.

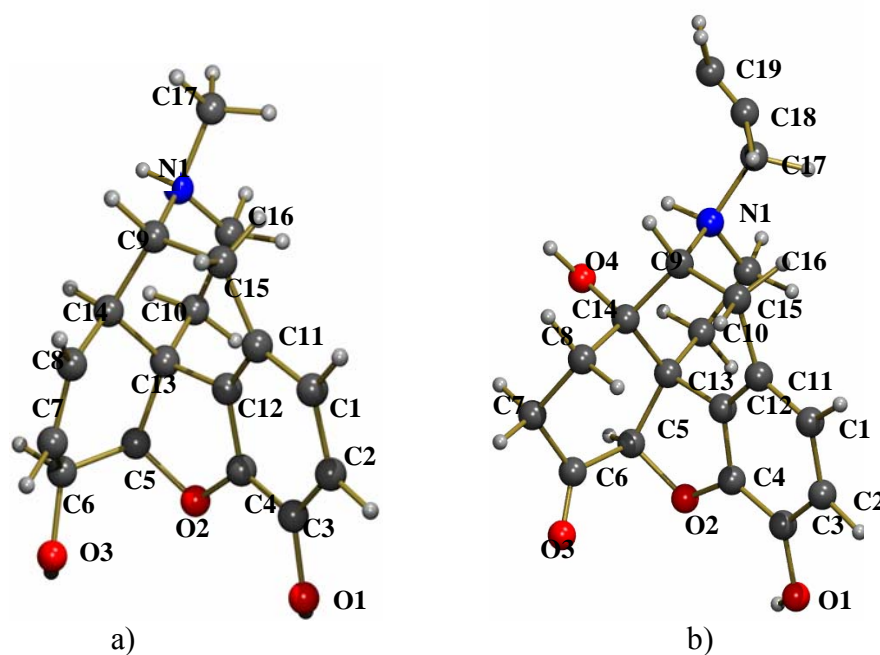


Figure 5.3. The molecular conformations used for the Z-matrices of: a) morphine; b) naloxone

Morphine does not have free rotatable torsion angles. The 20 solutions obtained after the simulated annealing processes showed χ^2 profile values of 18.66 for morphine hydrochloride anhydrate and 19.17 for morphine anhydrate.

Naloxone has two rotatable torsion angles: C18:C17:N1:C9 and C19:C18:C17:N1, optimized during the simulated annealing (SA) process. The simulated annealing process ended up with 20 solutions having a χ^2 profile values of 40.87 for naloxone hydrochloride anhydrate and 28.62 for naloxone anhydrate.

The fit of the observed and calculated diffraction data for the best solutions found after simulated annealing are shown in Fig. 5.4 for all four investigated forms.

5.3.2 Rietveld refinement

After structure solution, full Rietveld refinements were applied to the best solutions returned by the SA processes (Young, 1996). To the crystal structure of naloxone monohydrate determined with the FIDDLE software, a full Rietveld refinement was also applied. Almost all coordinates of the non-hydrogen atoms were freely refined, but soft restraints on bond lengths and angles were introduced in order to reduce the number of free parameters. The full Rietveld refinements proceeded smoothly to reach a minimum characterized by an excellent fit to the diffraction profiles presented in Fig. 5.5 for all five investigated forms. The crystallographic data of the refined crystal structures is presented in Table 5.3.

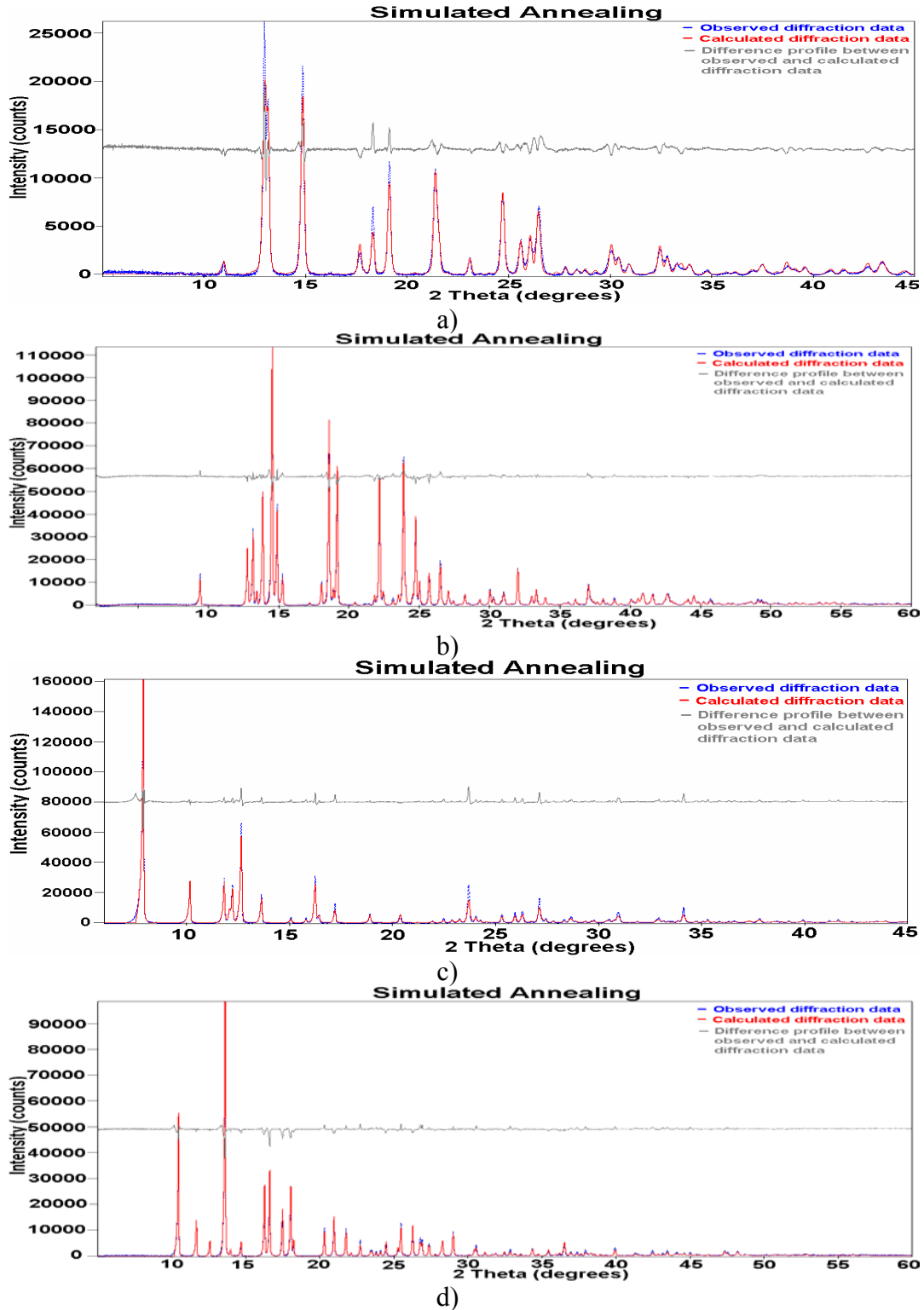


Figure 5.4. The fit to the diffraction data returned by the SA processes for the anhydrate forms of: a) morphine hydrochloride anhydrate; b) morphine anhydrate; c) naloxone hydrochloride anhydrate; d) naloxone anhydrate

Table 5.3. Crystallographic data of the refined forms after full Rietveld refinement

<i>Cell parameters</i>	Morphine hydrochloride anhydrate	Morphine anhydrate	Naloxone hydrochloride anhydrate	Naloxone monohydrate	Naloxone anhydrate
<i>System</i>	Orthorhombic	Orthorhombic	Orthorhombic	Orthorhombic	Monoclinic
<i>Space group</i>	$P2_12_12_1$	$P2_12_12_1$	$P2_12_12_1$	$P2_12_12_1$	$P2_1$
<i>a</i> (Å)	16.079(4)	13.861(7)	17.452(4)	13.903(5)	8.539(2)
<i>b</i> (Å)	12.874(6)	12.777(1)	14.681 (4)	7.257(7)	12.678 (4)
<i>c</i> (Å)	7.494(6)	7.690(4)	7.978 (2)	16.641(1)	7.652(2)
β (°)	-	-	-	-	97.078
<i>V</i> (Å ³)	1551.50	1362.06	2044.10	1678.99	822.16
<i>Final profiles</i>					
<i>R_{wp}</i>	4.161	4.157	2.650	2.901	5.212
<i>R_p</i>	3.034	3.016	1.850	2.211	3.492
<i>GOF</i>	2.373	3.643	2.600	1.527	3.344

5.4 DISCUSSION

Many pharmaceutical compounds are available on the market in crystalline form mainly due to reasons of stability during the time between the manufacture of the active ingredient and used by the patient. Most of the crystalline drugs are able to form solvates or hydrates. Hydrates are solid adducts containing the parent compound (*e.g.*, the anhydrate of a drug) and water. Due to its small molecular volume, high ability to form H-bonds and non-toxic properties, water is an ideal solvent for linking drug molecules into stable crystalline forms. The environment of the water molecules may exhibit various defined packing patterns, which will reflect in the drug behavior.

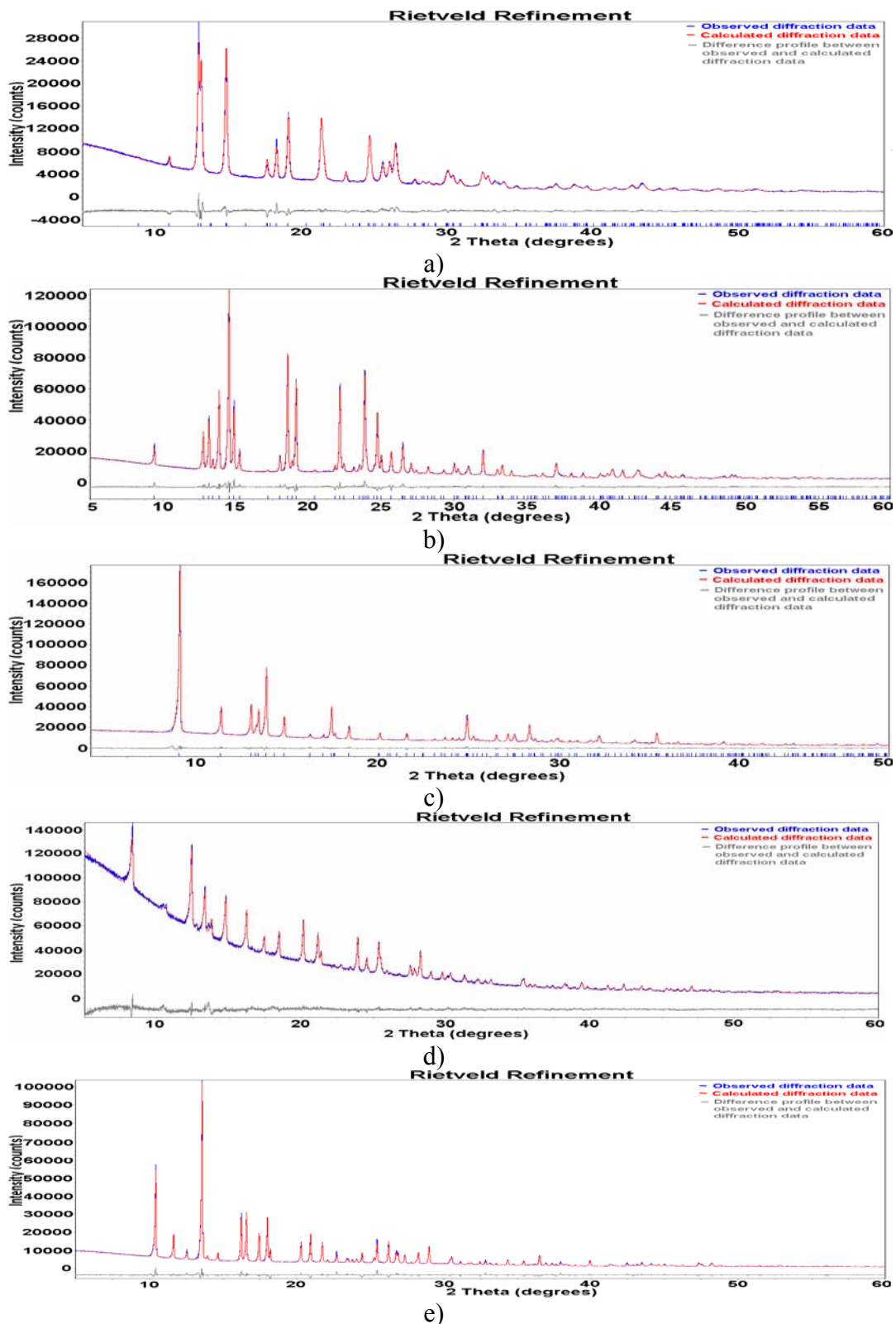


Figure 5.5. The fit after the final Rietveld refinement for: a) morphine hydrochloride anhydrate; b) morphine anhydrate; c) naloxone hydrochloride anhydrate; d) naloxone monohydrate; e) naloxone anhydrate

The presence of water molecules influences the intermolecular interactions (affecting the internal energy and enthalpy) and the crystalline disorder (entropy), hence influences the free energy, the thermodynamic activity, solubility, dissolution rate, stability, and bioavailability (Khankari *et al.*, 1995). Therefore we will further discuss various structural features and in particular typical H-bonds formed by morphine, naloxone and their hydrochloride forms in order to evaluate the influence of the subtle molecular differences between these two agonist and antagonist opioids, the role of water and the effect of the chloride counter-ion on structural properties of morphine and naloxone in the solid state.

In morphine hydrochloride tri-hydrate, the morphine molecules are packed in a *zigzag* head-to-tail fashion. H-bonds are formed between the –OH group attached to C(6) and the N atom from another morphine molecule. With the aid of the water molecules, the *zigzag* layers in morphine hydrochloride tri-hydrate are assembled in a three-dimensional network. The three-dimensional network is formed by H-bonds between the –OH groups attached to C(3), respectively C(6) and water molecules. The Cl⁻ is involved in H-bonding with the water molecules as well. H-bonds are also observed between different water molecules. The anhydrate form of morphine hydrochloride has the *zigzag* packing pattern like in the tri-hydrate, but this time the morphine molecules are bonded in a head-to-Cl⁻-to-tail fashion forming a one-dimensional network between the N atom, the Cl⁻ and –OH groups attached to C(3) and C(6). The packing of the morphine molecules in morphine hydrochloride tri-hydrate and hydrochloride anhydrate is presented in Fig. 5.6.

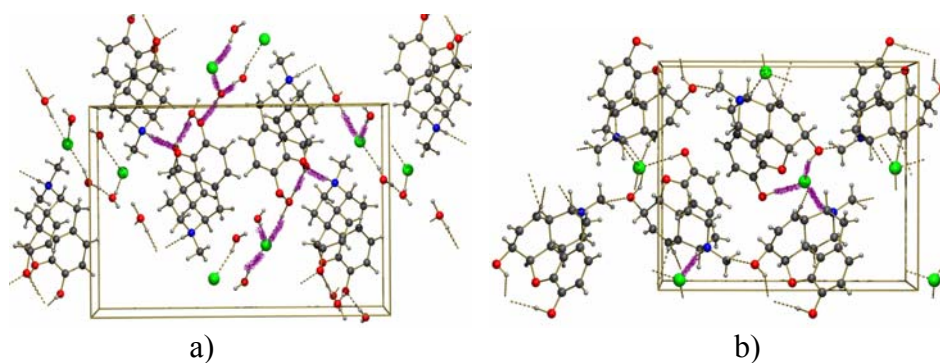


Figure 5.6. The packing of the morphine: a) hydrochloride tri-hydrate, b) hydrochloride anhydrate (characteristic H-bonds are depicted in gray)

The molecules of morphine in morphine monohydrate are H-bonded in a head-to-tail fashion forming layers assembled together by the water molecules in to a three-dimensional network. The H-bonds are formed between the $-OH$ group attached to C(3) and the N atom. The water molecules are also involved in H-bonding on one hand with the $-OH$ groups attached to C(3) and C(6) and on the other hand with other water molecules. In the absence of water molecules the morphine molecules are packed in a head-to-head fashion, forming a one-dimensional network. The $-OH$ group attached to C(3) of a morphine molecule is then involved in H-bonding with the $-OH$ group attached to C(6) of another morphine molecule. The packing of the morphine molecules in morphine monohydrate and anhydrate is presented in Fig. 5.7.

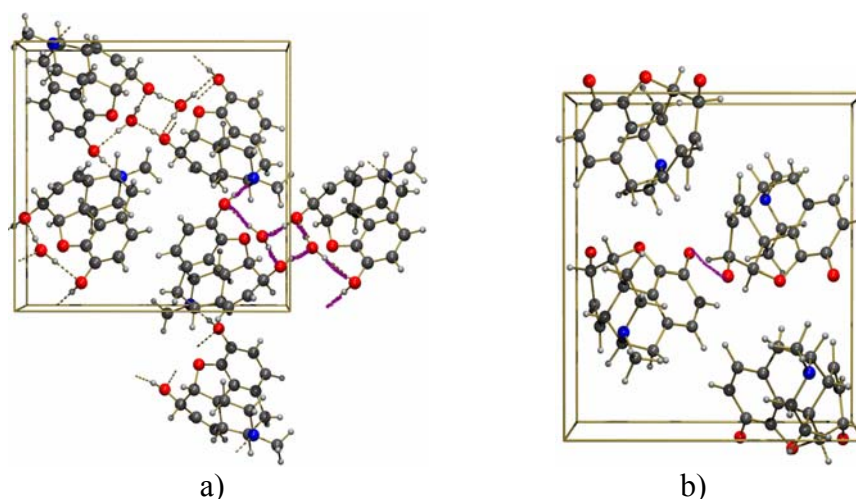


Figure 5.7. The packing of the morphine: a) monohydrate, b) anhydrate (characteristic H-bonds are depicted in gray)

The naloxone molecules in naloxone hydrochloride di-hydrate are also packed in a three-dimensional network with the aid of water molecules. H-bonds are formed between the –OH group attached to C(3), respectively C(14) and water molecules. The carboxyl group and the Cl⁻ are also involved in H-bonding with the water molecules. As expected, H-bonds between different water molecules are also observed. Obviously, the water molecules play a stabilizing role in the network formation of naloxone hydrochloride di-hydrate. The naloxone molecules in naloxone hydrochloride anhydrate are also assembled in a three-dimensional network, but this time with the aid of the Cl⁻ anion. Cl⁻ forms H-bonds with the N atom and with the (-OH) groups attached to C(3), and C(14). The packing of the naloxone molecules in naloxone hydrochloride di-hydrate and hydrochloride anhydrate is presented in Fig. 5.8.

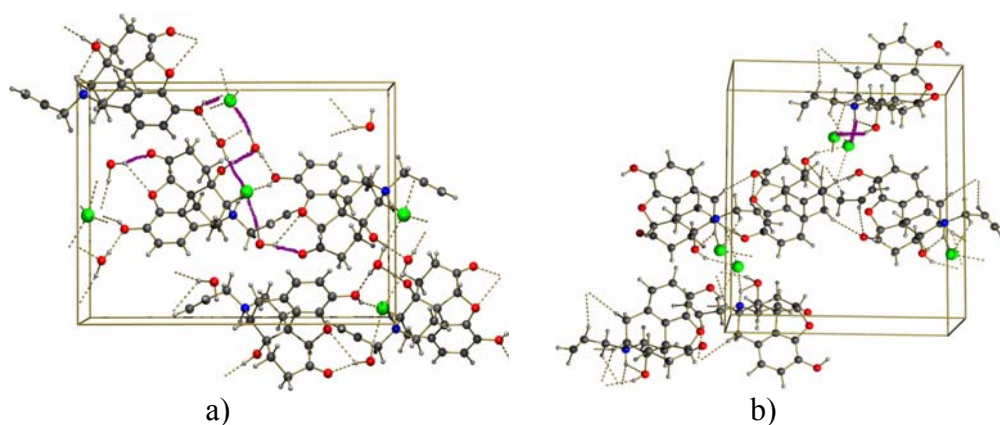


Figure 5.8. The packing of the naloxone: a) hydrochloride di-hydrate, b) hydrochloride anhydrate (characteristic H-bonds are depicted in gray)

Naloxone monohydrate and anhydrate form one-dimensional chains of naloxone molecules H-bonded in a *zigzag* fashion. The $-OH$ groups attached to C(3), respectively C(14) are involved in H-bonding in both forms. Thus, in the monohydrate form the H-bonds are formed between the $-OH$ groups of the naloxone molecules and the water molecules. In the anhydrate, intermolecular H-bonds between the $-OH$ groups from different naloxone molecules are observed. The allylic tail of the naloxone molecule is also involved in H-bonding. The $-OH$ group attached to C(14) is forming H-bonds with the allylic tail. The packing of the naloxone molecules in naloxone monohydrate and anhydrate is presented in Fig. 5.9.

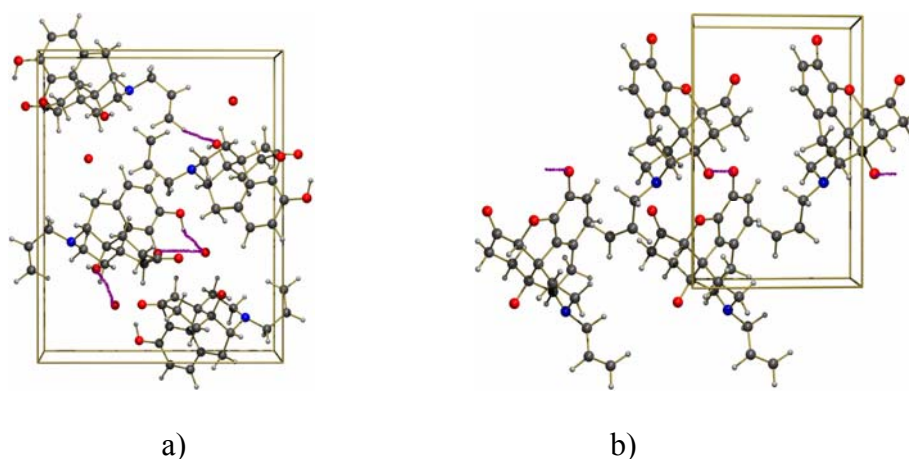


Figure 5.9. The packing of the naloxone: a) monohydrate, b) anhydrate (characteristic H-bonds are depicted in gray)

The presence of water molecules leads to the formation of three-dimensional networks in the hydrated forms of the agonists' morphine, morphine hydrochloride and the antagonist naloxone hydrochloride. On the other hand, the anhydrate forms of morphine, morphine hydrochloride and naloxone are able to form only one-dimensional networks due to the absence of water molecules and their involvement in H-bonding.

Dehydration of the hydrate forms of both the salt and the free base of morphine, induces a change in the H-bond network dimensionality from *3D* to *1D*. For naloxone, the dehydration takes place without any change in the H-bond network dimensionality.

The salt forms of naloxone show a higher dimensionality than the free base forms due to the involvement of Cl^- in additional H-bonding. Naloxone hydrochloride anhydrate forms a three-dimensional network due to the favorable position of the Cl^- in the crystal structure. Morphine hydrochloride

anhydrate is only able to form a one-dimensional network due to a different position of the Cl^- in the crystal structure.

All the hydrate forms of the investigated opioids form *3D* H-bond networks, except naloxone monohydrate that forms a *1D* H-bond network. Naloxone monohydrate dehydrates to form the anhydrate with breaking of the orthorhombic symmetry, ending up in a monoclinic one with space group $P2_1$. Apparently, in this case, the water molecules play a role in stabilizing the orthorhombic symmetry. By dehydrating the monohydrate water molecules disappear from the net, however, without disturbing the one-dimensional network of naloxone.

In the anhydrate forms of the investigated opioids, the counter ion Cl^- usually takes over the role of the water molecules. Cl^- can form H-bonds with the N atom as well, but when water molecules are present in the crystal structure, Cl^- prefers the water molecules instead of the N atom. When Cl^- and water molecules are not present (morphine anhydrate and naloxone anhydrate), intermolecular H-bonds are formed between the $-\text{OH}$ groups, taking over the role of the counter ion and/or water molecules. While in the monohydrate form of naloxone the allylic group is involved in H-bonding, in the anhydrate form the allylic group is no longer involved.

The characteristic structural features of the hydrate and anhydrate forms of naloxone, naloxone hydrochloride, morphine, and morphine hydrochloride are presented in Table 5.4.

Table 5.4. Characteristic structural data of the eight investigated forms

Opioids	H-bond network	Packing pattern of the molecules	Characteristic of H-bond
<i>Morphine hydrochloride tri-hydrate</i>	<i>3D</i>	head-to-tail	C(6)-OH...N C(3)-OH...O _(water) C(6)-OH...O _(water) OH _(water) ...Cl ⁻ OH _(water) ...O _(water)
<i>Morphine hydrochloride anhydrate</i>	<i>1D</i>	head-to-Cl ⁻ -to-tail	N-H... Cl ⁻ C(3)-OH...Cl ⁻ C(6)-OH...Cl ⁻
Morphine monohydrate	3D	head-to-tail	C(3)-OH...N C(3)-OH...O_(water) C(6)-OH...O_(water)
Morphine anhydrate	1D	head-to-head	C(3)-OH...O-C(6)
<i>Naloxone hydrochloride di-hydrate</i>	<i>3D</i>	head-to-tail	C(3)-OH...O _(water) C(14)-OH...O _(water) OH _(water) ...Cl ⁻ OH _(water) ... O-C(6)
<i>Naloxone hydrochloride anhydrate</i>	<i>3D</i>	head-to-tail	N-H... Cl ⁻ C(3)-OH...Cl ⁻ C(14)-OH...Cl ⁻
Naloxone monohydrate	1D	head-to-allyl	C(3)-OH...O(water) OH(water)... O-C(14) OH(water)...O(2) C(19)-H...O-C(14)
Naloxone anhydrate	1D	head-to-tail	C(3)-OH...O-C(14)

Besides having a different substituent on the N atom, the OH group attached to C(6) in morphine is substituted with a carboxyl group in naloxone. But on the other hand, in naloxone another OH group is attached to C(14). In the general H-bonding scheme of morphine, the two OH groups attached to C(3) and respectively to C(6) are always involved in H-bonding. For naloxone this also holds for the two OH groups attached to C(3) and C(14). The carboxyl group attached to C(6) is only involved in H-bonding with water molecules in naloxone hydrochloride di-hydrate. Although the OH groups are differently

positioned in morphine and naloxone, they are equally involved in the general H-bonding scheme.

Incorporation of water into the crystal lattice produces a new unit cell different from that of the anhydrate and, consequently, the physical properties and the behavior of the solvate may differ from those of the anhydrate (Evans et al., 2004). In all cases, the dehydration processes of morphine hydrochloride tri-hydrate, morphine monohydrate, naloxone hydrochloride di-hydrate and naloxone monohydrate to form the anhydrates induce only an anisotropic shrinkage of the unit cells.

5.5 CONCLUSIONS

The crystal structures of the anhydrate forms of morphine hydrochloride, morphine, naloxone hydrochloride and naloxone were successfully determined from X-ray powder diffraction data collected in transmission capillary geometry. The DASH software was used for structure determination and the Topas software for Rietveld refinement. The crystal structure of naloxone monohydrate was determined by the FIDDLE software and successfully refined by Topas software as well.

Comparison of the crystal structures of the hydrated and the anhydrate forms of morphine hydrochloride, morphine, naloxone hydrochloride and naloxone reveals similarities. The hydrate and anhydrate forms of morphine hydrochloride, morphine, naloxone hydrochloride and naloxone crystallize all, except one, in the orthorhombic space group $P2_12_12_1$. The dehydration processes of morphine hydrochloride tri-hydrate, morphine monohydrate,

naloxone hydrochloride di-hydrate and naloxone monohydrate induces only an anisotropic shrinkage of the unit cells of the hydrated forms.

The dehydration process of the hydrate forms of the investigated opioids takes place without any change in symmetry except for naloxone monohydrate which shows a lowering of the orthorhombic symmetry to the monoclinic one during dehydration. The H-bond dimensionality reduces to lower values for the anhydrate forms of the agonist opioid, while for the antagonist there is no change in dimensionality.

The counter ion Cl^- takes over the role of the water molecules in the anhydrates forming H-bonds with the N atom as well. When water molecules are present, Cl^- prefers the water molecules instead of the N atom. If water molecules and the counter ion are not present, intermolecular H-bonds are formed between different -OH groups. The allylic group of the naloxone molecule takes over the role of the counter ion Cl^- only in its absence. For the rest, the N atom can act as a donor as well as an acceptor.

For morphine and naloxone, the introduction of water or counter-ions like chlorine generates structures with higher dimensional hydrogen bonding networks than the corresponding anhydrate or free base structures.

Chapter 6

STRUCTURAL INSIGHT INTO THE DEHYDRATION AND HYDRATION BEHAVIOR OF NALTREXONE AND NALOXONE HYDROCHLORIDE. DEHYDRATION- INDUCED EXPANSION VS. CONTRACTION

This chapter is based on:

C. Guguta
E.R.H. van Eck
R. de Gelder

Submitted to

Crystal Growth & Design

2009

(accepted for publication)

ACKNOWLEDGMENT

This research was supported by the Technology Foundation STW, applied science division of NWO and the technology programme of the Ministry of Economic Affairs. Carmen Guguta would like to acknowledge Dr. Anja Stiewe for supplying naltrexone and naloxone hydrochloride salts and all her help during this research. We would also like to acknowledge the technical assistance of I. Eeuwijk, G.E. Janssen, J.W.G. Janssen, and J.W.M. van Os with the solid-state NMR measurements.

For the chemically and structurally related antagonists naltrexone and naloxone, hydrate and anhydrate forms exist for the hydrochloride salts, the generic forms that are on the market. The hydration/dehydration behavior of these salts was studied by applying hot-humidity stage X-ray powder diffraction, microscopy, differential scanning calorimetry, thermogravimetric analysis and solid-state NMR. The combination of these techniques shows consistent results and yields a detailed conversion scheme. A new crystal structure, determined from X-ray powder diffraction data, for naltrexone hydrochloride anhydrate is presented. The structure was solved by the DASH program and was refined with TOPAS. This new structure, together with the already known structures of naltrexone and naloxone hydrochloride, enabled us to investigate the influence of the subtle molecular differences between the two antagonists and the role of water on structural properties in the solid state. All known hydrate and anhydrate forms of naltrexone and naloxone hydrochloride crystallize in the orthorhombic space group $P2_12_12_1$, although the crystal packings show clear differences. Dehydration causes in both cases no breaking of the symmetry but the change in unit cell is for naltrexone profoundly different from naloxone. Dehydration of naltrexone hydrochloride tetra-hydrate takes place with shrinkage of the volume of the unit cell, while dehydration of naloxone hydrochloride di-hydrate results in an expansion of the unit cell. The H-bonding patterns corresponding to the two opioids seem to be footprints for the crystal structures and also for the hydration/dehydration behavior of the two antagonists. Despite naltrexone and naloxone hydrochloride are chemically and structurally related and show similarities in their biological behavior, the overall hydration and dehydration process is fundamentally different.

6.1 INTRODUCTION

An agonist is a compound which binds to a specific receptor and triggers a response in the cell. An antagonist can compete with an agonist for a receptor site and can prevent an agonist from acting (Karle, 1974). Narcotic antagonists are 10 to 1000 times more potent in enhancing receptor binding than their corresponding agonists (Pert *et al.*, 1973). The molecular structures of two antagonist opioids, naloxone and naltrexone, that are the subject of the present study, are presented in Fig. 6.1.

Naltrexone is an opioid receptor antagonist used primarily in the management of alcohol and/or opioid dependence. Synthesized in 1965 and tested during the 1970s and early 80s, naltrexone represents actually the pharmacotherapy for helping eliminate drug cravings and opiate-seeking behaviors, thus preventing opiate relapse (Ginzburg and Glass, 1984). Naltrexone is marketed in the generic form as its hydrochloride salt. The naltrexone hydrochloride tetra-hydrate form (CSD refcode PABCEA) crystallizes in the orthorhombic system with space group $P2_12_12_1$ and cell parameters: $a=7.768(11)$ Å, $b=15.926(6)$ Å, $c=18.099(5)$ Å, $V=2239.085$ Å³ (Le Dain *et al.*, 1992). The malonate form (CSD refcode JEXRAF) crystallizes also in the orthorhombic system with space group $P2_12_12_1$ and has cell parameters: $a=8.434(3)$ Å, $b=15.469(4)$ Å, $c=16.047(4)$ Å, $V=2093.581$ Å³ (Amato *et al.*, 1990).

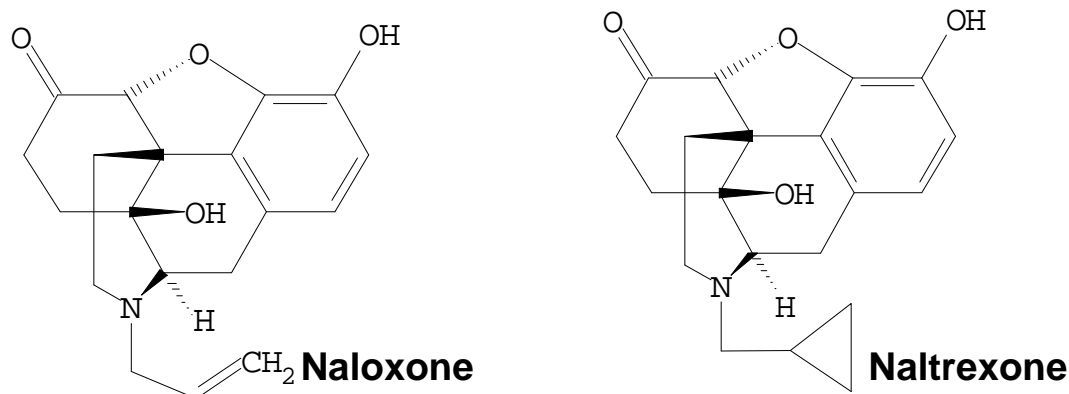


Figure 6.1. The molecular structure of the agonists: morphine, codeine and antagonist opioids: naloxone and naltrexone

Naloxone is a drug used to counter the effects of opioid overdose. Although differing only slightly from narcotics, the antagonist naloxone can completely block the analgesic and euphoric effects of agonists. The naloxone hydrochloride di-hydrate (CSD refcode NALOXC01) is the generic marketed form and crystallizes in the orthorhombic system with space group $P2_12_12_1$ and cell parameters: $a=7.833(3)$ Å, $b=13.185(5)$ Å, $c=18.569(5)$ Å, $V=1917.77$ Å³ (Sime et al., 1975), and was determined for the first time by Karle in 1974. The naloxone hydrochloride anhydrate crystallizes also in the orthorhombic system with space group $P2_12_12_1$ and cell parameters: $a=17.452(4)$ Å, $b=14.681(4)$ Å, $c=7.978(2)$ Å, $V=2044.10$ Å³ (Guguta et al., 2008). The monohydrate form of naloxone free base crystallizes in the orthorhombic system with space group $P2_12_12_1$ and cell parameters: $a=13.903(5)$ Å, $b=7.257(7)$ Å, $c=16.641(1)$ Å, $V=1678.99$ Å³ (Guguta et al., 2008). However, the anhydrate form of naloxone free base crystallizes in the monoclinic system with space group $P2_1$ and cell parameters: $a=8.539(2)$ Å, $b=12.678(4)$ Å, $c=7.652(2)$ Å, $\beta=97.078^\circ$, $V=822.16$ Å³ (Guguta et al., 2008).

The well-known T-shape of opioid compounds is also observed for naltrexone and naloxone (Fig. 6.2). The five-ring system forms two planes. The stock of the T-shape is formed by the B, C and D rings and the arms of the T by the A and E rings. There are no significant differences in bond lengths and angles. The B and D rings take an envelope conformation, while the E ring has a chair conformation and the C ring is flat. The A ring has a twisted chair conformation in the known forms of naloxone and naltrexone. The different substituent on the nitrogen atom or the existence of a counter ion is hardly affecting the molecular structure of the opioids.

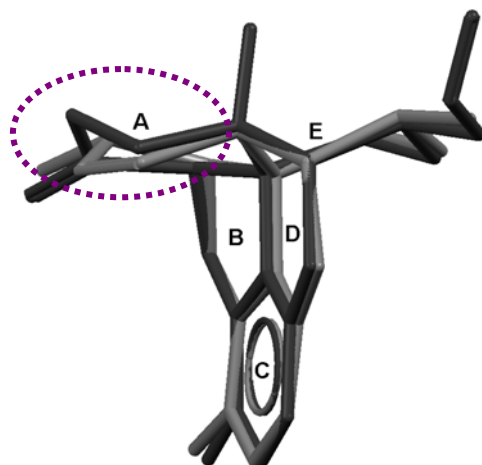


Figure 6.2. The T-shape five-ring system, depicting with gray the molecule of naltrexone and with black for the molecule of naloxone (the dashed circle points to the different A ring conformation)

In a previous paper a comparison of the crystal structures of the hydrate and anhydrate forms of the agonist morphine and antagonist naloxone hydrochloride, and naloxone hydrochloride revealed similarities. Although they act completely different in the human body, the two agonist and antagonist opioids showed to be crystallographically related (Guguta *et al.*, 2008).

It is interesting to determine how the different substituents in naltrexone and naloxone are influencing the hydration and dehydration behavior of these antagonists, also on the molecular scale. The hydration/dehydration behavior of these salts was therefore studied by applying hot-humidity stage X-ray powder diffraction, microscopy, differential scanning calorimetry, thermogravimetric analysis and solid-state NMR. The crystal structure of naltrexone hydrochloride anhydrate was determined from X-ray powder diffraction data in order to be able to study the changes in the crystal structures during dehydration.

6.2 EXPERIMENTAL

6.2.1 Materials

Naltrexone and naloxone hydrochloride were obtained from Diosynth commercial supply. The preparation procedures for the hydrate/anhydrate forms are described below.

6.2.2 Preparation of naltrexone hydrochloride tetra-hydrate

The tetra-hydrate form was prepared at room temperature from a diluted aqueous HCl solution of starting material (1.5g naltrexone hydrochloride : 30mL H₂O). After complete evaporation of the solvent, needle shaped crystals were obtained.

6.2.3 Preparation of naltrexone hydrochloride anhydrate

Naltrexone hydrochloride anhydrate was obtained by dehydrating the tetra-hydrate form at 110°C, under vacuum (10⁻²mbar) and in presence of P₂O₅ drying agent. Before and after the experiment, argon gas was flushed into the

reaction vessel. The sample was stored in a glove box under nitrogen atmosphere. Several attempts to grow crystals suitable for single-crystal diffraction failed.

6.2.4 Preparation of naloxone hydrochloride di-hydrate

The di-hydrate form of naloxone hydrochloride was prepared at room temperature from a diluted aqueous HCl solution of starting material (1g naloxone hydrochloride : 100mL H₂O). After complete evaporation of the solvent, needle shaped crystals were obtained.

6.2.5 Preparation of naloxone hydrochloride anhydrate

Naloxone hydrochloride anhydrate was obtained by dehydrating the di-hydrate form at 140°C, under vacuum (10⁻²mbar) and in presence of P₂O₅ drying agent. Before and after the experiment, argon gas was flushed into the reaction vessel. The sample was stored in a glove box under nitrogen atmosphere.

6.2.6 Analytical Methodology

X-ray Powder Diffraction (XRPD)

X-ray powder diffraction measurements for crystal structure determination of naltrexone hydrochloride anhydrate were performed using a Bruker D8 AXS Advance X-ray Diffractometer. The D8 was equipped with a Johansson type monochromator with a focusing curved Ge 111 crystal. A VÅNTEC-1 detector was used with an effective angular region of 2°. The data was collected in transmission capillary geometry using monochromatic Cu K_{α1} radiation. The

anhydrate sample was lightly ground, using an agate mortar and pestle and mounted in order to reduce preferred orientation effects (Howard et al., 2000). A 0.5 mm glass capillary tube was filled with the material and sealed in a glove box under nitrogen atmosphere. The capillary tube was spun at 15 rpm during data collection to minimize instrumental and sample packing aberrations (Dollase et al., 1986).

X-ray powder diffraction employed for investigating the hydration and dehydration behavior of the naltrexone and naloxone hydrochloride forms was done using a hot-humidity stage attached to the above-mentioned diffractometer and controlled by an Ansyco humidity and temperature control unit. The most important instrumental and data collection parameters are presented in Table 6.1.

Data analysis for crystal structure determination

The diffraction pattern was indexed using DICVOL91 (Boultif & Louër, 1991) to obtain lattice parameters that were subsequently refined in a Pawley fit (Pawley, 1981). Z-matrices describing the molecular topology of the fragments in the compound were generated automatically by DASH (David et al., 2004) from the structural data of the tetra-hydrate form. Twenty runs with 10^7 SA (simulated annealing) moves per run were performed for structure solution. To the best solution obtained after the SA process, a final full Rietveld refinement was performed using the Topas software (Cheary et al., 1992).

Table 6.1. Instrumental and data collection parameters

<i>Typical instrument settings</i>	
System	Bruker AXS D8 Advance $\theta/2\theta$
Generator	40 kV, 40 mA
Measuring circle (mm)	435
Radiation (Å)	Cu $K_{\alpha 1}$, $\lambda=1.54056\text{\AA}$
Monochromator	Primary, focusing curved Ge 111
Geometry	Transmission capillary configuration
Sample holder	0.5 mm glass capillary tube
Detector	VÅNTEC-1
<i>Measuring conditions for structure determination</i>	
Range ($^{\circ} 2\theta$)	5-60
Spatial resolution (Å)	1.5407 Å
Step size ($^{\circ} 2\theta$)	0.0084696
Step time (s)	50
Total data collection time (h)	ca 92
Spinning (rpm)	15
<i>Typical measuring conditions for hot-humidity measurements</i>	
Range ($^{\circ} 2\theta$)	2 - 40
Step size ($^{\circ} 2\theta$)	0.05
Step time (s)	1
Humidity range (%RH)	0 – 80
Temperature range ($^{\circ}\text{C}$)	25 - 125
Heating rate ($^{\circ}\text{C}/\text{min}$)	1
Carrier gas	Nitrogen

Microscopy

Scanning electron microscopy photographs were taken with a JEOL JSM 6330F, operating at 3 kV, 12 μ A and equipped with a secondary electron detector. In order to induce good conductivity of the samples, prior to SEM

analysis, the crystals were coated with gold at 10^{-5} Torr using a Cressington 208HR Sputter Coater.

The polarized light microphotographs were taken with a Leica DM-RX microscope.

Differential Scanning Calorimetry (DSC)

Differential scanning calorimetry curves were obtained using a Mettler Toledo 822 DSC with a TSO 801RO Sample Robot. The instrument was calibrated using indium standards. The samples were scanned at $1^{\circ}\text{C}/\text{min}$ or $5^{\circ}\text{C}/\text{min}$ from 25 to 280°C under nitrogen purge at $40\text{ mL}/\text{min}$ in punched aluminum pans.

Thermogravimetry Analysis (TGA)

Thermogravimetry analysis curves were generated using a TA Instruments Q500 TGA. The instrument was temperature calibrated using indium, tin and zinc standards. A weight calibration was performed using standard weights under nitrogen purge. The samples were scanned at $1^{\circ}\text{C}/\text{min}$ from 25 to 300°C under nitrogen purge at $40\text{ mL}/\text{min}$ in punched aluminum pans.

Solid-State NMR Spectroscopy (SSNMR)

100.6 MHz solid-state ^{13}C cross-polarization/magic angle spinning (CP/MAS) spectra for the naltrexone hydrochloride samples were obtained using a Bruker AXS 400MHz spectrometer. The samples were packed into a 4 mm rotor and spun with a rate of 12 kHz. The contact time for CP was 2.5ms. A signal was acquired with proton decoupling.

The ^{13}C NMR spectra for the naloxone hydrochloride were obtained on a CMX-300 spectrometer (300.15 MHz for ^1H , 75.46 MHz for ^{13}C) using a Bruker 4mm double resonance MAS probe spinning at 4 kHz. The CP/MAS spectra were recorded employing a variable amplitude CP (1 ms contact time, an rf field of 64 kHz on ^1H with a ± 1 kHz ramp and a 60 kHz rf field on ^{13}C). Protons were decoupled using the CM sequence with an rf field strength of 84 kHz (Gerbaud et al., 2003). A 5-pulse TOSS sequence was used to suppress spinning sidebands for the amorphous and anhydrous sample (Song et al., 1993).

6.3 RESULTS AND DISCUSSION

6.3.1 Crystal structure determination of naltrexone hydrochloride anhydrate

Indexing, Pawley refinement and simulated annealing process

Twenty-three reflections with low and high intensity were introduced into DICVOL91 and an orthorhombic cell with a volume of 1820.73 \AA^3 was found. Space group determination in DASH resulted in $P2_12_12_1$. The volume and space group $P2_12_12_1$ correspond to $Z' = 1$ (molecules per asymmetric unit). The lattice parameters obtained after indexing were subsequently refined along with background, zero point, peak shape parameters and reflection intensities in a Pawley fit. The characteristic parameters of the orthorhombic cell obtained after the Pawley fit are presented in Table 6.2.

The peak shape is implemented in DASH as a convolution of Gaussian, Lorentzian and axial divergence terms (asymmetry). Actually, the X-ray line

shape is a full Voigt function, which uses two parameters σ_1 and σ_2 to describe the angle-dependent Gaussian component:

$$\sigma^2 = \sigma_1^2 \sec^2 \theta + \sigma_2^2 \tan^2 \theta$$

and two parameters γ_1 and γ_2 to describe the angle-dependent Lorentzian component:

$$\gamma = \gamma_1 \sec \theta + \gamma_2 \tan \theta$$

The two other asymmetry parameters are fully defined by the peak fitting procedure and cannot be refined by Pawley fitting. The sample gave sharp diffraction lines with a mean FWHM = 0.092° and a minimum value FWHM = 0.078° for the first twelve fitted peaks.

The profile Pawley χ^2 is described in DASH as:

$$\chi^2 = \left\{ \sum_i^N w_i [y_i(\text{obs}) - y_i(\text{calc})]^2 \right\} / (N - P + C),$$

where $y_i(\text{obs})$ is the observed intensity at the i^{th} step in the powder diffraction pattern; $y_i(\text{calc})$ is the associated calculated intensity; $w_i = 1/\sigma_i^2$, where σ_i is the standard deviation of the observed intensity at that point. The summation is performed over all N data points, where N is the number of data points, P the number of parameters and C the number of parameter constraints. The profile χ^2 for the Pawley fit had a final value of 3.36.

Table 6.2. Lattice parameters and Pawley fit results

<i>Lattice parameters</i>	
System	Orthorhombic
Space group	$P2_12_12_1$
a (Å)	15.529
b (Å)	14.991
c (Å)	7.840
V (Å ³)	1825.44
Zero point correction	0.0201
<i>Pawley fit results</i>	
Number of reflections	328
Data points	6309
Pawley χ^2	3.36

The molecular conformations of the Z-matrices describing the molecular geometry are shown in Fig. 6.3.

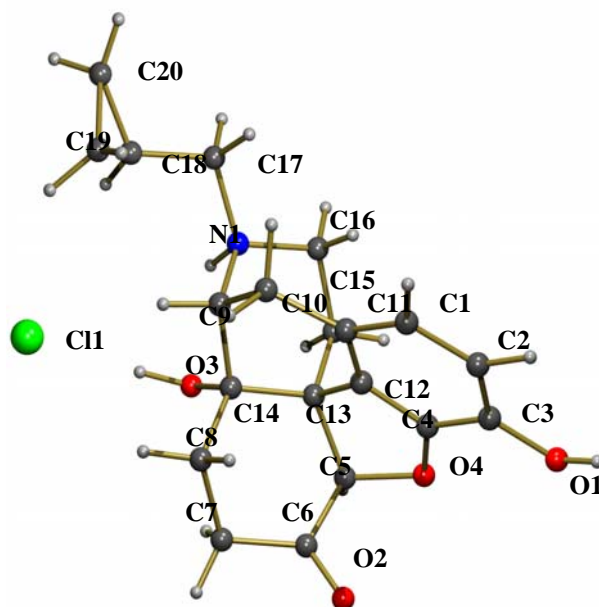


Figure 6.3. The molecular conformations used for the Z-matrices

Naltrexone hydrochloride has two torsion angles: C18:C17:N1:C9 and C19:C18:C17:N1, optimized during the simulated annealing (SA) process. The simulated annealing process ended up with 13 solutions having low χ^2 profile values out of 20. The structure of the best solution had a profile χ^2 of 15.32. The fit of the observed and calculated diffraction data for this solution is shown in Fig. 6.4.

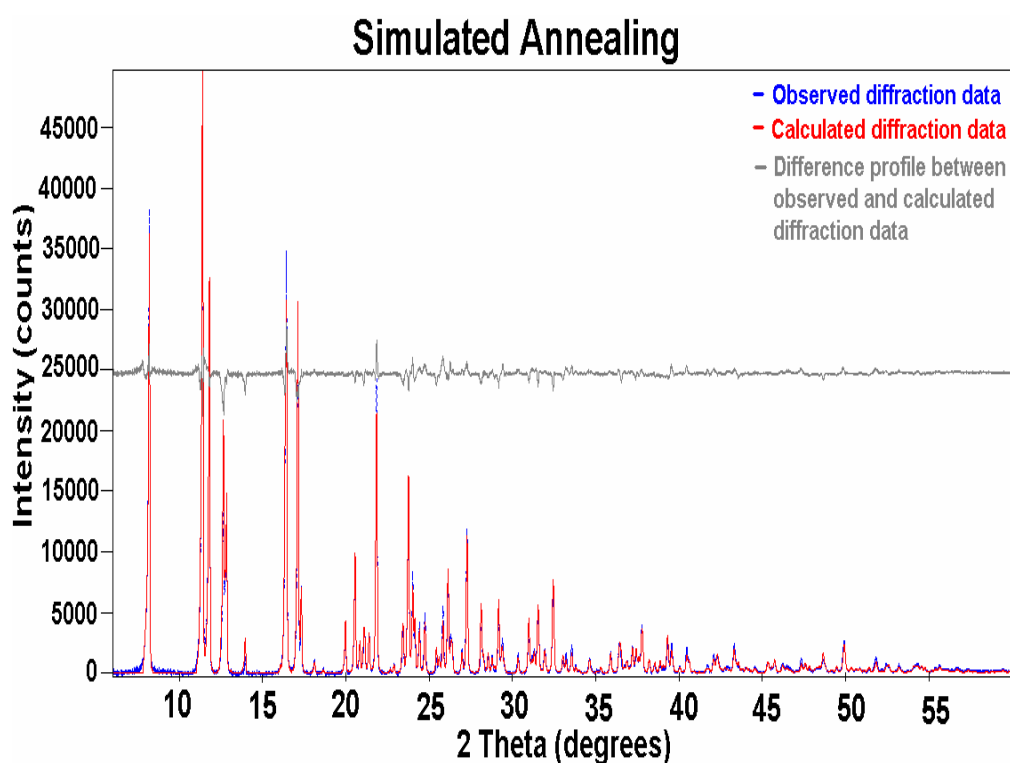


Figure 6.4. The fit to the diffraction data returned by the SA process

Rietveld refinement

A full Rietveld refinement (Young, 1996) of the best solution returned by the SA process gave a final profile $R_{wp}=3.65$, $R_p=2.64$ and a GOF of 2.54. The fit of the final calculated diffraction data to the observed data is shown in Fig. 6.5.

All coordinates of the non-hydrogen atoms were freely refined, but soft restraints on bond lengths and angles were introduced in order to reduce the number of free parameters. The final crystal structure of naltrexone hydrochloride anhydrate is presented in Fig. 6.6. The crystallographic data of the refined crystal structure is presented in Table 6.3.

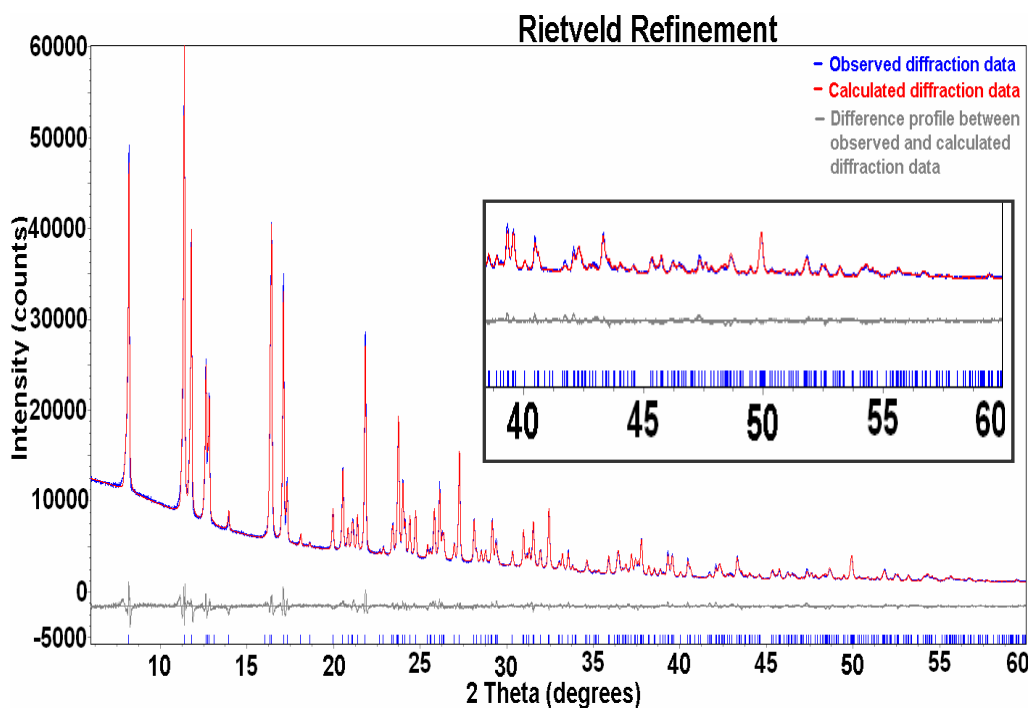
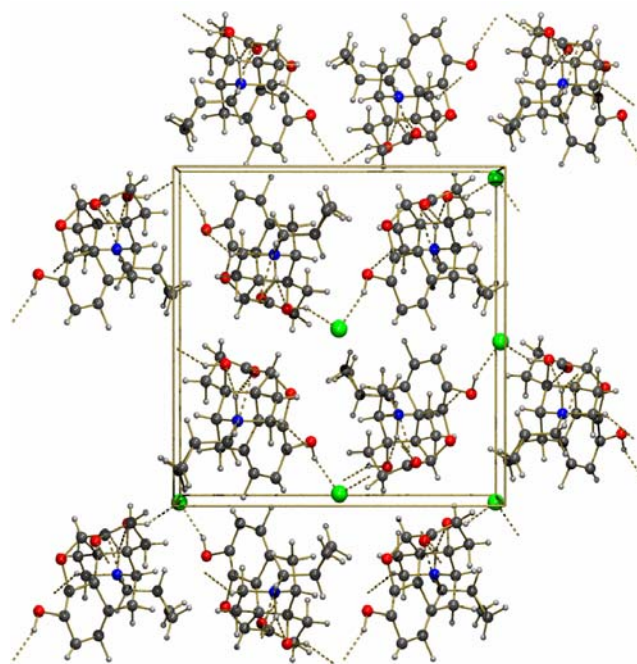
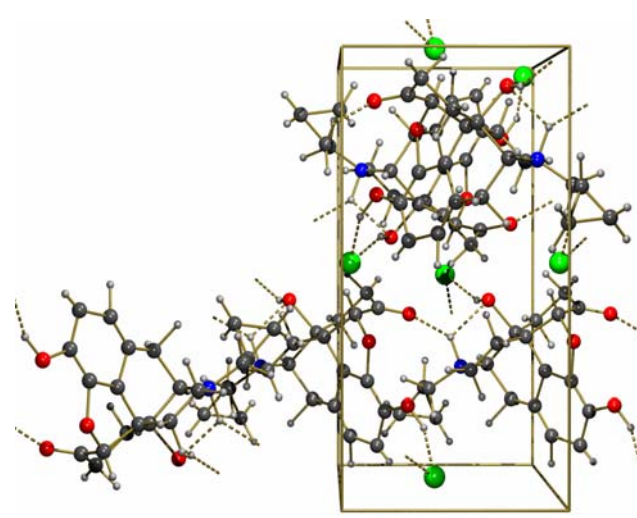


Figure 6.5. The fit after the final Rietveld refinement (high 2 theta angle is enlarged)



a)



b)

Figure 6.6. Crystal structure of naltrexone hydrochloride anhydrate: a) c-projection, b) a-projection

Table 6.3. Crystallographic data of the refined naltrexone hydrochloride anhydrate structure after full Rietveld refinement

<i>Cell parameters</i>	Naltrexone hydrochloride anhydrate	<i>Final profiles</i>
<i>System</i>	Orthorhombic	$R_{wp} = 3.65$ $R_p = 2.64$ $GOF = 2.54$
<i>Space group</i>	$P2_12_12_1$	
<i>a</i> (Å)	15.5338(4)	
<i>b</i> (Å)	14.9942(4)	
<i>c</i> (Å)	7.8420(2)	
<i>V</i> (Å ³)	1826.53(8)	

6.3.2 Hot-humidity stage X-ray powder diffraction (XRPD)

The conversions recorded with hot-humidity stage X-ray powder diffraction for *naltrexone hydrochloride* tetra-hydrate are presented in Fig. 6.7.

To study the dehydration of naltrexone hydrochloride tetra-hydrate, the compound was heated in a temperature range between 25 - 75°C at 0%RH and kept at 75°C for 1hr. A complete conversion to the anhydrate form was already observed at 30°C.

In order to study the reverse process, i.e. the conversion of the anhydrate to the tetra-hydrate, naltrexone hydrochloride anhydrate was subjected to 40°C and 80% RH. After 40 min this resulted in the formation of an unknown hydrate form Y. Continued exposure of form Y to 80%RH and 40°C lead to further conversion to the tetra-hydrate form. Leaving the tetra-hydrate form at

40°C and 80% RH for 12 hours did not lead to other forms with a higher amount of hydration water.

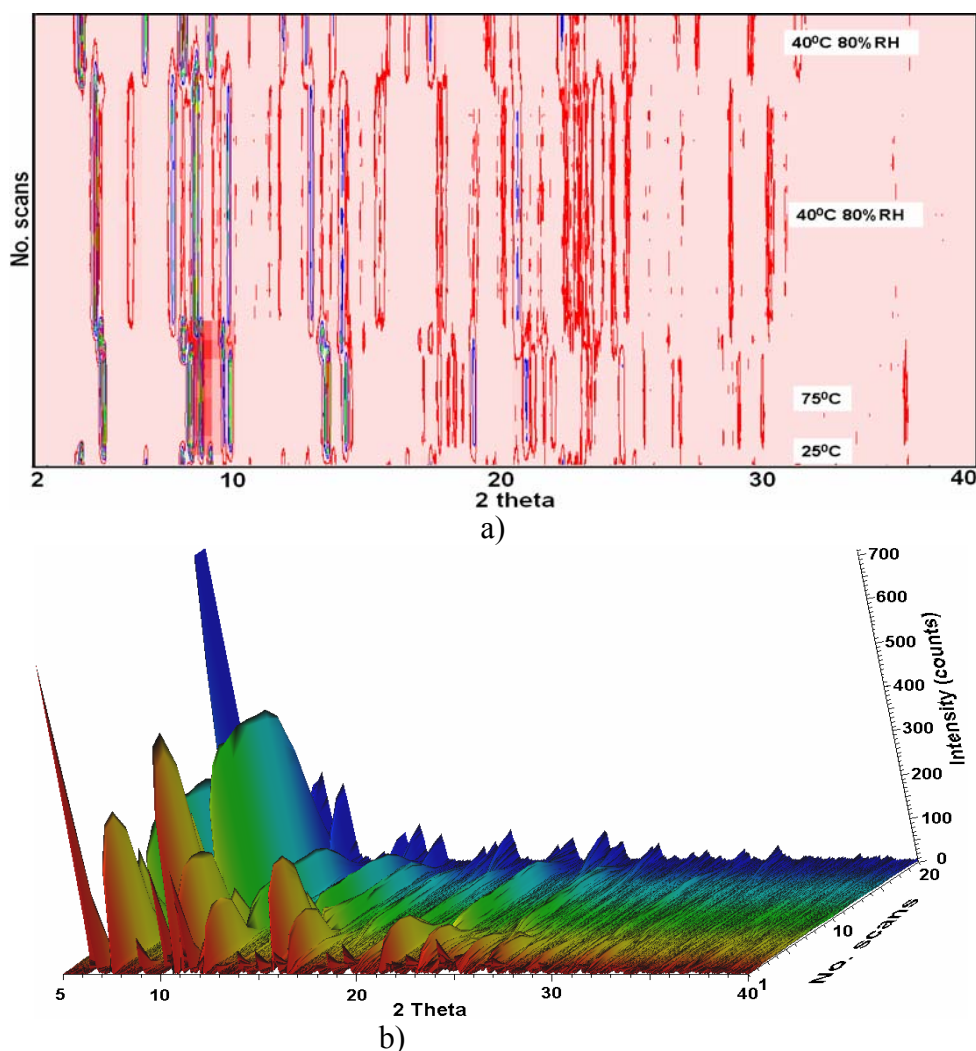


Figure 6.7. Top view (a) and 3D pictures (b) of the hot-humidity stage X-ray powder diffraction experiments recorded for the conversion of naltrexone hydrochloride tetra-hydrate (bottom) to the anhydrate, further on to an unknown hydrate form Y and back to the tetra-hydrate (top)

The conversions recorded with hot-humidity stage X-ray powder diffraction for *naloxone hydrochloride* di-hydrate are presented in Fig. 6.8. To study the dehydration of the di-hydrate form, the samples were heated in a temperature range between 25 - 145°C at 0%RH and kept at 145°C for 1hr. A complete

conversion to the anhydrate form was observed at 75°C. No intermediate forms were observed. In order to study the reverse process, *i.e.* the conversion of the anhydrate to the tetra-hydrate form, the anhydrate was subjected to 40°C and 80% RH. After 1 hour and 20 min this resulted in the formation of an amorphous form.

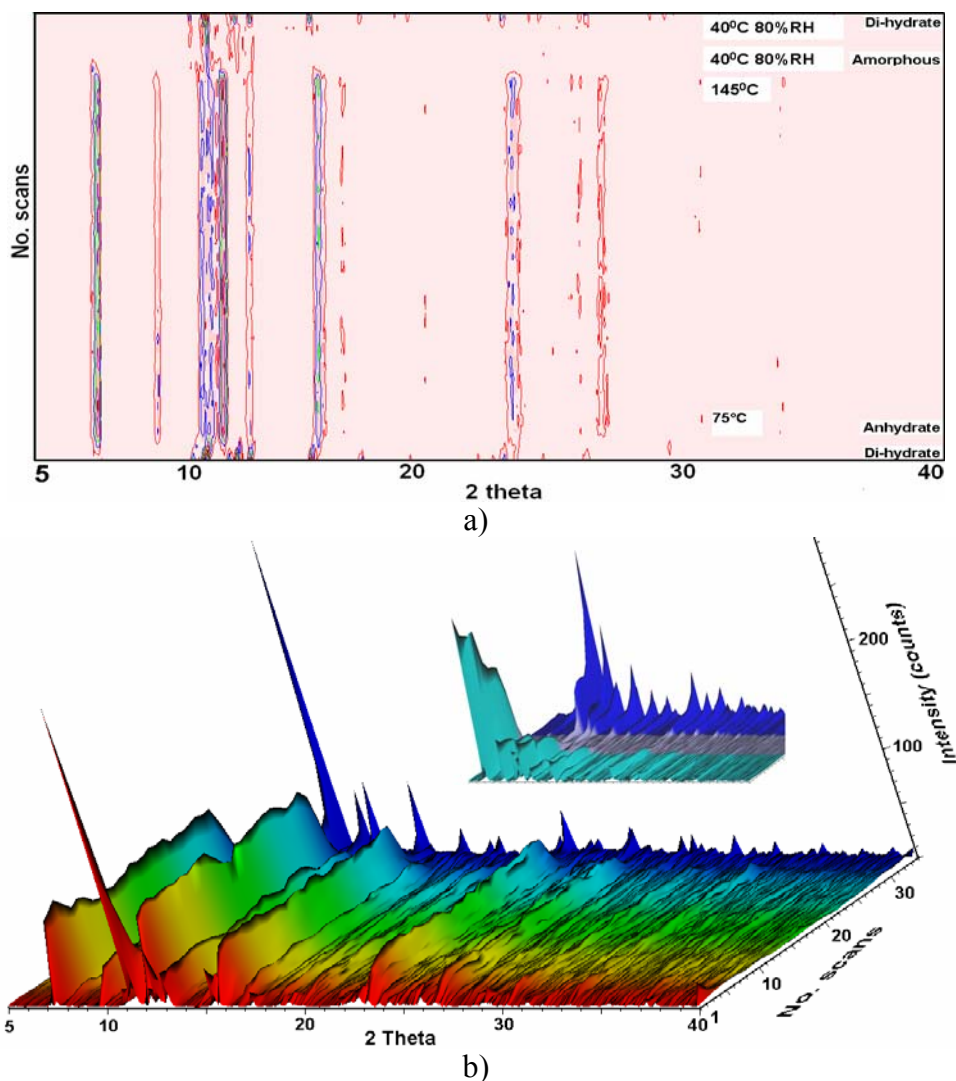


Figure 6.8. Top view (a) and 3D pictures (b) of the hot-humidity stage X-ray powder diffraction experiments recorded for the conversion of naloxone hydrochloride di-hydrate (bottom) to the anhydrate form, further on to the amorphous form and back to the di-hydrate form (top) (enlarged picture of the conversion anhydrate - amorphous - di-hydrate).

Continued exposure of the amorphous form to 80%RH and 40°C lead to the formation of the di-hydrate form of naloxone hydrochloride. Leaving the di-hydrate form at 40°C and 80% RH for 12 hours did not lead to other forms with a higher amount of hydration water.

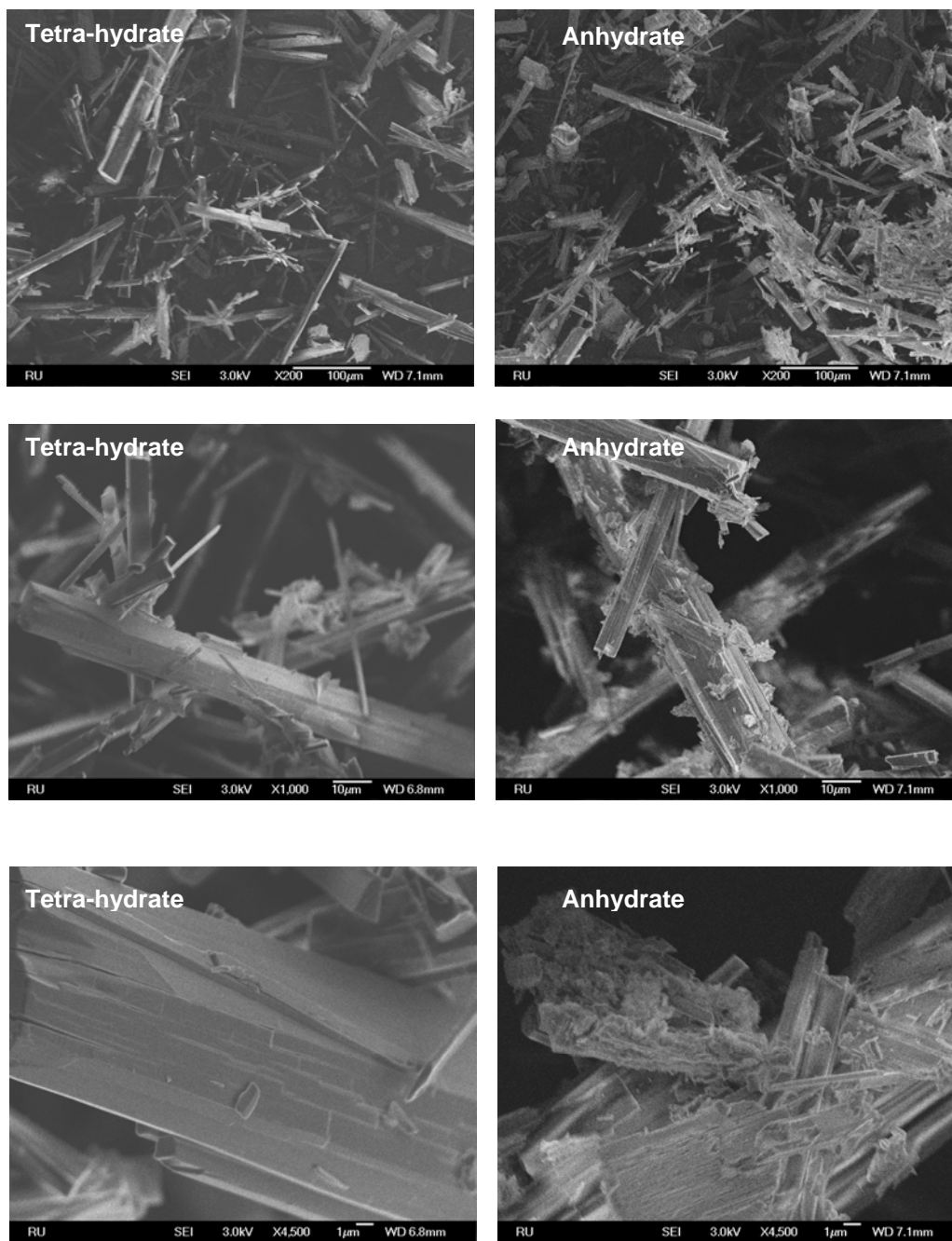
6.3.3 Microscopy

The scanning electron microphotographs of naltrexone hydrochloride samples are presented in Fig. 6.9. Three different magnifications were used in order to emphasize the small differences between the morphology of the two morphs.

The *naltrexone hydrochloride* tetra-hydrate consists of acicular crystal found in stacked ordered aggregates with chord thickness of 2 to 18µm (Fig. 6.9a). The anhydrate form of naltrexone hydrochloride exhibits in general the same characteristics as the tetra-hydrate form, although the anhydrate seems to consist of more defected and thinner needle crystals. The chord thickness for the anhydrate form varies from 1 to 12µm (Fig. 6.9b).

Naloxone hydrochloride di-hydrate crystallizes in rather large pyramidal crystals (Fig. 6.10a). Therefore an examination using an optical microscope was possible. During a close investigation, droplets of water coming out on the surface of the crystals could be detected. It seems that the crystals of the naloxone hydrochloride di-hydrate are not stable and loose at least part of the hydration water already at room temperature. Applying vacuum (10^{-2} mbar) the di-hydrate pyramidal crystals brake apart in order to form the anhydrate form within a few minutes. The morphology of the naloxone hydrochloride anhydrate crystals was investigated using scanning electron microscopy. The

naltrexone hydrochloride anhydrate shows needle shaped crystals stacked in ordered aggregates with chord thickness of 2 to 15 μm (Fig. 6.10b).



a)

b)

Figure 6.9. Scanning electron microphotographs of naltrexone hydrochloride forms at different magnifications (x200; x1000; x4500) of: a) tetra-hydrate ; b) anhydrate

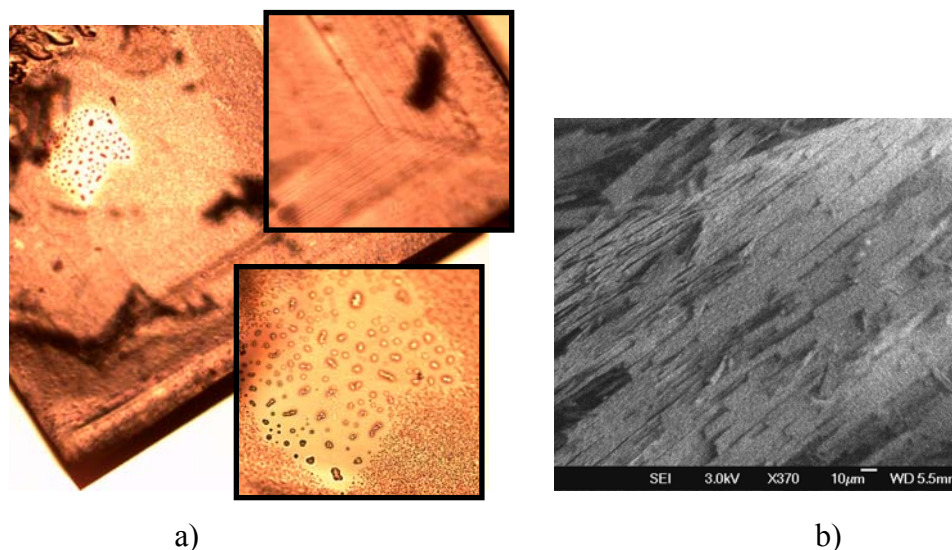


Figure 6.10. Microphotographs of naloxone hydrochloride: a) di-hydrate form with enlarged zoom on the water droplets (down) and the pyramidal shaped crystal (up); b) anhydrate form at x370 magnification

6.3.4 Differential Scanning Calorimetry (DSC)

Differential scanning calorimetry curves of *naltrexone hydrochloride* tetra-hydrate at different heating rates are shown in Figure 6.11. The DSC measurements of the tetra-hydrate form shows an endothermic effect due to solvent loss and anhydrate formation at temperatures from 25 - 110°C, confirming the results obtained with hot-humidity stage X-ray powder diffraction. The endothermic event observed at 220°C indicates the decomposition of naltrexone hydrochloride.

The anhydrate form yielded no thermal events measurable by DSC until 220°C, where the onset of decomposition appears. The shifts recorded with 1°C/min in comparison with the ones observed at 5°C/min are attributed to the higher heating rates.

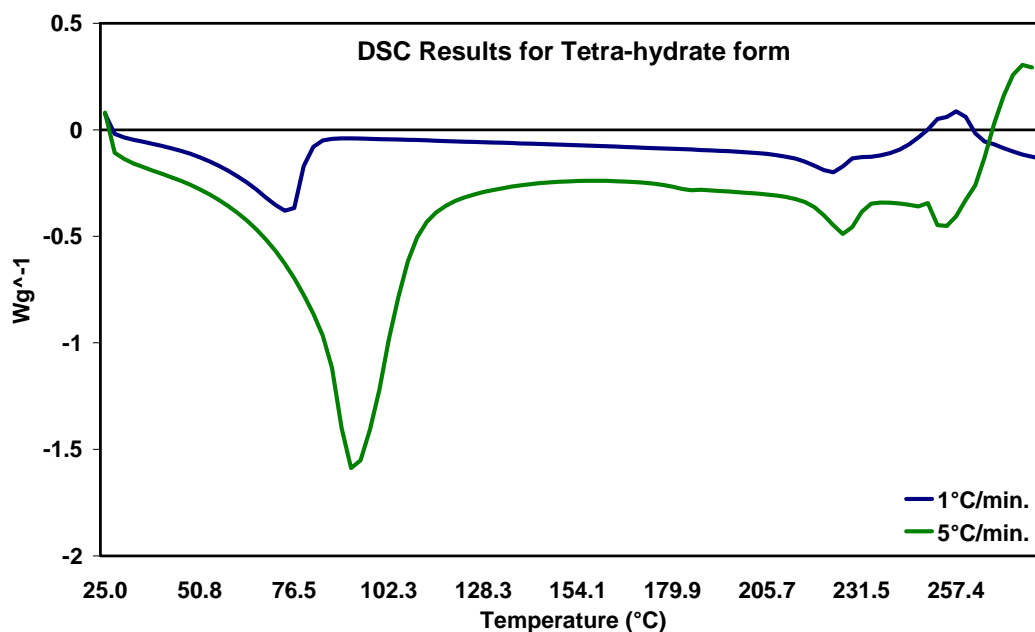


Figure 6.11. DSC curves with 1 $^{\circ}C/min$ and 5 $^{\circ}C/min$ for naltrexone hydrochloride tetra-hydrate

Differential scanning calorimetry curves of *naloxone hydrochloride dihydrate* at different heating rates are shown in Figure 6.12. The DSC measurements of the naloxone hydrochloride dihydrate show a two-step endothermic effect due to solvent loss and the final anhydrate formation at temperatures between 75 - 150 $^{\circ}C$. Taking into account that the hot-humidity stage XRPD data did not show the formation of another form besides the anhydrate during dehydration, this suggests that part of the water molecules can be removed from the hydrate without a structural change.

The obtained anhydrate form yielded an endothermic event measurable by DSC at 175 $^{\circ}C$. Due to the total solvent loss and anhydrate formation at 150 $^{\circ}C$, the recorded endothermic event at 175 $^{\circ}C$ must be due to partial decomposition of the sample. The onset of further decomposition of naloxone hydrochloride is observed at 250 $^{\circ}C$. The shifts recorded for all the investigated forms with

1°C/min in comparison with the ones observed at 5°C/min are attributed to the higher heating rates.

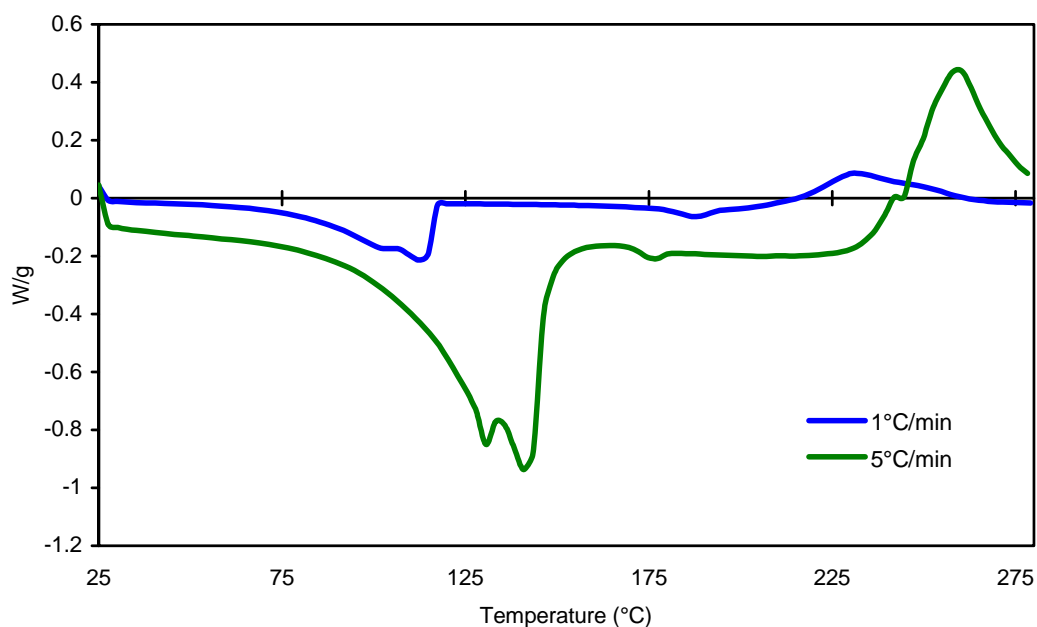


Figure 6.12. DSC curves with 1°C/min. and 5°C/min. for naloxone hydrochloride di-hydrate

6.3.5 Thermal Gravimetric Analysis (TGA)

The thermal profile of the *naltrexone hydrochloride* tetra-hydrate is shown in Fig. 6.13. The TGA curve is denoted by a normal font line on a percentage of initial weight scale.

Dehydration of the *naltrexone hydrochloride* tetra-hydrate was observed gradually as a mass loss of 15.57% in a temperature range from 25 - 75°C. The dehydration of the tetra-hydrate form results in the release of water with a theoretical weight loss of 16.01% close to the observed weight loss of 15.57% (3.89 molecules H₂O/molecule NTX). The investigated sample of *naltrexone hydrochloride* tetra-hydrate decomposed in a temperature range of 220 to

280°C. The TGA data confirms the results obtained with hot-humidity stage X-ray powder diffraction and DSC.

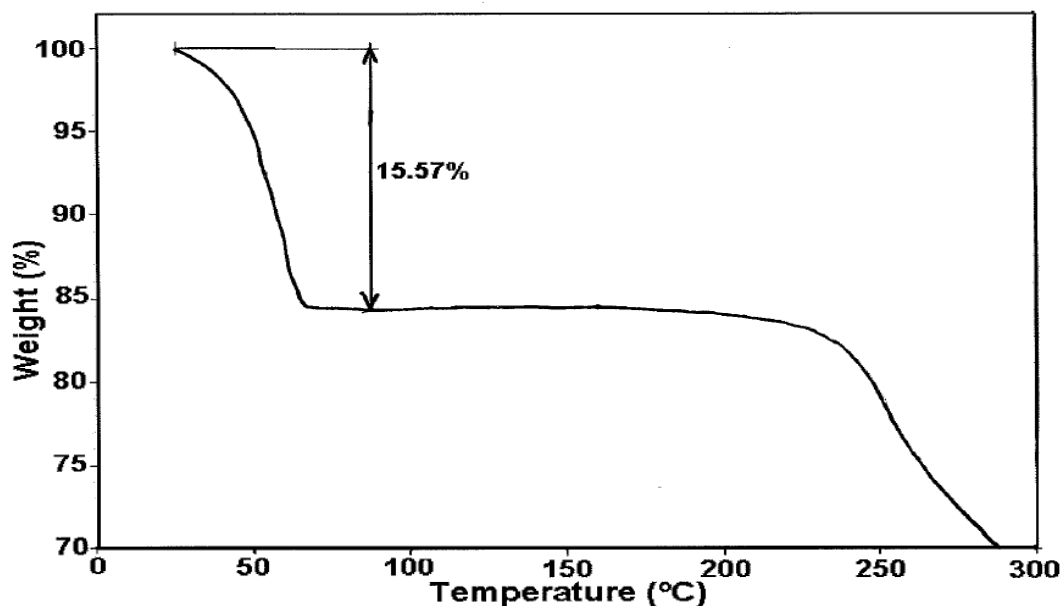


Figure 6.13. TGA curves with 1°C/min heating rate for naltrexone hydrochloride tetra-hydrate

The thermal profile of the *naloxone hydrochloride* di-hydrate is shown in Fig. 6.14. Dehydration of the naloxone hydrochloride di-hydrate was observed gradually as a mass loss of 8.81% in a temperature range from 25 - 75°C. The dehydration of the di-hydrate form results in the release of water with a theoretical weight loss of 9% close to the observed weight loss of 8.81% (1.95 molecules H₂O/molecule NLX). The investigated sample of naloxone hydrochloride di-hydrate decomposed partially in a temperature range from 175 - 250°C continued by the final decomposition process in a temperature range of 250 to 300°C. The TGA data confirm the results obtained with hot-humidity

stage X-ray powder diffraction and DSC, however, the separate steps in dehydration as seen in DSC are not visible here.

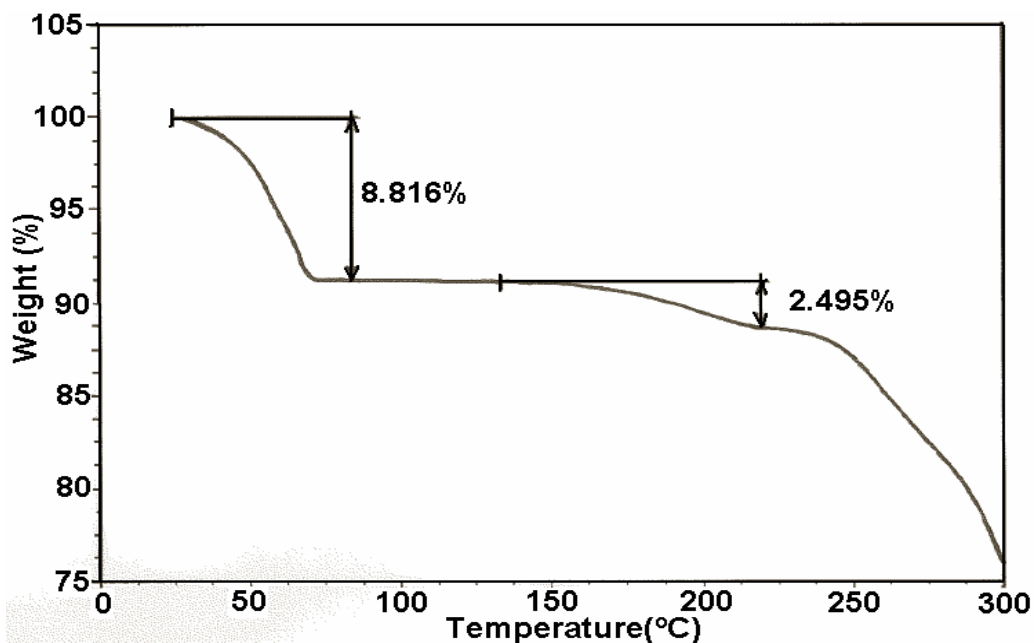


Figure 6.14. TGA curves with 1°C/min heating rate for naloxone hydrochloride di-hydrate

6.3.6 Solid-State NMR Spectroscopy (SSNMR)

The ^{13}C CPMAS spectra of the naltrexone hydrochloride samples are displayed in Fig.6.15. Compared to the tetra-hydrate form of *naltrexone hydrochloride*, the undetermined hydrate Y and the anhydrate forms show significant differences. The tetra-hydrate and the anhydrate forms both have single resonances per carbon atom, a clear indication of one molecule per asymmetric unit cell. However, for the undetermined hydrate Y there seem to be 3 resonances per carbon atom, of more or less equal intensity within each carbon species. Some groups of 3 carbon resonances have shifts that neither occur in the anhydrate, nor in the tetra-hydrate. This excludes the existence of a

mixture of the anhydrate and the tetra-hydrate and together with another unknown form. Although a mixture of 3 unknown compounds is still a possibility, $Z'=3$ is much more likely for this unknown form.

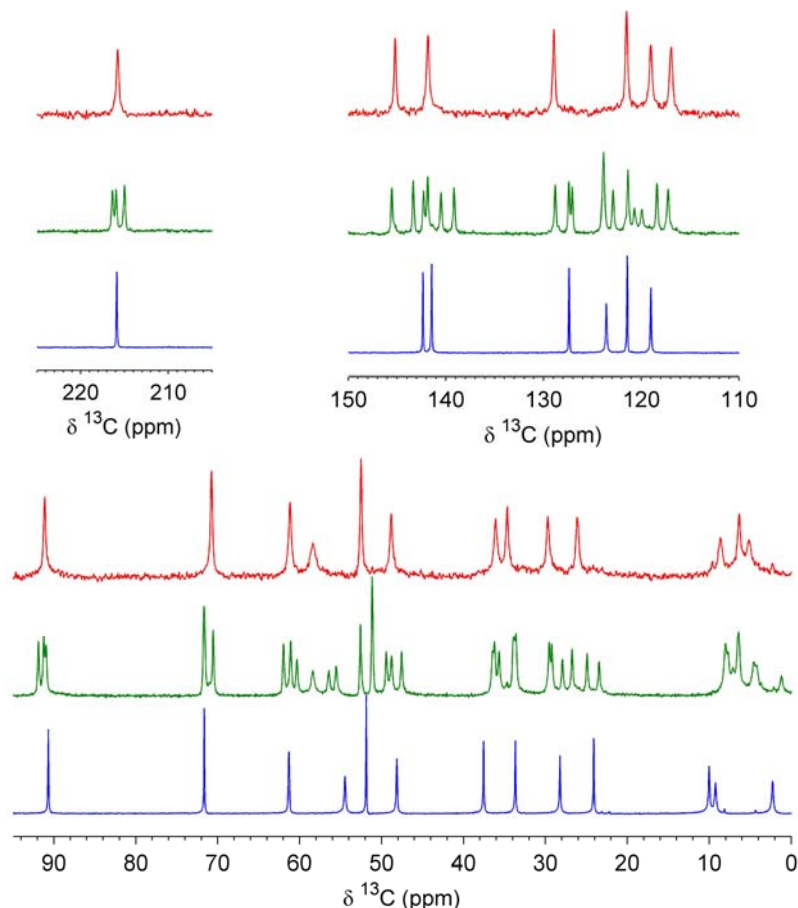


Figure 6.15. Solid-state ^{13}C CP/MAS NMR spectra of naltrexone hydrochloride forms: tetra-hydrate (bottom spectra), anhydrate (top), undetermined hydrate (middle)

The ^{13}C -NMR spectra for *naloxone hydrochloride* di-hydrate, anhydrate and amorphous forms are shown in Fig. 6.16. The spectra of the di-hydrate and the anhydrate forms indicate the existence of one molecule per asymmetric unit cell. Clear differences can be observed between the di-hydrate and anhydrate. The spectrum of the amorphous compound displays broad resonances, at the

position of the originating anhydrate, at the position of the di-hydrate, or in between. This clearly indicates the structural heterogeneity. Amorphous and materials of poor crystallinity have broader resonances because of the heterogeneity of structural forms found in the sample. This heterogeneity results in a distribution of isotropic shifts for a given carbon.

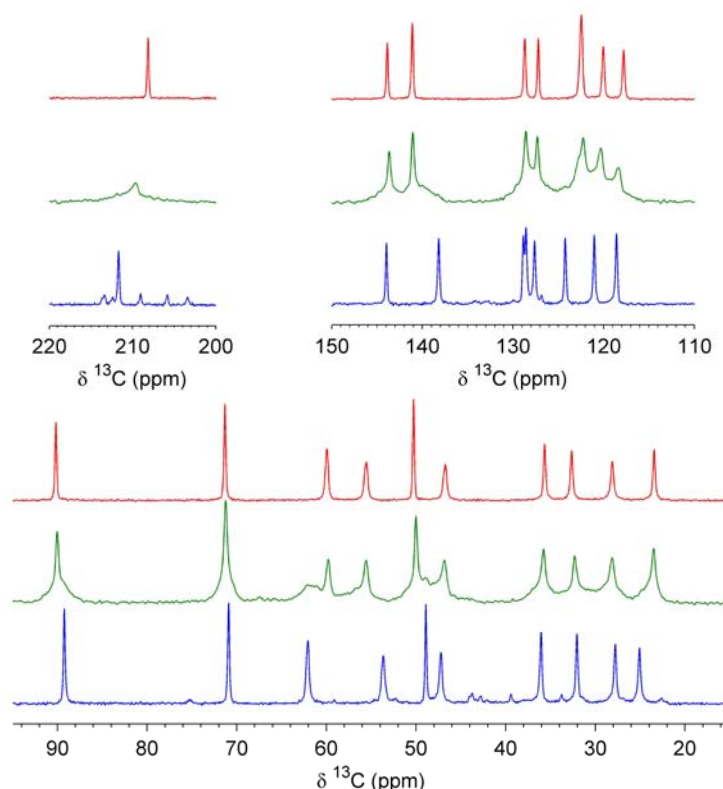


Figure 6.16. Solid-state ^{13}C CP/MAS NMR spectra of naloxone hydrochloride forms: di-hydrate (bottom spectra), anhydrate (top), amorphous (middle)

6.3.7 Structural aspects of hydration and dehydration

The characteristic structural features of the hydrated and anhydrate forms of naltrexone and naloxone hydrochloride are presented in Table 6.5.

The naltrexone molecules in *naltrexone hydrochloride tetra-hydrate* are packed in a three-dimensional network with the aid of water molecules. H-

bonds are formed between the –OH group attached to C(3), respectively C(14) and water molecules (for atom numbering see Fig. 6.3). The Cl⁻ is involved in H-bonding with the water molecules and also with the –OH group attached to C(14) (Table 6.5). The carboxyl group forms H-bonds only with the N atom. H-bonds between different water molecules are also observed. Obviously, the water molecules play a stabilizing role in the network formation of naltrexone hydrochloride tetra-hydrate. The naltrexone molecules in *naltrexone hydrochloride anhydrate* are assembled in a two-dimensional network, this time with the aid of the Cl⁻ anion and N atom. The Cl⁻ forms H-bonds with the (-OH) groups attached to C(3), and C(14). As for the case of the tetra-hydrate form, the carboxyl group forms only H-bonds with the N atom. The packing of the naltrexone molecules in naltrexone hydrochloride tetra-hydrate and hydrochloride anhydrate is presented in Fig.6.17 a and b.

Comparing the SSNMR spectra of the anhydrate with the tetra-hydrate, significant differences can be found in the cyclopropane substituents (C18, C19, C20 between 0-11 ppm) which can be easily traced back to their significantly different surroundings in the crystal lattice (presence of chlorine in the anhydrate vs hydroxyl in the tetra-hydrate, see Fig. 6.17 a-b). It is interesting to note that the shift of the carboxyl hardly changes between the two forms (215.9 ppm in the tetra-hydrate vs 215.8 ppm in the anhydrate), in line with the fact that in both the tetra-hydrate and the anhydrate this carboxyl is only involved in the same type of hydrogen bond to N. By contrast, the unknown form shows 3 peaks with different shifts (215.0, 216.0, and 216.4), a strong indication that the hydrogen bonding in this form is significantly changed.

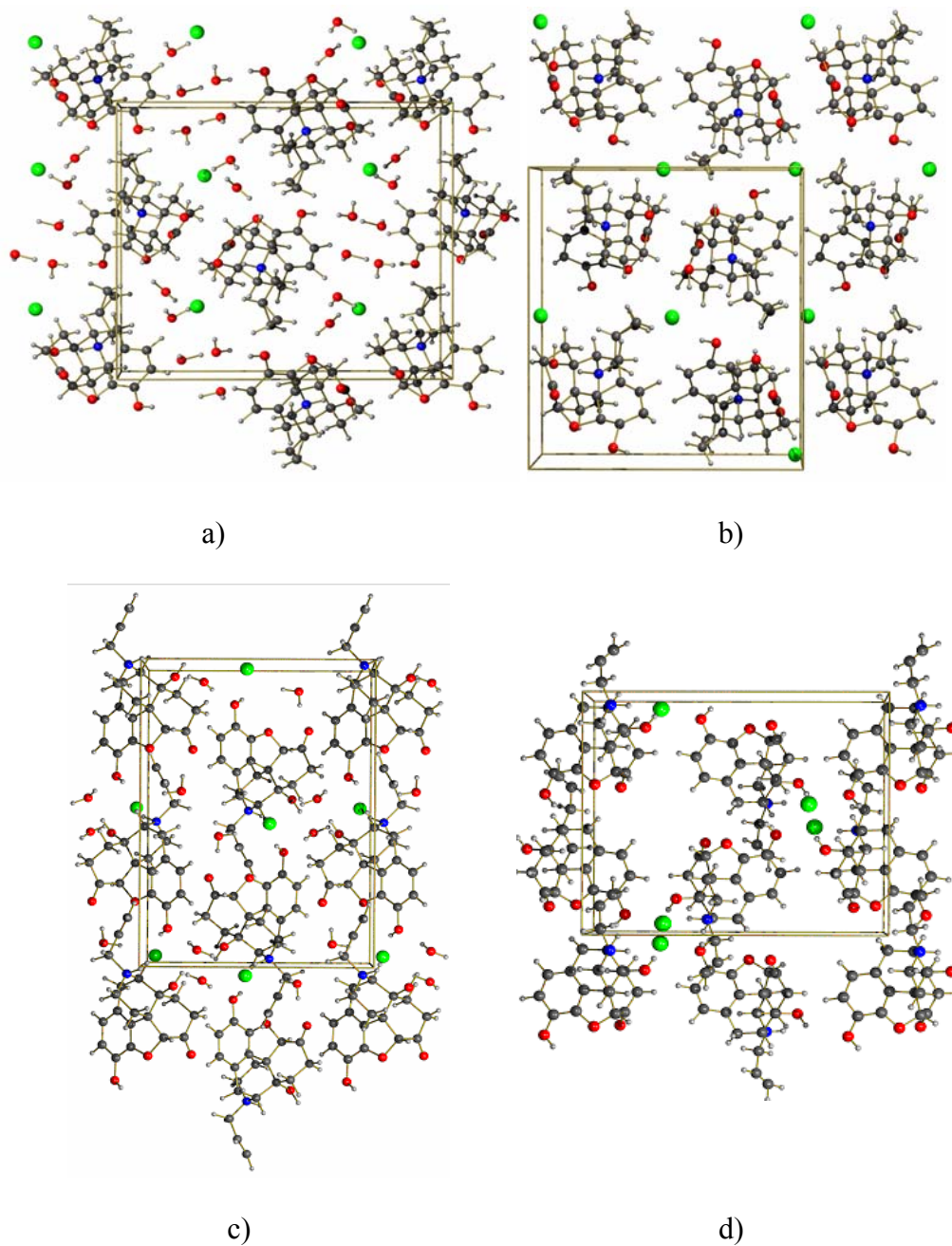


Figure 6.17. The crystal structures of the: a) naltrexone hydrochloride tetrahydrate, b) naltrexone hydrochloride anhydrate, c) naloxone hydrochloride dihydrate, d) naloxone hydrochloride anhydrate

The naloxone molecules in *naloxone hydrochloride di-hydrate* are also packed in a three-dimensional network with the aid of water molecules. H-bonds are formed between the –OH group attached to C(3), respectively C(14)

and water molecules. The carboxyl group and the Cl⁻ are also involved in H-bonding with the water molecules. The N atom forms H-bonds only with the Cl⁻. The naloxone molecules in *naloxone hydrochloride anhydrate* are also assembled in a three-dimensional network, this time with the aid of the Cl⁻ anion. Cl⁻ forms H-bonds with the N atom and with the (-OH) groups attached to C(3), and C(14) (Guguta *et al.*, 2008). The packing of the naloxone molecules in naloxone hydrochloride di-hydrate and hydrochloride anhydrate is presented in Fig. 6.17 c and d.

The SSNMR data showed that for those carbon atoms involved in the hydrogen bonding, going from the anhydrate to the di-hydrate, the chemical shift changes in the C3 hydroxyl at 141.1 ppm shifts -2.9 ppm (becomes more shielded) and the C6 carboxyl at 208.1 ppm shifts +3.6 ppm in the di-hydrate (more deshielding). Interestingly, also other carbon atoms are affected: C17 and C10 are not involved in hydrogen bonding but still their chemical shifts change going from anhydrate to di-hydrate from 50.3 ppm to 48.9 ppm for C17 and from 23.4 ppm to 25.1 ppm for C10. Because the conformation of the naloxone molecules is virtually the same for the anhydrate and the di-hydrate, these changes in chemical shift therefore reflect the effect of the differences in stacking of the molecules. One should note that all peaks that are present in the anhydrate still exist in the amorphous form, except the carboxyl. On the whole this indicates that locally, for at least a significant number of molecules, the environment still resembles the anhydrate structure. The positions of the carboxyl on the other hand seem to be the first to be entirely affected by hydration. From the crystal structure one can see that the carboxyls are located in the voids in the structure and are therefore most readily hydrated.

Table 6.4. Characteristic structural data of the investigated forms

Antagonist Opioids	H-bond network	H-bonds formed by N atom	H-bonds formed by Cl ⁻ anion	Other H-bond
<i>Naltrexone hydrochloride tetra-hydrate</i>	3D	<ul style="list-style-type: none"> • carboxyl group 	<ul style="list-style-type: none"> • water • C(14)-OH 	C(3)-OH...O _(water) C(14)-OH...O _(water) OH _(water) ...Cl ⁻ OH _(water) ...O _(water)
<i>Naltrexone hydrochloride anhydrate</i>	2D	<ul style="list-style-type: none"> • carboxyl group 	<ul style="list-style-type: none"> • C(3)-OH • C(14)-OH 	-
<i>Naloxone hydrochloride di-hydrate</i>	3D	<ul style="list-style-type: none"> • Cl⁻ anion 	<ul style="list-style-type: none"> • C(3)-OH • water • N-H 	C(3)-OH...O _(water) C(14)-OH...O _(water) OH _(water) ...Cl ⁻ OH _(water) ... O-C(6)
<i>Naloxone hydrochloride anhydrate</i>	3D	<ul style="list-style-type: none"> • Cl⁻ anion 	<ul style="list-style-type: none"> • C(3)-OH • C(14)-OH • N-H 	-

A comparison between the crystal structures of the hydrated and anhydrate forms of naltrexone and naloxone hydrochloride can now be made. By dehydrating the naltrexone hydrochloride tetra-hydrate, the water disappears from the net without breaking of the symmetry, but with lowering of the dimensionality of the H-bond network. The dehydration process of the tetra-hydrate form induces shrinkage of the unit cell in two directions and small expansion in the third direction (Table 6.5).

By dehydrating the naloxone hydrochloride di-hydrate, the water disappears from the net again without breaking of the symmetry but without lowering of the dimensionality of the H-bond network. In contrast to naltrexone hydrochloride tetra-hydrate the water molecules in the naloxone di-hydrate are isolated and therefore are not mutually attached by H-bonds. The DSC

measurements indicate that the dehydration of the naloxone hydrochloride dihydrate takes place in two steps, but at the same time hot-humidity stage XRPD could only record the powder patterns corresponding to the dihydrate and anhydrate forms. The structural data together with the DSC and XRPD data suggest the formation of an intermediate hydrate form isostructural to the dihydrate. The two water molecules in naloxone hydrochloride dihydrate form different H-bonds. One of the water molecules forms H-bonds with the -OH group attached to C(3) and C(14). The second water molecule forms H-bonds with the carboxyl group and with the Cl⁻ anion. The H-bonds formed by the water molecule with the -OH groups are significantly shorter ($L_1=1.731$ and $L_2=1.864$) than those formed by the second water molecule ($L_3=2.882$ and $L_4=2.184$). Therefore the first dehydration event noticed in the DSC data probably corresponds to the loss of the water molecules that are involved in H-bonding with the carboxyl group and Cl⁻ anion. The same loosely bonded water molecules are probably also responsible for loss of water noticed in the microphotographs that were taken at room temperature. Figure 6.18 presents the two water molecules involved in H-bonds with different lengths, together with the symmetry related water molecules.

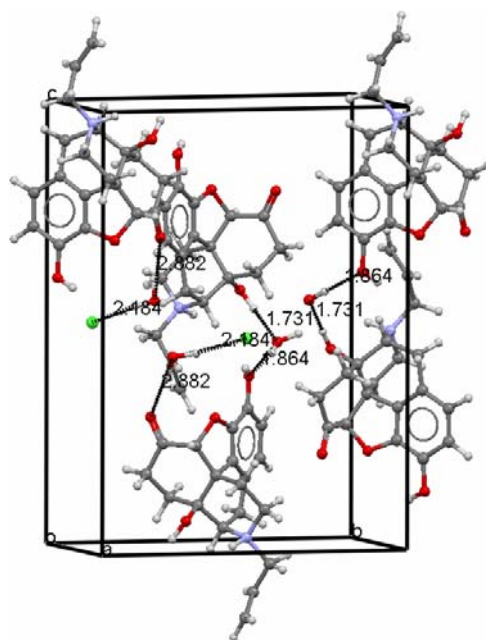


Figure 6.18. The H-bonds and their lengths formed by the two water molecules present in naloxone hydrochloride di-hydrate, together with the symmetry related water molecules

Table 6.5. Unit cell parameters of the investigated forms showing the dehydration pathway

<i>Cell parameters</i>	Naltrexone hydrochloride tetra-hydrate	Naltrexone hydrochloride anhydrate	Naloxone hydrochloride di-hydrate	Naloxone hydrochloride anhydrate
<i>System</i>	Orthorhombic	Orthorhombic	Orthorhombic	Orthorhombic
<i>Space group</i>	$P2_12_12_1$	$P2_12_12_1$	$P2_12_12_1$	$P2_12_12_1$
<i>a</i> (Å)	18.099(5) →	14.9942 (4)	18.569(5) →	14.681 (4)
<i>b</i> (Å)	15.926(6) →	15.5338(4)	13.185(5) →	17.452(4)
<i>c</i> (Å)	7.768(1) →	7.8420(2)	7.833(3) →	7.978 (2)
<i>V</i> (Å ³)	2239.08	1826.53	1917.77	2044.11

The dehydration process of the di-hydrate form induces shrinkage of the unit cell in one direction and expansion in two directions (Table 6.5).

The hot-humidity stage XRPD data showed that the anhydrate form of naloxone hydrochloride converts (at similar conditions) faster to the di-hydrate than the anhydrate form of naltrexone hydrochloride converts to the tetra-hydrate form. In both cases, the conversions to the hydrated forms of naloxone and naltrexone hydrochloride are taking place via an intermediate form. Naloxone hydrochloride di-hydrate is obtained via an amorphous form and the naltrexone hydrochloride tetra-hydrate via an unknown crystalline hydrate. The principal packing of the molecules in the naloxone hydrochloride anhydrate is considerably changed in comparison with the di-hydrate, leaving voids in the crystal structure (Fig. 6.19) that are not present in the anhydrate of naltrexone hydrochloride. This could be a reason that the hydration process of naloxone is faster compared to naltrexone.

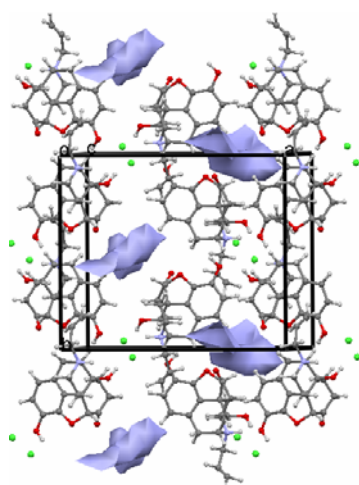


Figure 6.19. Naloxone hydrochloride anhydrate and the voids created after dehydration, depicted in gray

Another significant structural difference is that the N atom prefers to form H-bonds with the carboxylic group in the naltrexone hydrochloride forms, and with the Cl⁻ anion in the naloxone hydrochloride forms.

Moreover, dehydration of naltrexone hydrochloride tetra-hydrate takes place with shrinkage of the volume of the unit cell with 18.42%, while naloxone hydrochloride di-hydrate shows an expansion of the unit cell with 6.18% during dehydration.

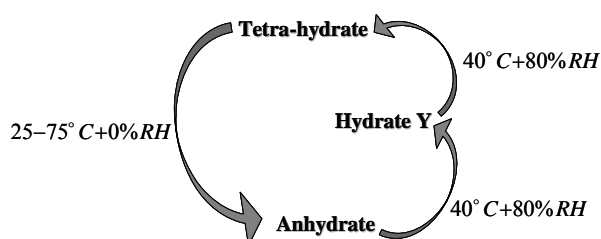
Despite naltrexone and naloxone hydrochloride are chemically and structurally related and show some similarities in their behavior, the overall hydration and dehydration process is fundamentally different.

6.4 CONCLUSIONS

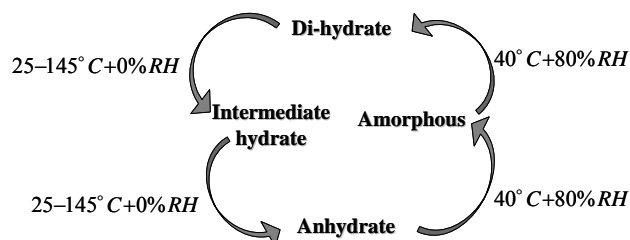
The crystal structure of naltrexone hydrochloride anhydrate was determined successfully from X-ray powder diffraction data collected in transmission capillary geometry and using the DASH software for structure determination and Topas software for the final Rietveld refinement.

The combination of the applied techniques (DSC, TGA, SSNMR, hot-humidity XRPD) together with the structural data show consistent results and yields a detailed conversion scheme for naltrexone hydrochloride as well as for naloxone hydrochloride. Hot-humidity stage X-ray powder diffraction showed complete and reversible conversion between the tetra-hydrate and the anhydrate forms of naltrexone hydrochloride, respectively between the di-hydrate and the anhydrate forms of naloxone hydrochloride. The conversion of naltrexone hydrochloride anhydrate to the tetra-hydrate form takes place via an

intermediate hydrate form. The conversion of the naloxone hydrochloride anhydrate to the di-hydrate form takes place via an amorphous form. The existence of a intermediate hydrate isostructural to naloxone hydrochloride di-hydrate is suggested from the combination of DSC, XRPD and SSNMR measurements. The conversions can be summarized in the following scheme for naltrexone hydrochloride:



and for naloxone hydrochloride:



SSNMR confirmed the existence of another hydrate form for naltrexone hydrochloride and discharged the existence of a mixture of the anhydrate and tetra-hydrate forms. In the case of naloxone hydrochloride, the existence of the amorphous form was also confirmed. The impact of dehydration and hydration on the H-bonding networks is clearly reflected in the solid state NMR C^{13} spectra.

Comparison of the crystal structures of the hydrated and the anhydrate forms of naltrexone and naloxone hydrochloride reveals some similarities but also

significant differences. The investigated forms of the two antagonists crystallize all in the orthorhombic space group $P2_12_12_1$. The dehydration processes for naltrexone hydrochloride tetra-hydrate and naloxone hydrochloride di-hydrate induces different changes in the unit cells of the hydrated forms in order to form the anhydrated forms. The difference in the H-bonding pattern showed by the two opioids seems to be a footprint for the crystal structures and also for the hydration/dehydration behavior of the two antagonists. Remarkably, dehydration of naltrexone hydrochloride tetra-hydrate takes place with shrinkage of the volume of the unit cell with 18.42%, while naloxone hydrochloride di-hydrate shows an expansion of the unit cell with 6.18% during dehydration. Despite the fact that naltrexone and naloxone hydrochloride are chemically and structurally related and show some similarities in their behavior, the overall hydration and dehydration process is fundamentally different.

Chapter 7

FIDDLE. SIMULTANEOUS INDEXING AND STRUCTURE SOLUTION FROM POWDER DIFFRACTION DATA

This chapter is based on:

C. Guguta
J. M. M. Smits
R. de Gelder

Submitted to

*Journal of
Applied
Crystallography*

ACKNOWLEDGMENT

This research was supported by the Technology Foundation STW, applied science division of NWO and the technology program of the Ministry of Economic Affairs.

The usual process for crystal structure determination from powder diffraction data consists of (1) indexing of the powder pattern, (2) space group determination, (3) structure solution and (4) structure refinement. Despite the success of methods for powder indexing, there are many cases in which the very first step in a structure determination fails or is far from straightforward. Due to a number of fundamental and experimental problems, like peak broadening, the presence of impurity phases, dominant zones and geometrical ambiguities, powder indexing will remain difficult in many cases, thereby hampering the next steps in the structure determination.

FIDDLE is a method for the determination of crystal structures from powder diffraction data that circumvents the difficulties associated with separate indexing. Structure determination from powder diffraction data can be seen as a process of global optimization of all model parameters, including the unit cell parameters. This strategy is applied in the *FIDDLE* program. For the simultaneous optimization of the parameters that describe a crystal structure a genetic algorithm is used together with a pattern matching technique based on auto and cross correlation functions. This "one-pot" strategy for indexing and structure determination was successfully used for determining the unknown crystal structures of ethinyl estradiol anhydrate, naloxone monohydrate and creatine anhydrate, cases for which indexing was problematic.

7.1 INTRODUCTION

Nowadays, single-crystal X-ray diffraction is a standard method for the determination of molecular structures and for the elucidation of intra and intermolecular interactions in various materials. Often, however, crystals suitable for single-crystal diffraction cannot be obtained (easily). Compounds that show polymorphism or solvate (hydrate) formation frequently cause difficulties in the crystallization of one of the modifications. In addition, most of the times recrystallization of unstable compounds that are initially obtained as microcrystalline powders is not feasible.

A possible route for crystal structure analysis of "problematic" compounds is to make optimal use of powder diffraction data. These data contains less information than single crystal diffraction data but for a lot of compounds powder diffraction has allowed for a full crystal structure determination.

The complexity of crystal structures determined from powder diffraction data has steadily increased through further development of "traditional" methods for structure determination in reciprocal space and application of global optimization algorithms in direct space (Harris *et al.*, 2001; David *et al.* 2002; Favre-Nicolin *et al.*, 2002; Altomare *et al.*, 2004; Altomare *et al.*, 2004; Tremayne, 2004; David and Shankland, 2008). The published number of crystal structures determined by powder diffraction is still rather limited, compared to the enormous amount of structures determined by single crystal diffraction. Clearly, structure determination from powder diffraction data is not a generally applicable method yet.

The lack of success in the indexing step has become one of the major bottlenecks in structure determination from powder diffraction data. There are a number of fundamental and experimental problems that can make powder indexing problematic or simply impossible: peak broadening (leading to a loss in resolution), increasing peak density at higher angles, peak shifts, systematic or accidental absences of reflections, the presence of impurity phases, inaccuracies in the experimental measurements, dominant zones and geometrical ambiguities. Problems that originate from the use of laboratory instruments, like peak broadening caused by the instrumental profile and experimental inaccuracies, can be reduced by measuring on synchrotron facilities. However, problems originating from specific powder imperfections (impurities, crystallite size, strain, lattice mistakes) cannot be solved by going to more sophisticated instruments. This means that for powder patterns measured on laboratory as well as synchrotron facilities the problem of limited quality can exist.

It is clear that particularly for compounds for which no suitable single crystals can be grown the powder method is an attractive alternative. Often, however, the problematic crystallization behavior of these compounds is also reflected by the moderate quality of their microcrystalline powders and their corresponding powder diffraction data.

Despite the success of standard methods for powder indexing, like ITO (Visser, 1969), TREOR (Werner, 1985) and DICVOL91 (Boultif, 1991), there are many cases in which the very first step in structure determination fails or is far from straightforward. New strategies and enhancements will certainly

extend the possibilities of powder indexing methods (Coelho, 2003; Neumann, 2003; Altomare *et al.*, 2000). However, the problems associated with the nature of powder diffraction data (absences, increasing peak density etc.) together with the usual strategy of applying a separate indexing step, which may lead to geometrical ambiguities, will be a fundamental limitation for improvement.

Recently, a method called *OCEANA* was reported for structure determination from powder diffraction data without prior indexing (Padgett *et al.*, 2007). *OCEANA* is a grid search based method which uses a genetic algorithm to adjust the cell parameters, potential packing energy and R_{wp} to locate the global minimum in a given space group. The method is limited to $Z' \leq 1$.

In this paper a different methodology (*FIDDLE*) for the determination of crystal structures from powder diffraction data is presented that circumvents the difficulties associated with separate indexing. The method implemented in *FIDDLE* has the possibility of searching through the most common space groups, while varying Z' and without taking into account any energy or packing considerations. By using correlations functions for pattern matching the method is able to optimize cell and structural parameters simultaneously using a genetic algorithm, without any assumptions on cell parameters or density. Results from several tests of the method on various organic compounds are presented to demonstrate the effectiveness of the concept. Moreover, using *FIDDLE*, three previously unknown crystal structures, cases for which indexing was problematic, could be determined successfully.

7.2 COMPUTATIONAL METHODOLOGY

7.2.1 Program description

There is no fundamental reason to separate, as is usual today, the process of unit cell determination and the process of structure solution. If one is able to describe the main part of a crystal structure by a model consisting of a discrete set of parameters (cell parameters $\{a, b, c, \alpha, \beta, \gamma\}$, space group number S and - using information on molecular structures - a limited set of structural parameters describing the positional parameters $\{(x, y, z)_j\}$), then a structure determination from powder diffraction data can be seen as a process of (global) optimization of all crystal structure parameters, including the unit cell parameters. This is the strategy implemented in the *FIDDLE* program. Structure solution then means that in the end the calculated powder diffraction pattern corresponding to the complete set of optimized parameters, including the cell parameters, must match the experimental pattern, assuming that there is one unique structure which has this property.

The *FIDDLE* method is a direct space method. Prior knowledge of the structure of molecular fragments (and the internal degrees of freedom) is needed to define a model of the crystal structure in terms of structural parameters that can be optimized. Like in other direct space methods *FIDDLE* reduces the set of positional parameters to a set of rotation angles $\{\theta, \phi, \psi\}$, which define the orientation of a molecular fragment in the unit cell, a translation vector $\{x, y, z\}$, which defines the position of the molecular

fragment in the cell and a set of n torsion angles $\{\tau_1, \tau_2, \dots, \tau_n\}$, which describe the intramolecular geometry of the fragment.

Part of the parameters, the cell parameters, define the positions of the peaks in the powder pattern. The other parameters, space group and positional parameters, define the intensities of the peaks. Together, they define the total pattern (not regarding zero-point shifts and peak shapes). A suitable measure for similarity between experimental and calculated pattern must be used to be able to optimize both sets of parameters simultaneously. *FIDDLE* uses weighted auto and cross correlation functions for pattern matching and the mathematics for this fitness function are described below.

For space group determination *FIDDLE* uses a strategy that is also applied in crystal structure prediction: the frequency of the occurrence of space groups in the CSD (Cambridge Structural Database) is used and systematically the most common space groups are explored. About 79% of all organic and organometallic compounds crystallize in only 5 space groups: $P2_1/c$, $P-1$, $P2_12_12_1$, $C2/c$ and $P2_1$ (Allen, 2002). Chiral molecules (non-superimposable on their mirror image) crystallize in chiral space groups and this further reduces the number of possible space groups. *FIDDLE* now explores the space groups $P2_1/c$, $P-1$, $P2_12_12_1$, $P2_1$, $C2/c$, $Pbca$, $Pnma$, $Pbcn$, and $P1$ and varies Z' . Prior knowledge about Z' obtained from methods like solid-state NMR reduces of course the problem. Fig. 7.1 shows the main steps in the *FIDDLE* procedure.

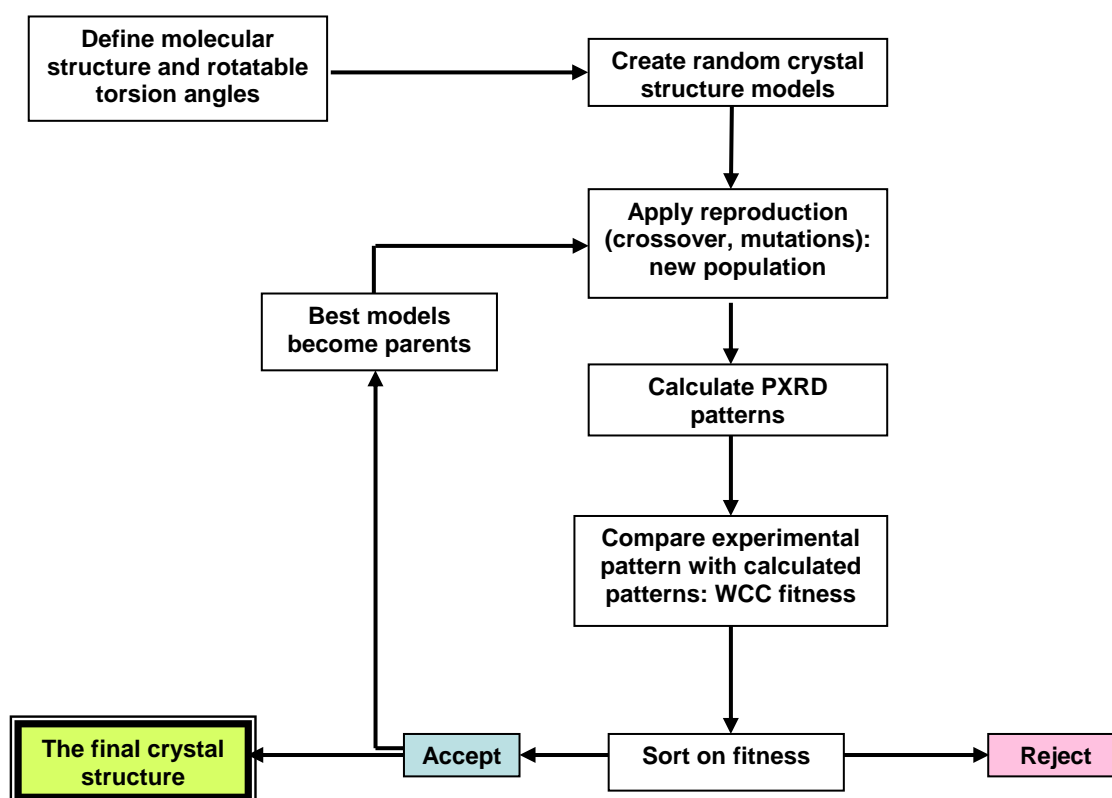


Figure 7.1. Overview of the main steps in the *FIDDLE* procedure

7.2.2 The Genetic Algorithm

A Genetic Algorithm (GA) is a global optimisation method based on evolution principles (Harris *et al.*, 1998). Evolutionary operations such as mating, mutation and "natural selection" are applied, through which members with the highest fitness value within a population survive and procreate. Genetic algorithms can be applied to any problem in which the quantity to be optimized can be written as a function of a set of variables (Goldberg, 1989; Cartwright, 1993; Keane, 1996).

The settings of the Genetic Algorithm implemented in the *FIDDLE* program were determined by trial and error and were initially based on experience with the determination of molecular constants from rovibronic spectra with genetic

algorithms (Hageman *et al.*, 2000). Table 7.1 shows the genetic algorithm settings used in *FIDDLE*.

Table 7.1. Genetic algorithm settings in *FIDDLE*

Settings	Value
Maximum number of generations	300
Population size	400
Elitism	200
Crossover type	Two-point crossover
Unit cell edges boundaries	3-40 Å
Unit cell angles boundaries	60-120°
Orientation angles boundaries	0-360°
Torsion angles boundaries	0-360°
Mutation type	New random value within boundaries
Mutation probability	0.02
Selection type	Probabilistic
Fitness type	Weighted cross correlation function

The unit cell parameters (cell edges and angles) and the positional parameters such as orientation angles and the torsion angles are randomly set within a range of values during initialization (see Table 7.1). This also holds for the translation vector(s) but the boundaries for these parameters are dependent on the space group.

7.2.3 Comparison of powder diffraction patterns in FIDDLE: the fitness function

The *RMS* (Root Mean Square) criterion is a well known criterion that is based on the sum of the squared differences between n observed and n calculated data values, respectively $y_i(obs)$ and $y_i(calc)$. A well-known criterion for powder pattern similarity is R_{wp} (R-weighted pattern). This criterion is used for the refinement of crystal structures on XRPD data and also for structure solution from XRPD data. R_{wp} is similar to an *RMS* criterion but the squared differences are weighted according to the standard deviations in the observed intensities.

$$R_{wp} = (\sum_{i=1, n} w_i (y_i(obs) - y_i(calc))^2)^{1/2} / (\sum_{i=1, n} w_i y_i(obs)^2)^{1/2}$$

$$w_i = 1/y_i(obs)$$

R_{wp} can only be used when the peak positions in the observed and calculated powder patterns are the same or at least very close. It is therefore useless for the comparison of powder patterns corresponding to structures with significantly different unit cells.

The *WCC* (Weighted Cross Correlation) criterion was developed to deal with cases where two patterns are different with respect to peak positions. It is based on correlation functions (de Gelder *et al.*, 2001):

$$WCC = \int w_{fg}(r) c_{fg}(r) dr / (\int w_{ff}(r) c_{ff}(r) dr \int w_{gg}(r) c_{gg}(r) dr)^{1/2}$$

$$c_{fg}(r) = \int f(x) g(x+r) dx$$

The weighting function, which extracts information from the correlation functions, can be adapted to influence the sensitivity for shifts in peak positions, in XRPD as a result of lattice parameter variations. This is done by changing the value of width l :

$$w_{fg}(r) = 1 - |r| / l \quad \text{if } |r| < l$$

$$w_{fg}(r) = 0 \quad \text{if } |r| \geq l$$

$$w_{ff}(r) = w_{gg}(r) = w_{fg}(r)$$

The *WCC* criterion is always normalized and scaling is unnecessary since this is done implicitly. Comparison of deformed patterns, caused by unit cell variations, is possible with the *WCC* criterion since it recognizes shifted peaks. When we divide the intensities of the powder patterns by the standard deviations in the observed intensities and calculate *WCC* at $r = 0$, we obtain the relation between *WCC* and R_{wp} , a relation between a sine and cosine function:

$$WCC_{r=0} = (1 - R_{wp}^2)^{1/2}$$

So, (only) for $r = 0$ there is a direct and clear relation between R_{wp} and *WCC*.

7.3 EXPERIMENTAL

16 compounds covering a range of structural complexity, number of torsion angles, different Z' and different space groups were selected from the CSD in order to test the methodology implemented in the *FIDDLE* program (Table 7.2).

The known crystal structure of morphine anhydrate was re-determined from laboratory X-ray powder diffraction data with the *FIDDLE* program. This re-determination was carried out to test the performance of the *FIDDLE* method for experimental data.

Table 7.2. Compound name and corresponding molecular formula

<i>Code</i>	<i>Compound name</i>	<i>Molecular formula</i>	<i>CSD Refcode</i>
1	Dihydroqinghaosu	C ₁₅ H ₂₄ O ₅	COTYAL
2	3-Methoxy-11-methyl-4a,5,9,10,11,12-hexahydro-6H-benzofuro(3a,3,2-ef)(2)benzazepin-6-ol	C ₁₇ H ₂₁ NO ₃	SIBHAM
3	17β-Hydroxy-7α-methyl-androst-5-en-3-one	C ₂₀ H ₃₀ O ₂	HMANDR
4	(-)-S-2-(2-Chlorophenyl)-2-methylaminocyclohexanone	C ₁₃ H ₁₆ ClNO	XURCAO
5	(+)-R-2-(2-Chlorophenyl)-2-methylaminocyclohexanone	C ₁₃ H ₁₆ ClNO	XURCES
6	2',4'-Difluoro-4-hydroxy-3-biphenylcarboxylic acid	C ₁₃ H ₈ F ₂ O ₃	FAFWIS02
7	(R)-(-)-3-Acetoxy-quinuclidine methiodide	C ₁₀ H ₁₈ NO ₂ ⁺ I ⁻	ACQUIN
8	2-Amino-6-ethyl-4,5,7,8-tetrahydro-6H-oxazolo(5,4-d)azepine	C ₉ H ₁₅ N ₃ O	BERFUZ
9	3-(2-Hydroxyphenyl)-4-methyl-1,2,4-Δ ² -triazoline-5-thione	C ₉ H ₉ N ₃ OS	HPMTZT
10	(R)-(+)-2-(2-Oxo-3-piperidiny)-1,2-benzisothiazol-3(2H)-one-1,1-dioxide	C ₁₂ H ₁₂ N ₂ O ₄ S	SUCROS01
11	Sucrose	C ₁₂ H ₂₂ O ₁₁	CAVGOV
12	2-(2,6-Dichloro-3-methylphenyl)-aminobenzoic acid	C ₁₄ H ₁₁ Cl ₂ NO ₂	MECLOF10
13	(3α,5α,6α)-4,4,6-Trichloro-7-methoxy-3,4,5,6-tetrahydro-2H-3a,5-methanoazulene	C ₁₂ H ₁₃ Cl ₃ O	RUWLOK
14	2-Phenyl-7-methyl-8-azahypoxanthine	C ₁₁ H ₉ N ₅ O	AZHPXA
15	10,11-Dihydro-10-hydroxy-5(H)-dibenz(b,f)azepine-5-carboxamide	C ₁₅ H ₁₄ N ₂ O ₂	KAMCEG
16	(3-(((2-((Aminoiminomethyl)amino)-4-thiazolyl)methyl)thio)-N-(aminosulfonyl)propanimidamide)-nickel(ii)	C ₈ H ₁₃ N ₇ NiO ₂ S ₃	BEVQAV

The unknown crystal structures of three compounds (ethinyl estradiol anhydrate, naltrexone monohydrate and creatine anhydrate) were determined from laboratory X-ray powder diffraction data using the *FIDDLE* program. Indexing the three powder patterns with the most commonly used indexing

programs, such as: DICVOL91, ITO and TREOR, was not successful and therefore the determination of these three crystal structures was of particular interest.

The X-ray powder diffraction measurements for the structure solutions were performed using a Bruker D8 AXS Advance X-ray Diffractometer. The D8 was equipped with a Johansson type monochromator with a focusing curved Ge 111 crystal. A VÅNTEC-1 detector was used with an effective angular region of 2°. The data were collected in transmission capillary geometry using monochromatic Cu K α_1 radiation. The most important instrumental and data collection parameters are presented in Table 7.3.

Table 7.3. Instrumental and data collection parameters

<i>Typical instrument settings</i>	
System	Bruker D8 AXS Advance $\theta/2\theta$
Generator	40 kV, 40 mA
Measuring circle (mm)	435
Radiation (Å)	Cu K α_1 , $\lambda=1.54056\text{Å}$
Monochromator	Primary, focusing curved Ge 111
Geometry	Transmission capillary configuration
Sample holder	0.5 mm glass capillary tube
Detector	VÅNTEC-1
<i>Typical measuring conditions</i>	
Range ($^{\circ}2\theta$)	2-50
Step size ($^{\circ}2\theta$)	0.0084696
Step time (s)	50
Total data collection time (h)	ca 74
Spinning (rpm)	15

7.4 TESTS APPLIED TO CALCULATED POWDER

DIFFRACTION DATA (A)

The crystal structures of 16 compounds selected from the CSD database were determined with *FIDDLE* to verify the effectiveness of the program and the methodology, for cases with various symmetries and structural complexities (Table 7.2 and 7.4). The input molecular models were also obtained from the CSD. The calculations were performed on 6 AMD Dual-Core Opteron 280 machines (two dual core 2.4GHz processors each), all running under the LINUX operating system. The total number of seeds used for the various crystal structure determinations was between 2400 and 4800. The maximum 2θ range used was 40° . For each compound the tests were done in the correct space group and for the true value for Z' . On the best *FIDDLE* solutions having the highest fitness values a full final Rietveld refinement was carried out using Topas 3. Fig. 7.2 shows a representative overlay between the solution with the highest fitness value obtained from *FIDDLE* and the known crystal structure in the CSD for one of the studied compounds (FAFWIS02). It is clear that the final result obtained with *FIDDLE* is close to the true crystal structure of this compound. The compound has one torsion angle and crystallizes in the orthorhombic space group $P2_12_12_1$ with unit cell parameters: $a=39.700(1)$ Å, $b=14.129(2)$ Å, $c=3.835(6)$ Å, $V=2151.51$ Å³, $Z'=2$. From the data presented in Table 7.4 it can clearly be seen that when the correct space group and Z' is used, the correct unit cell parameters are always found for the top twenty solutions. Always the first solution with the highest fitness value appeared to be the correct crystal structure.

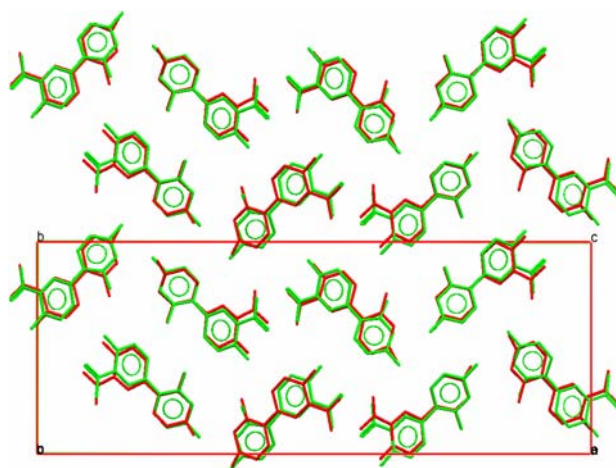


Figure 7.2. The overlay between the solution with the highest fitness value obtained from *FIDDLE* (red) and the known crystal structure in the CSD (green) for FAFWIS02

Table 7.4. CSD compounds selected for testing of *FIDDLE*

<i>CSD refcode</i>	<i>Space group</i>	<i>Z'</i>	<i>No. torsion angles</i>	<i>Width (Å)*</i>	<i>No. seeds</i>	<i>Best Fitness value</i>	<i>No. correct unit cells in the first 20</i>	<i>No. correct solutions in the first 20</i>
COTYAL	$P2_12_12_1$	1	0	1.5	2400	0.8369	20	20
SIBHAM	$P2_12_12_1$	1	1	1.5	2400	0.8236	20	20
HMANDR	$P2_12_12_1$	1	0	1.5	2400	0.8058	20	20
XURCAO	$P2_12_12_1$	1	2	1.5	2400	0.7946	20	20
XURCES	$P2_12_12_1$	1	2	1.5	2400	0.7973	20	20
FAFWIS02	$P2_12_12_1$	2	4	0.5	4800	0.7477	20	2
ACQUIN	$P1$	1	2	1.5	2400	0.9796	19	19
BERFUZ	$P2_1/c$	1	1	1.5	4800	0.9491	20	19
HPMTZT	$P2_1/c$	1	1	1.5	4800	0.9631	20	20
SUCROS01	$P2_1$	1	5	1.5	2400	0.9619	20	20
CAVGOV	$P2_1$	1	1	1.5	4800	0.9706	20	20
MECLOF10	$P-1$	1	3	1.5	4800	0.9510	17	17
RUWLOK	$Pna2_1$	1	1	1.5	4800	0.9763	20	20
AZHPXA	$C2/c$	1	1	1.5	4800	0.9664	20	20
KAMCEG	$Pbca$	1	1	1.5	4800	0.9730	20	20
BEVQAV	$Pbcn$	1	2	1.5	4800	0.9797	20	20

* See point 7.5 Tests applied to calculated powder diffraction data (B)

To illustrate that in general the correct crystal structure is the one having the highest fitness value and that the correct unit cell parameters are more often found than a complete solution, a simple test on sucrose data was performed. Sucrose is a compound crystallizing in the monoclinic space group $P2_1$, with unit cell parameters: $a=7.7235(5) \text{ \AA}$, $b=8.6786(7) \text{ \AA}$, $c=10.824(1) \text{ \AA}$, $\beta=102.982(3)^\circ$, $V= 706.98 \text{ \AA}^3$, $Z'=1$ and having five torsion angles. For this compound 20 optimizations were performed. The graph showing the different fitness values vs. the number of generations for sucrose is presented in Fig.7.3. The simple test for sucrose showed that the correct unit cell parameters are found for all 20 optimizations and that the solution with the highest fitness value corresponds to the correct crystal structure.

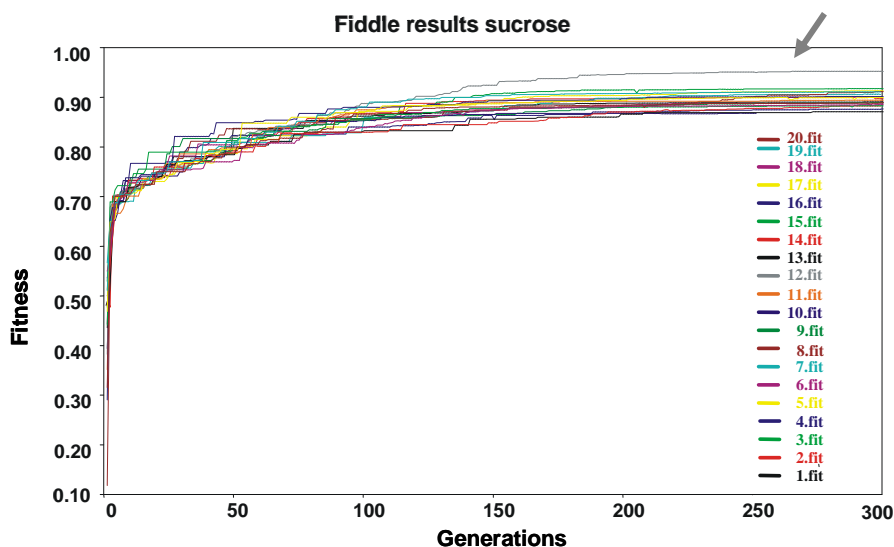


Figure 7.3. The different fitness values vs. the number of generations for sucrose

The overlay between the solution with the highest fitness value and the known crystal structure in the CSD (green) is presented in Fig. 7.43 as well as a

comparison between its corresponding pattern and the theoretical pattern for sucrose.

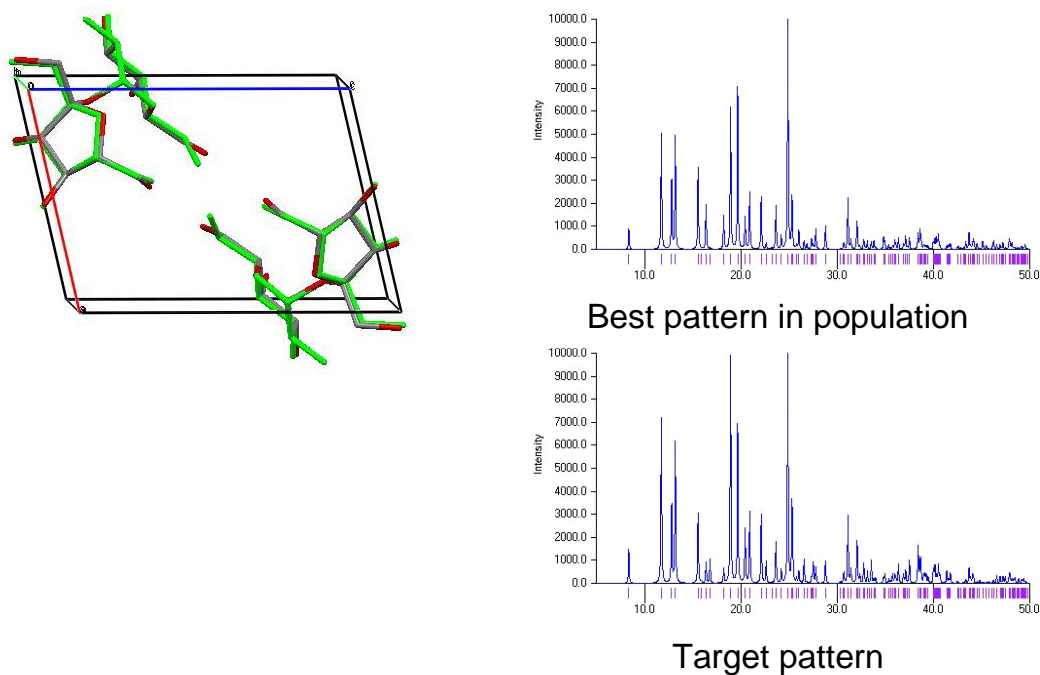


Figure 7.4. The overlay between the solution with the highest fitness value obtained from *FIDDLE* and the known crystal structure in the CSD (green) for sucrose as well as a comparison between the best pattern in the population and the theoretical pattern for sucrose

7.5 TESTS APPLIED TO CALCULATED POWDER

DIFFRACTION DATA (B)

Another experiment was carried out on the sucrose data in order to check the influence of the value of the width of the weighting function. For this test the space group and Z' were again fixed. 2400 Seeds and a maximum 2θ value of

40° were used. Fig. 7.5 shows the width vs. the number of correct solutions found in the top 80. There is a tendency to a smaller number of correct solutions for smaller values of the width, which indicated again that going to narrow weighting functions, with R_{wp} as an extreme case, reduces the performance of the genetic algorithm. On the other hand there is a wide range for the value of the width for which good results are obtained. Experience showed that a width of 0.7 Å is a good compromise between calculation speed and efficiency.

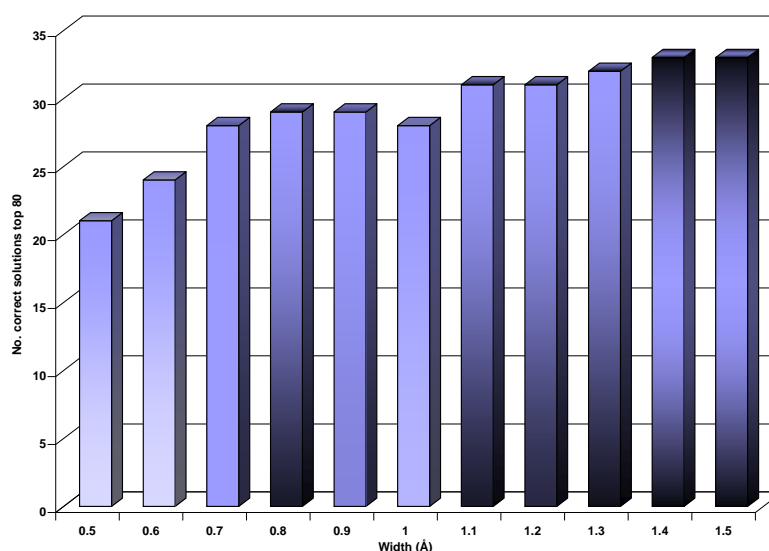


Figure 7.5. The number of correct solutions vs. the width

Searching through all ten space groups implemented in *FIDDLE* while varying Z' from 1 to 3 and using 1.5 Å for the width, the correct crystal structure of sucrose was again found, the best solution having a fitness value of 0.9690 (see Fig. 7.6). This experiment mimicks the actual situation in a structure solution from powder diffraction data where in principle space group and Z' are unknown.

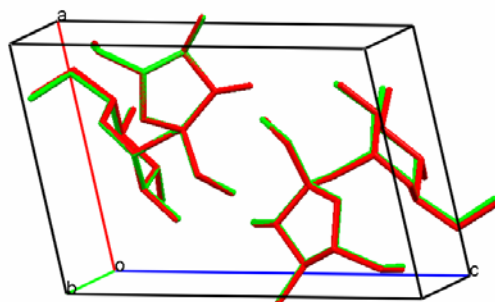


Figure 7.6. The overlay between the solution with the highest fitness value obtained from *FIDDLE* (red), obtained after varying the space group and Z' , and the known crystal structure in the CSD (green) for sucrose

7.6 TEST APPLIED TO EXPERIMENTAL DATA

When re-determining the crystal structure of morphine anhydrate, the effectiveness of the program was proved once again. For this test the space group and Z' were set to their correct value. The number of seeds used was 9600. A width of 0.7 Å and a maximum 2θ of 50° was used. The first 8 solutions having the highest fitness value returned the correct crystal structure, although the correct unit cell parameters were found within the first 37 solutions. The quality of the best solution returned by *FIDDLE* could be used directly for Rietveld refinement. The full Rietveld refinement proceeded smoothly to reach a minimum characterized by a good fit to the diffraction profiles presented in Fig. 7.7 ($R_{wp}=4.31$). Morphine anhydrate crystallizes in the orthorhombic space group $P2_12_12_1$ with unit cell parameters: $a=13.8616(5)$ Å, $b=12.7775(4)$ Å, $c=7.6903(3)$ Å, $V= 1362.07$ Å³. A comparison between the best solution obtained from *FIDDLE* and the final structure obtained after Rietveld refinement is presented in Fig. 7.8.

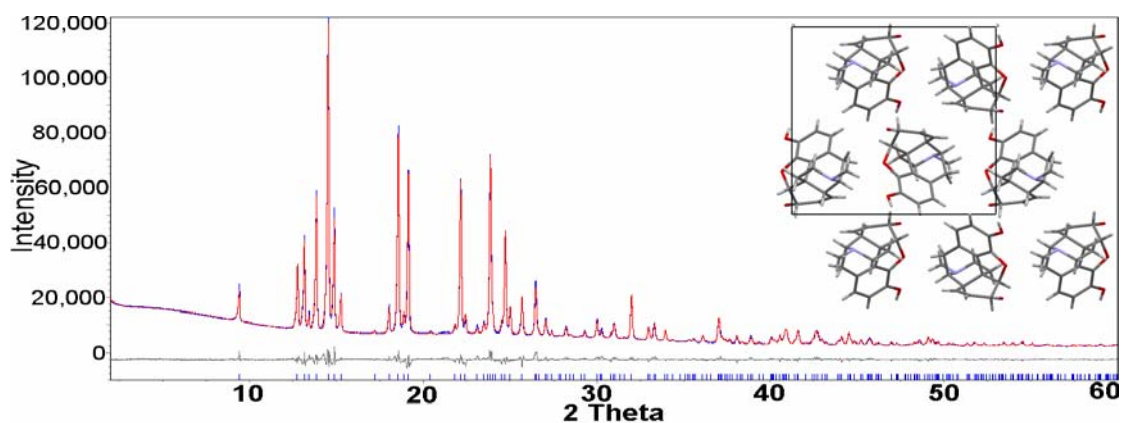


Figure 7.7. The fit after the final Rietveld refinement for morphine anhydrate

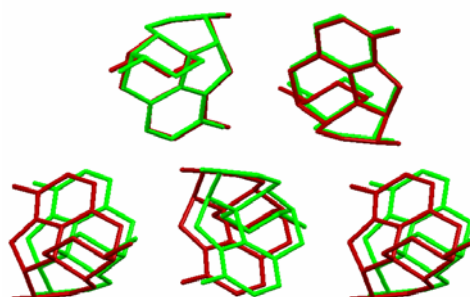


Figure 7.8. Comparison between the best solution obtained from *FIDDLE* (red) and the final structure obtained after Rietveld refinement (green) for morphine anhydrate

7.7 APPLICATION TO UNKNOWN CRYSTAL STRUCTURES

Of particular interest were the crystal structures of ethinyl estradiol anhydrate, naloxone monohydrate and creatine anhydrate. After collecting the X-ray powder diffraction data for the three compounds, indexing using DICVOL91, ITO and TREOR failed. The unknown crystal structures of ethinyl estradiol, naloxone monohydrate and creatine anhydrate could successfully be determined using *FIDDLE*. Prior information regarding the number of

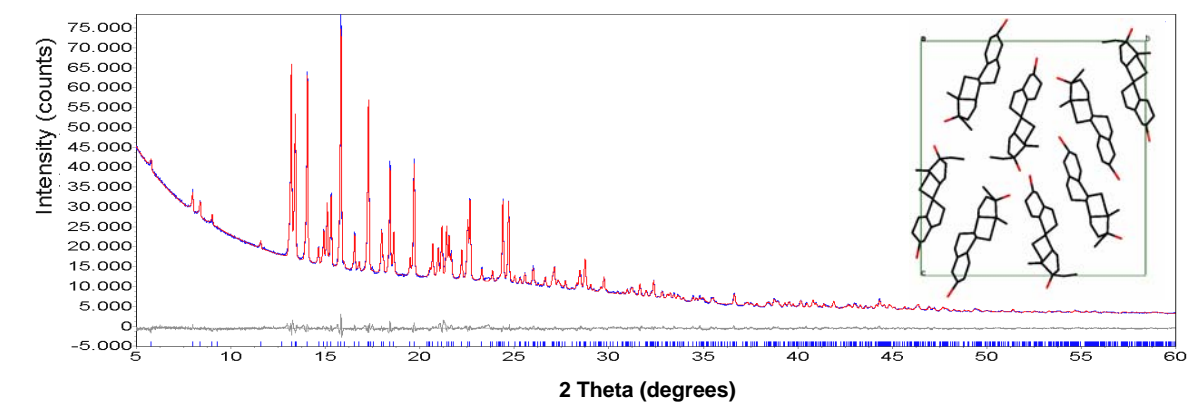
molecules per asymmetric unit was obtained from solid-state NMR and used as input in *FIDDLE*, in order to reduce the computing time. The input molecules were obtained from related structures in the CSD. Searching through all ten space groups implemented in *FIDDLE*, using the information about Z' obtained from solid-state NMR, and using a maximum 2θ of 40° and 0.7 \AA for the width, the final crystal structures of the three compounds were determined successfully. 4800 Seeds were used in total for all space groups. For ethinyl estradiol the first 40 solutions obtained from *FIDDLE* indicated the correct unit cell. In the case of naloxone monohydrate and creatine anhydrate the first 5, respectively 4 solutions indicated the correct unit cell. On the best *FIDDLE* solutions having the highest fitness value a full final Rietveld refinement was carried out using Topas 3. The full Rietveld refinements proceeded smoothly to reach a minimum characterized by a good fit to the diffraction profiles presented in Fig. 7.9 for all three cases. Comparisons between the best solution obtained from *FIDDLE* for ethinyl estradiol anhydrate, naloxone monohydrate and creatine anhydrate and the final structures obtained after Rietveld refinement are presented in Fig. 7.10.

Initially, the crystal structure of ethinyl estradiol was determined with the use of four programs: *IsoQuest*, *FIDDLE*, *DASH* and *TOPAS 3*. The *IsoQuest* program was used in order to get information about the unit cell parameters from isostructural compounds in the CSD. *IsoQuest* is a program, which can use as input the X-ray powder diffraction pattern and can search for isostructural compounds in the CSD (de Gelder *et al.*, 2006). As a result an isostructural compound (CSD refcode - EYHENO) was found. *IsoQuest* has an extremely low computing time and therefore is a good choice for obtaining

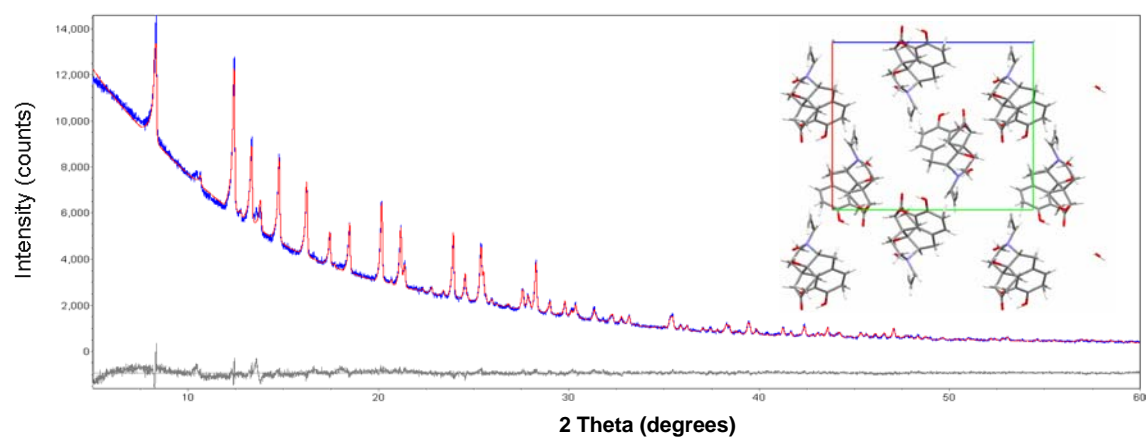
information about the space group and Z' . Therefore the computing time of *FIDDLE* can be reduced significantly. The information about the space group obtained from *IsoQuest* together with the information obtained from solid-state NMR about Z' was used in the *FIDDLE* program in order to determine the crystal structure of ethinyl estradiol anhydrate. After running 2400 seeds and a width of 1.5 Å the unit cell of ethinyl estradiol anhydrate was obtained. Using the unit cell from *FIDDLE*, the *DASH* program was applied, followed by a full Rietveld refinement (using *TOPAS 3*). Afterwards, several tests were performed on ethinyl estradiol anhydrate data using the *FIDDLE* program only. It was shown that ethinyl estradiol anhydrate could also be determined with *FIDDLE* alone ($R_{wp}=2.15$). Therefore, when *IsoQuest* does not give any useful results, performing a full determination with *FIDDLE* always can lead to a correct result although computing time is higher.

Ethinyl estradiol anhydrate crystallizes in the orthorhombic space group $P2_12_12_1$ with unit cell parameters: $a=6.918(2)$ Å, $b=21.109(5)$ Å, $c=22.147(6)$ Å, $V=3234.5$ Å³.

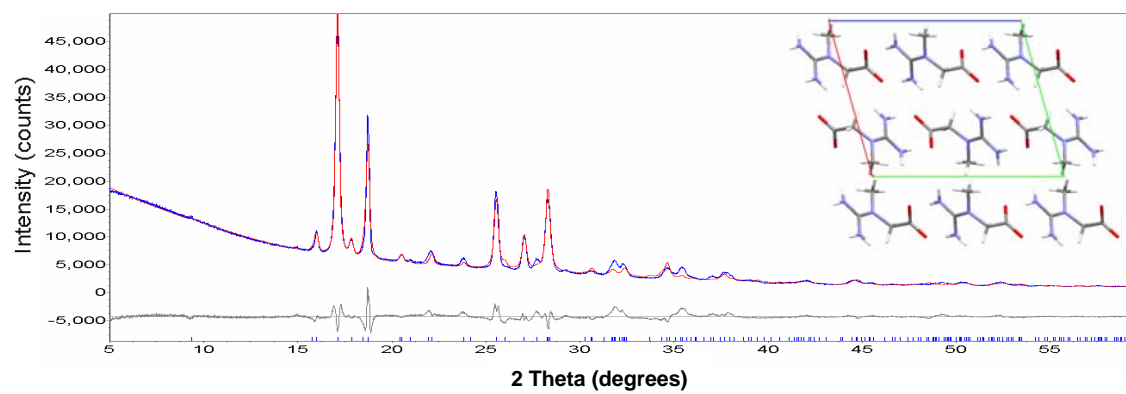
Naloxone monohydrate ($R_{wp}=2.901$) crystallizes in the orthorhombic space group $P2_12_12_1$ with unit cell parameters: $a=13.902(7)$ Å, $b=7.257(3)$ Å, $c=16.640(8)$ Å, $V=1678.98$ Å³.



a)

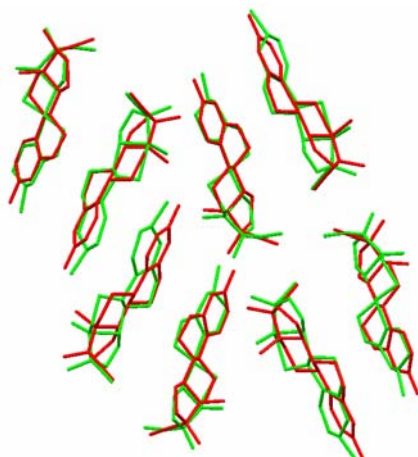


b)

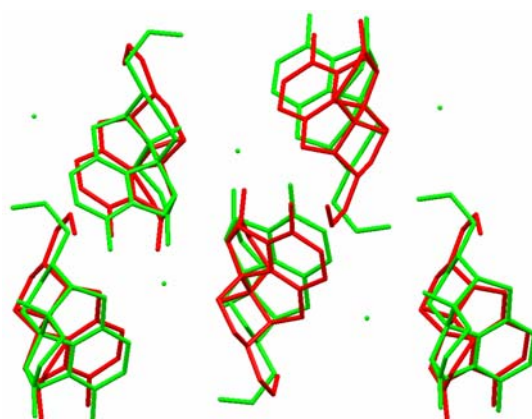


c)

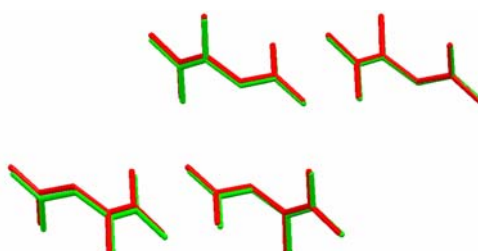
Figure 7.9. The fit after the final Rietveld for: a) ethinyl estradiol anhydrate; b) naloxone monohydrate; c) creatine anhydrate



a)



b)



c)

Figure 7.10. Comparison between the best solution obtained from *FIDDLE* (red) and the final structure obtained after Rietveld refinement (green) for: a) ethinyl estradiol anhydrate; b) naloxone monohydrate; c) creatine anhydrate

Creatine anhydrate was successfully determined with *FIDDLE* and refined using Topas3 ($R_{wp}=7.20$). Creatine anhydrate crystallizes in the monoclinic space group $P2_1/c$ with unit cell parameters: $a=9.838(8)$ Å, $b=5.831(5)$ Å, $c=11.679(9)$ Å, $\beta=74.31(2)^\circ$, $V=645.062$ Å³. Creatine monohydrate, which is obtained after hydration of creatine anhydrate, crystallizes in the monoclinic space group $P2_1/a$ with unit cell parameters: $a=12.159(1)$ Å, $b=5.038(2)$ Å, $c=12.491(2)$ Å, $\beta=108.87(1)^\circ$, $V=724.038$ Å³. From a comparison between the anhydrate form of creatine and the monohydrate it is clear that dehydration takes place with an anisotropic shrinkage of the unit cell of the monohydrate (Fig. 7.11).

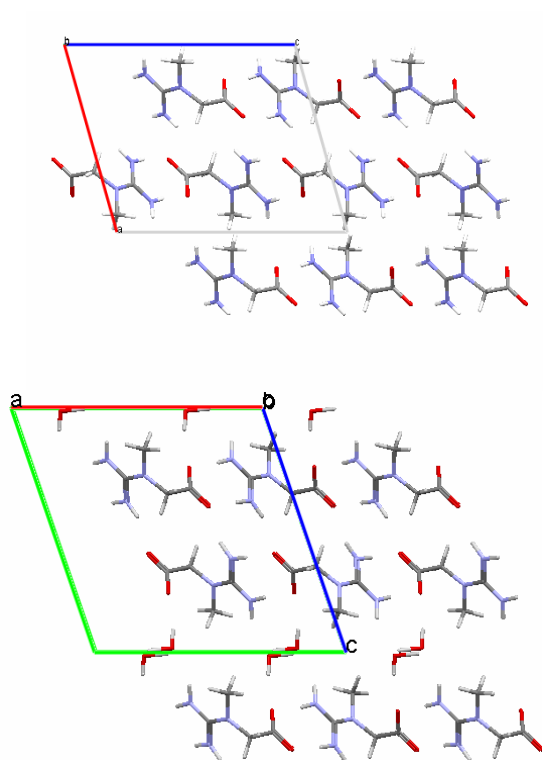


Figure 7.11. Comparison between the anhydrate (left) and the monohydrate (right) forms of creatine

Although the quality of the powder diffraction patterns recorded for ethinyl estradiol anhydrate and naloxone monohydrate was high enough for crystal structure determination, standard indexing proved not to be successful. After determining the crystal structure of the two forms, the *FIDDLE* results pointed at impurity peaks appearing at low 2θ angles, peaks that probably hampered the indexing process. The impurity in the case of ethinyl estradiol corresponds to the hemi-hydrate form and for naloxone monohydrate to the anhydrate form. Eventually we were able to obtain a pure form of ethinyl estradiol anhydrate and therefore the data presented here do not show any impurity corresponding to the hemi-hydrate form. This is not the case for naloxone monohydrate for which the most pure form of the monohydrate still had an impurity peak corresponding to the anhydrate form. In the case of creatine anhydrate, the quality of the X-ray powder diffraction pattern was low and therefore the indexing step was impeded by severe peak overlap. Even using the knowledge obtained from *FIDDLE* about the unit cell parameters, the quality of the recorded data restricted a Pawley refinement and subsequent structure solution with other programs.

7.8 CONCLUSIONS

Simultaneous indexing and structure solution is possible using a global optimization approach. *FIDDLE* was successfully used to determine known and unknown crystal structures and can be applied to compounds for which the indexing step is impeded, for several reasons. Indexing with *FIDDLE* is computationally cheaper than complete structure determination, meaning that when a structure is not fully solved the program can still deliver the correct unit cell. Any information related to the number of molecules per asymmetric unit

obtained from solid-state NMR or knowledge about the chirality of the compounds may be input into the program in order to reduce the computational time. Nevertheless, *FIDDLE* is capable of solving structures for which unit cell, space group and Z' are unknown.



References

Chapter 1

Altomare A., Caliendo R., Camalli M., Cuocci C., da Silva I., Giacobuzzo C., Moliterni A. G. G., Spagna R. *J. Appl. Cryst.*, **2004**, *37*, 957-966.

Altomare A., Caliendo R., Camalli M., Cuocci C., Giacobuzzo C., Moliterni A.G.G., Rizzia R. *J. Appl. Cryst.*, **2004**, *37*, 1025-1028.

Brittain H.G., Byrn S.R. *Polymorphism in Pharmaceutical Solids*, **1999**, 73–124, Marcel Dekker Inc., New York.

Brouwer D.H., Darton R.J., Morris R.E., Levitt M.H. *J. Am. Chem. Soc.*, **2005**, *127*, 10365-10370.

Brouwer D.H. *J. Magnetic Resonance*, **2008**, *194*, 136–146.

Clawson J.S., Vogt F.G., Brum J., Sisko J., Patience D.B., Dai W., Sharpe S., Jones A.D., Pham T.N., Johnson M.N., Copley R.C.P. *Cryst. Growth & Design*, **2008**, future publication.

David W.I.F., Shankland K., McCusker L.B., Baerlocher Ch. *Structure determination from powder diffraction data*, **2002**, Oxford University Press, Oxford.

David W. I. F. *J. Appl. Cryst.*, **2004**, *37*, 621-628.

David W.I.F., Shankland K. *Acta Cryst.*, **2008**, *A64*, 52-64.

Favre-Nicolin V., Cerny R. *J. Appl. Cryst.*, **2002**, *35*, 734–743.

Guguta C., Peters Th.P.J., de Gelder R. *Cryst. Growth & Design*, **2008**, future publication.

Harris K.D.M., Tremayne M., Kariuki B.M. *Angew. Chem. Int. Ed.*, **2001**, *40*, 1626–1651.

Harris K.D.M., Cheung E.Y. *Chem. Soc. Rev.*, **2004**, *33*, 526 - 538.

Loisel C., Keller G., Lecq G., Bourgaux M., Ollivon M. *J. Am. Oil Chem. Soc.*, **1998**, 75, 425-439.

McCrone W.C. *Physics and Chemistry of the organic solid state*, **1965**, 2, 725-767, Wiley Interscience, New York, USA.

McCusker L.B., VonDreele R.B., Cox D.E., Louer D., Scardi P. *J. Appl. Cryst.*, **1999**, 32, 36–50.

Morris K.R., Griesser U.J., Eckhardt C.J., Stowell J.G. *Adv. Drug Deliv. Reviews*, **2001**, 48, 91-114.

Padgett C.W., Arman H.D., Pennington W.T. *Cryst.Growth Des.*, **2004**, 2, 367-372.

Reutzel-Edens S.M. *Engineering of Crystalline Materials Properties*, **2007**, 351-374, NATO Science for Peace and Security Series B: Physics and Biophysics, Springer Netherlands.

Shankland K., Florence A.J., Shankland N., David W. I. F., Johnston A., Markvardsen A.J. *Am. Pharm. Review*, **2004**, 7, 80-86.

Timken M.D., Chen J.K., Brill T.B. *Applied Spectrosc.*, **1990**, 44, 701-706.

Tremayne M. *Phil. Trans. R. Soc. Lond. A.*, **2004**, 362, 2691–2707.

Vippagunta S.R., Brittain H.G., Grant D.J.W. *Advanced Drug Delivery Reviews*, **2001**, 48, 3–26.

Webster S., Smith D.A., Batchelder D.N. *Vib. Spectrosc.*, **1998**, 18, 51-59.

Williams K.P.J, Pitt G.D., Batchelder D.N., Kip B.J. *Appl. Spectros.*, **1994**, 48, 232-235.

Williams K.P.J, Pitt G.D., Smith B.J.E., Whitley A., Batchelder D.N., Hayward I.P. *J. Raman Spectros.*, **1994**, 25, 131-138.

Young R.A. *The Rietveld Method*, **2002** Oxford University Press, Oxford.

Chapter 2

Boultif A., Louër D. *J.Appl.Cryst.*, **1991**, 24, 987-993.

Bruker AXS, *TOPAS V2.1: General profile and structure analysis software for powder diffraction data. - User's Manual*, **2003**, Bruker AXS, Karlsruhe, Germany.

Cambridge Structural Database, **2005**, *Cambridge Crystallographic Data Centre*, Cambridge, UK.

Cerius², *User Guide*, **2002**, Accelrys Inc., San Diego, CA, USA.

Cheary R.W., Coelho A.A. *J. Appl. Cryst.*, **1992**, 25, 109-121.

Cuppen H.M., van Eerd A.R.T., Meekes H. *Cryst.Growth Des.*, **2004**, 4, 989-997.

Cuppen H.M., Beurkens G., Kozuka S., Tsukamoto K., Smits J.M.M., de Gelder R., Grimbergen R.F.P., Meekes H. *Cryst.Growth Des.*, **2005**, 5, 917-923.

David W.I.F., Shankland K., Van de Streek J., Pidcock E., Motherwell S. *DASH version3.0*, **2004**, Cambridge Crystallographic Data Centre, UK.

Dollase W.A. *J.Appl.Cryst.*, **1986**, 19, 267-272.

Florence A.J., Shankland N., Shankland K., David W.I.F., Pidcock E., Xu X., Johnston A., Kennedy A.R., Cox P.J., Evans J.S.O., Steele G., Cosgrove S.D., Frampton C.S. *J.Appl.Cryst.*, **2005**, 38, 249-259.

Hatada M., Jancarik J., Graves B., Kim S. *J.Am.Chem.Soc.*, **1985**, 107, 4279-4282.

Howard C.J., Kisi E.H. *J.Appl.Cryst.*, **2000**, 33, 1434-1435.

Leung S.S., Grant D.J.W. *J.Pharm.Sci.*, **1997**, *86*, 64-71.

Leung S.S., Padden B.E., Munson E.J., Grant D.J.W. *J.Pharm.Sci.*, **1998**, *87*, 501-507.

Leung S.S., Padden B.E., Munson E.J., Grant D.J.W. *J.Pharm.Sci.*, **1998**, *87*, 508-513.

Meguro T., Kashiwagi T., Satow Y. *J.Pep.Res.*, **2000**, *56*, 97-104.

Pawley G.S. *J.Appl.Cryst.*, **1981**, *14*, 357-361.

Young R.A. *The Rietveld Refinement*, **1996**, Oxford University Press.

Chapter 3

Cerius², *User Guide*, **2002**, Accelrys Inc., San Diego, CA, USA.

Chauvet A., Saint-Julien H., De Maury G., Masse J. *Thermoch. Acta*, **1983**, *71*, 79-91.

Cui Y. *Int. J. Pharm.*, **2007**, *339*, 3-18.

Cuppen H.M., van Eerd A.R.T., Meekes H. *Cryst. Growth Des.*, **2004**, *5*, 989-997.

Cuppen H.M., Beurkens G., Kozuka S., Tsukamoto K., Smits J.M.M., de Gelder R., Grimbergen R.F.P., Meekes H. *Cryst. Growth. Des.*, **2005**, *5*, 917-923.

Guguta C., Meekes H., de Gelder R. *Cryst. Growth. Des.*, **2006**, *4*, 989-997.

Hatada M., Jancarik J., Graves B., Kim S. *J. Am. Chem. Soc.*, **1985**, *107*, 4279-4282.

Kishimoto S., Naruse M. *J. Chem. Tech. Biotechnol.*, **1988**, *43*, 71-82.

Leung S.S., Grant D.J.W. *J. Pharm. Sci.*, **1997**, *86*, 64-71.

Leung S.S., Padden B.E., Munson E.J, Grant D.J.W. *J. Pharm. Sci.*, **1998**, 87, 501-507.

Leung S.S., Padden B.E., Munson E.J., Grant D.J.W. *J. Pharm. Sci.*, **1998**, 87, 508-513.

Meguro T., Kashiwagi T., Satow, Y. *J. Pep. Res.*, **2000**, 56, 97-104.

Rastogi S., Zakrewski M., Suryanarayanan R. *Pharm. Res.*, **2001**, 3, 267-273.

Spek A.L. *Acta Cryst.*, **1990**, A46, C34.

Chapter 4

Beurskens P.T., Beurskens G., Bosman W.P., de Gelder R., Garcia-Granda S., Gould R.O., Israel R., Smits J.M.M. *DIRDIF-96*, **1996**, Crystallography Laboratory: University of Nijmegen, The Netherlands; <http://www.crystallography.nl>.

Byrn S.R., Pfeiffer R.R., Stowell J.G. *Solid State Chemistry of Drugs*, **1999**, West Lafayette, IN.

Cambridge Structural Database, **2005**, Cambridge Crystallographic Data Centre, Cambridge, UK.

Desiraju G.R. *Acc.Chem.Res.*, **1991**, 24, 290-296.

van Geerestein V.J. *Acta Cryst.*, **1987**, C43, 1206-1209.

de Gelder R., de Graaff, R.A.G., Schenk H. *Acta Cryst.*, **1993**, A49, 287-293.

Gu C.-H., Li H., Gandhi R.B., Raghavan K. *Int.J.Pharm.*, **2004**, 283, 117-125.

Ishida T., Doi M., Shimamoto M., Minamino N., Nonaka K., Inoue M. *J.Pharm.Sci.*, **1989**, 4, 274-280.

Morris K.R., Rodriguez-Hornedo N. *Encyclopedia of Pharmaceutical Technology*, **1993**, 7, 393-441.

Nangia A., Desiraju G.R. *Chem. Commun.*, **1999**, 605-606.

North A.C.T., Phillips D.C., Mathews F.S.A. *Acta Cryst.*, **1968**, A24, 351-359.

Sheldrick G.M. *SADABS*, **1996**, University of Göttingen, Germany.

Sheldrick G.M. *SHELXL97*, **1997**, University of Göttingen, Germany.

Chapter 5

Boultif A., Louër D. *J. Appl. Cryst.*, **1991**, 24, 987-993.

Bye E. *Acta Chem. Scand. B*, **1976**, 30, 549-554.

Cheary R.W., Coelho A.A. *J. Appl. Cryst.*, **1992**, 25, 109-121.

David W.I.F., Shankland K., Van de Streek J., Pidcock E., Motherwell S. *DASH version 3.0*, **2004**, Cambridge Crystallographic Data Centre, UK.

Dollase W.A. *J. Appl. Cryst.*, **1986**, 19, 267-272.

Duchamp D.J., Olson E.C., Chidester C.G. *ACA, Ser. 2*, **1977**, 5, 83.

Evans J.S.O., Radosavljevic Evans I., *Chem. Soc. Rev.*, **2004**, 33, 539-547.

Gates M., Tschudi G. *J. Amer. Chem. Soc.*, **1952**, 74, 1109-1110.

Guguta C., Smits J.M.M., de Gelder R. submitted to *Cryst. Growth & Design*

Gulland J.M., Robinson R. *Mem. Proc. Manchester Lit. Phil. Soc.*, **1925**, 69, 79-86.

Gylbert L. *Acta Cryst.*, **1973**, B29, 1630-1635.

Howard C.J., Kisi E.H. *J. Appl. Cryst.*, **2000**, 33, 1434-1435.

Karle I.L. *Acta Cryst.*, **1974**, B30, 1682-1686.

Khankari K.R., Grant D.J.W. *Thermochimica Acta*, **1995**, 248, 61-79.

Klein C.L., Majeste R.J., Stevens E.D. *J.Am.Chem.Soc.*, **1987**, *109*, 6675-6681.

MacKay M., Hodgkin D.C. *J.Chem.Soc.*, **1955**, 3261.

Pawley G.S. *J.Appl.Cryst*, **1981**, *14*, 357-361.

Pert C.B., Snyder S.H. *Molecular Pharmacology*, **1974**, *10*, 868-879.

Young R.A. *The Rietveld Refinement*, **1996**, Oxford University Press.

Chapter 6

Amato M.E., Bandoli G., Grassi A., Nicolini M., Pappalardo G.C. *J. Chem. Soc., Perkin Trans.*, **1990**, *2*, 1757 - 1762.

Balbach S.; Korn C. *Int. J. Pharm.*, **2004**, *275*, 1-12.

Belskii V.K., Babilev F.V., Arzamastsev A.P., Simonova L.L. *Chem. Pharm. J.*, **1988**, *22*, 506.

Boultif,A.; Louër D. *J.Appl.Cryst.* **1991**, *24*, 987-993.

Byrn S. R., Pfeiffer R. R., Stowell J. G. *Solid-State Chemistry of Drugs*, **1999**, SSCI Inc.

Canfield D.V., Barrick J., Giessen B.C. *Acta Cryst.*, **1987**, *C43*, 977-979.

Chang C. J., Diaz L. E., Morin F., Grant D. M. *Magn. Reson. Chem.*, **1986**, *24*, 768-771.

Cheary R. W.; Coelho A. A. *J. Appl. Cryst.*, **1992**, *25*, 109-121.

Le Dain A.C., Madsen B.W., Skelton B.W., White A.H. *Aust. J. Chem.*, **1992**, *45*, 635-640.

David W. I. F., Shankland K., Van de Streek J., Pidcock E., Motherwell S. *DASH version3.0*, **2004**, Cambridge Crystallographic Data Centre, UK.

Diaz L. E., Frydman L., Olivieri A. C., Frydman B. *Anal. Lett.*, **1987**, *20*, 1657-1666.

Dollase W. A. *J.Appl.Cryst.* **1986**, *19*, 267-272.

Gates M., Tschudi G. *J.Amer.Chem.Soc.*, **1952**, *74*, 1109-1110.

Gerbaud G., Ziarelli F., Caldarelli S. *Chem. Phys. Lett.*, **2003**, *377*, 1.

Ginzburg H. M., Glass W.J. *J. Clin. Psychiatry*, **1984**, *45*, 4-6.

Guguta et. al 2008 manuscript submitted to *Crystal Growth & Design*.

Howard C. J., Kisi E. H. *J.Appl.Cryst.* **2000**, *33*, 1434-1435.

Jagannathan N. R. *Curr. Sci.*, **1988**, *56*, 827-830.

Karle I.L. *Acta Cryst.*, **1974**, *B30*, 1682-1686.

Pawley G. S. *J.Appl.Cryst* **1981**, *14*, 357-361.

Pert C.B., Snyder S.H. *Molecular Pharmacology* **1974**, *10*, 868-879.

Saindon P. J., Cauchon N. S., Sutton P. A., Chang C.-j., Peck G. E., Byrn S. R. *Pharm. Res.*, **1993**, *10*, 197-203.

Sime R.L., Forehand R., Sime R.J. *Acta Cryst.*, **1975**, *B31*, 2326-2330.

Song Z., Antzutkin O.N., Feng X., Levitt M.H. *Solid State Nucl. Magn.Reson.*, **1993**, *2*, 143-146.

Spek A. L. *Acta Cryst.*, **1990**, *A46*, C34.

Venkatesh S., Lipper R.A. *J. Pharm. Sci.* **2000**, *89*, 145-154.

Young R. A. *The Rietveld Refinement* **1996**, Oxford University Press.

Chapter 7

Altomare A., Caliandro R., Camalli M., Cuocci C., da Silva I., Giacobozzo C., Moliterni A. G. G., Spagna R. *J. Appl. Cryst.*, **2004**, *37*, 957-966.

Altomare A., Caliendo R., Camalli M., Cuocci C., Giacobozzo C., Moliterni A.G.G., Rizzia R. *J. Appl. Cryst.*, **2004**, 37, 1025-1028.

Altomare A., Giacobozzo C., Guagliardi A., Moliterni A.G.G., Rizzi R., Werner P.-E. *J. Appl. Cryst.*, **2000**, 33, 1180-1186.

Boultif A., Louër D. *J. Appl. Cryst.*, **1991**, 24, 987-993.

Cartwright H.M. *Applications of Artificial Intelligence in Chemistry*, **1993**, Oxford University Press.

Coelho A.A. *J. Appl. Cryst.*, **2003**, 36, 86-95.

David W.I.F., Shankland K., McCusker L.B., Baerlocher Ch. *Structure determination from powder diffraction data*, **2002**, Oxford University Press, Oxford.

David W.I.F., Shankland K. *Acta Cryst.*, **2008**, A64, 52-64.

Favre-Nicolin V., Cerny R. *J. Appl. Cryst.*, **2002**, 35, 734-743.

de Gelder R., Wehrens R., Hageman J.A. *J. Comp. Chem.*, **2001**, 22, 273-289.

de Gelder R. *IUCr CompComm Newsletter*, **2006**, 59-69.

Goldberg D.E. *Genetic Algorithms in Search, Optimization and Machine Learning*, **1989**, MA: Addison Wesley.

Hageman J.A., Wehrens R., de Gelder R., Leo Meerts W., Buydens L.M.C. *J. Chem. Phys.*, **2000**, 113, 7955-7962.

Harris K.D.M., Johnston R.L., Kariuki B.M. *Acta Cryst.*, **1998**, A54, 632-645.

Harris K.D.M., Tremayne M., Kariuki B.M. *Angew. Chem. Int. Ed.*, **2001**, 40, 1626-1651.

Keane A. J. *Modern Heuristic Search Methods*, **1996**, 255-272, New York: Wiley.

Neumann M.A. *J. Appl. Cryst.*, **2003**, 36, 356-365.

Padgett C.W., Arman H.D., Pennington W.T. *Cryst.Growth Des.*, **2004**, 2, 367-372.

Tremayne M. *Phil. Trans. R. Soc. Lond. A.*, **2004**, 362, 2691–2707.

Visser J. W. *J. Appl. Cryst.*, **1969**, 2, 89-95.

Werner P.-E., Eriksson L., Westdahl M. *J. Appl. Cryst.*, **1985**, 18, 367-370.



Summary

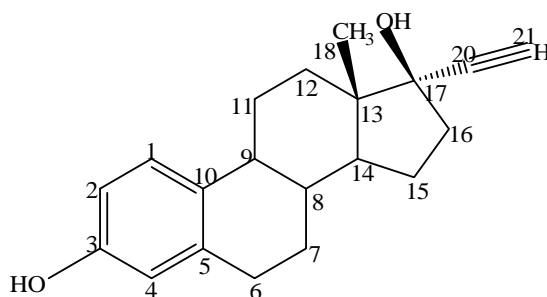
Pharmaceutical compounds have the tendency to crystallize in various polymorphs, solvates or hydrates as a function of the crystallization medium, temperature and humidity. This can cause many practical problems, including changes in stability, dissolution rates, bioavailability, morphology, vapor pressure, and packaging: the key factors to the development of appropriate dosage forms. Therefore, understanding polymorphism and solvate or hydrate formation at the molecular level is of particular interest. It critically depends, however, on the availability of powerful structure elucidation methods and other methods for solid-state analysis.

This thesis presents a new strategy for crystal structure determination from powder diffraction data that circumvents the difficulties associated with separate indexing, one of the major bottlenecks in the powder method. Moreover, this thesis deals also with application of different solid-state techniques in combination with crystal structure determination for the study of solvate and hydrate formation of pharmaceutical compounds and excipients.

Chapter 2 and 3 deal with aspartame, a sweetener and excipient in drug formulation. The crystal structure of aspartame anhydrate was determined successfully by collecting X-ray powder diffraction data. Comparison of the structures of the hydrates and the anhydrate reveals a remarkable similarity between the structures of IA and IB on the one hand and between IIA and IIB on the other hand. Minimization experiments suggest that another hemi-hydrate polymorph exists and that the ordering of the water molecules inside the channels is an essential step in the dehydration mechanism of the hemi-hydrate. The hydration/dehydration behavior of aspartame was investigated using hot-humidity stage X-ray powder diffraction (XRPD) and molecular mechanics

modeling in combination with differential scanning calorimetry (DSC) and thermogravimetric analysis (TGA). The results are compared to earlier studies on aspartame as described in literature. It is shown that earlier transition studies were hampered by incomplete conversions and wrong assignment of the forms. The combination of the techniques applied in this study now shows consistent results for aspartame and yields a clear conversion scheme for the hydration/dehydration behavior of the four forms. The systematic study on aspartame as presented in this thesis may be of importance for a further understanding of the formation of hydrates and shows that the availability of crystal structures together with analytical data provides a detailed insight into the hydration/dehydration behavior of compounds.

Chapter 4 presents the crystal structures of four new ethinyl estradiol solvates together with a structural study of H-bond formation and isostructurality. The characteristic H-bonds formed by the ethinyl estradiol pseudo-polymorphs are between the –OH groups attached to C(3) and/or C(17) and the corresponding solvent molecules, as well as hydrogen bonds between different ethinyl estradiol molecules, namely between the –OH groups attached to C(3) and those attached to C(17).



The molecular structure of ethinyl estradiol

Ethinyl estradiol forms pseudo-polymorphs mainly with solvents having H-bond accepting or both accepting and donating propensity and shows a remarkable flexibility in forming distinctly different hydrogen-bonding patterns, resulting in a diverse set of solvate structures. A high degree of similarity can be observed between the crystal packing of the nitromethane and dioxane solvates, forming isostructural sheets of ethinyl estradiol molecules arranged parallel in a head-to-tail fashion.

In Chapter 5 the crystal structures of naloxone monohydrate and four new anhydrate forms of morphine, naloxone, and their hydrochloride salts, all determined from X-ray powder diffraction data, are presented. These new structures, together with already known structures from the Cambridge Structural Database, enabled us to investigate the influence of the subtle molecular differences between these agonist and antagonist, the role of water and the effect of the chloride counter-ion on structural properties of morphine and naloxone in the solid state. The results suggest that the introduction of water or counter-ions like chlorine generate structures with higher dimensional hydrogen bonding networks than the corresponding anhydrate or free base structures. The counter ion Cl^- takes over the role of the water molecules in the anhydrates forming H-bonds with the N atom as well. When water molecules are present, Cl^- prefers the water molecules instead of the N atom. If water molecules and the counter ion are not present, intermolecular H-bonds are formed between different -OH groups. The allylic group of the naloxone molecule takes over the role of the counter ion Cl^- only in its absence. Furthermore, the N atom can act as a H-bond donor as well as an acceptor.

Chapter 6 deals with two antagonists, naloxone and naltrexone, chemically and structurally related. All known hydrate and anhydrate forms of naltrexone and naloxone hydrochloride crystallize in the orthorhombic space group $P2_12_12_1$, although the crystal packings show clear differences. Dehydration causes in both cases no breaking of the symmetry but the change in unit cell is for naltrexone profoundly different from naloxone. Dehydration of naltrexone hydrochloride tetra-hydrate takes place with shrinkage of the volume of the unit cell, while dehydration of naloxone hydrochloride di-hydrate results in an expansion of the unit cell. The H-bonding patterns corresponding to the two antagonists seem to be footprints for the crystal structures and also for their hydration/dehydration behavior. Despite naltrexone and naloxone hydrochloride are chemically and structurally related and show similarities in their biological behavior, the overall hydration and dehydration process is fundamentally different.

In Chapter 7 a new methodology for structure determination is proposed for non-indexable powder patterns. *FIDDLE* is a method for determination of crystal structures from powder diffraction data that circumvents the difficulties associated with separate indexing. Structure determination from powder diffraction data can be seen as a process of global optimization of all model parameters, including the unit cell parameters. This strategy is applied in the *FIDDLE* program. For the simultaneous optimization of the parameters that describe a crystal structure a genetic algorithm together with a pattern matching technique based on auto and cross correlation functions is used. This "one-pot" strategy for indexing and structure determination, as applied in *FIDDLE*, was successfully used for determining the unknown crystal structures of ethinyl

estradiol anhydrate, naloxone monohydrate and creatine anhydrate, cases for which indexing was problematic.



Samenvatting

Farmaceutische verbindingen hebben vaak de neiging om in verschillende polymorfen, solvaten of hydraten te kristalliseren, afhankelijk van het kristallisatiemedium, de temperatuur en/of luchtvochtigheid. Dit kan vele praktische problemen geven, zoals veranderingen in stabiliteit, oplossnelheid, biobeschikbaarheid, morfologie, dampspanning en verpakking: de belangrijkste factoren bij de ontwikkeling van de juiste dosis-formulering. Inzicht in polymorfie, solvaat- en/of hydraatvorming op moleculair niveau is hierbij van bijzonder belang. Bepalend hiervoor is echter wel de beschikbaarheid van krachtige methodes voor structuuropheldering en andere methodes voor de analyse van vaste stoffen.

Dit proefschrift stelt een nieuwe strategie voor de bepaling van de kristalstructuur uit poederdiffractiegegevens voor die problemen bij indicering van poederpatronen, één van de belangrijkste stappen en knelpunten bij de poedermethode, kan omzeilen. Voorts behandelt dit proefschrift ook de toepassing van verschillende vaste stof technieken, in combinatie met kristalstructuurbepaling, op de bestudering van solvaat- en hydraatvorming van een aantal farmaceutische verbindingen en vulstoffen.

Hoofdstuk 2 en 3 behandelen aspartaam, een zoetstof en een vulmiddel gebruikt in medicijnformuleringen. De kristalstructuur van aspartaam anhydraat kon met succes bepaald worden uit gegevens verkregen met Röntgenpoederdiffractie. Vergelijking van de structuren van de hydraten en het anhydraat levert een opmerkelijke gelijkenis op tussen de structuren van vorm IA en IB enerzijds en die van IIA en IIB anderzijds. Uit minimalisatie-experimenten komt naar voren dat er misschien nog een ander hemi-hydraat

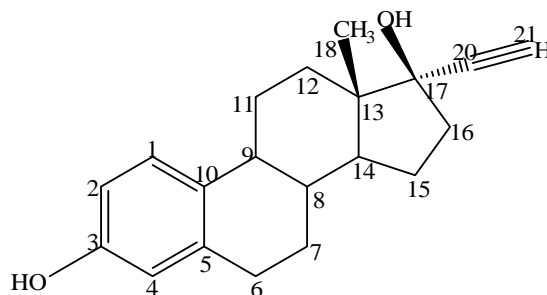
bestaat en dat het ordenen van de watermoleculen binnen de kanalen een essentiële stap is in het dehydratatiemechanisme van het hemi-hydraat van aspartaam.

Het hydratatie/dehydratatiegedrag van aspartaam wordt ook onderzocht gebruik makend van "hot-humidity stage" Röntgenpoederdiffractie (XRPD) en moleculaire mechanica in combinatie met differential scanning calorimetry (DSC) en thermogravimetrische analyse (TGA). De resultaten worden vergeleken met vroegere studies van aspartaam zoals beschreven in de literatuur. Er wordt hierbij aangetoond dat de vroegere overgangsstudies door onvolledige omzettingen en verkeerde toekenningen van de verschillende vormen werden belemmerd.

De combinatie van technieken, zoals in deze studie worden toegepast, laten nu consistente resultaten zien voor aspartaam en leveren een duidelijk omzettingsschema op voor het hydratatie/dehydratatiegedrag van de vier vormen. De systematische studie van aspartaam zoals in dit proefschrift wordt toegepast kan van belang zijn voor een verder inzicht in de vorming van hydraten en toont aan dat de beschikbaarheid van kristalstructuren tezamen met analytische gegevens een gedetailleerd inzicht geeft in het hydratatie/dehydratatiegedrag van verbindingen.

Hoofdstuk 4 beschrijft de kristalstructuren van vier nieuwe ethynylestradiol solvaten tezamen met een studie van waterstofbrugvorming en isostructuraliteit. De kenmerkende waterstofbruggen die door de pseudo-polymorfen van ethynylestradiol worden gevormd bevinden zich tussen de -OH groepen die aan C(3) en/of C(17) zijn gebonden en de betreffende oplosmiddelmoleculen,

evenals tussen verschillende moleculen van ethinylestradiol, te weten tussen de -OH groepen die aan C(3) zijn gebonden en die aan C(17).



De moleculaire structuur van ethinylestradiol

Ethinylestradiol vormt hoofdzakelijk pseudo-polymorfen met oplosmiddelen die waterstofbruggen kunnen accepteren of zowel waterstofbruggen kunnen accepteren als doneren en vertoont een opmerkelijke flexibiliteit in het vormen van duidelijk verschillende waterstofbrugpatronen, resulterend in een uiteenlopende reeks solvaatstructuren. Een hoge graad van gelijkheid kan tussen de kristalpakking van het nitromethaan- en dioxaansolvaat worden waargenomen. In beide gevallen worden isostructurele lagen van ethinylestradiol moleculen in een kop-staart configuratie waargenomen.

In Hoofdstuk 5 worden de kristalstructuren van naloxon monohydraat en vier nieuwe anhydraatvormen van morfine, naloxon, en hun waterstofchloridezouten, allen bepaald uit poederdiffractiegegevens, gepresenteerd. Deze nieuwe structuren, tezamen met reeds bekende structuren uit de Cambridge Structural Database, stelden ons in staat om de invloed van de subtiele moleculaire verschillen tussen deze agonist en antagonist, de rol van water en het effect van het chloride tegenion op structurele eigenschappen van morfine en naloxon in de vaste toestand te onderzoeken. De resultaten

suggereren dat het introduceren van water of tegenionen zoals chloor structuren met hogerdimensionale waterstofnetwerken dan het overeenkomstige anhydraat of de vrije base opleveren. Het Cl⁻ tegenion neemt de rol van de watermoleculen over in de anhydraten waarbij waterstofbruggen met het stikstofatoom worden gevormd. Wanneer watermoleculen aanwezig zijn, verkiest Cl⁻ de watermoleculen in plaats van het stikstofatoom. Als zowel de watermoleculen als het tegenion niet aanwezig zijn, worden de intermoleculaire waterstofbruggen gevormd tussen verschillende -OH groepen. De allylgroep van het naloxonmolecuul neemt de rol van het Cl⁻ tegenion over zodra Cl⁻ afwezig is. Verder treedt het stikstofatoom zowel als waterstofbrugdonor als -acceptor op.

Hoofdstuk 6 behandelt twee antagonisten, naloxon en naltrexon, die chemisch en structureel verwant zijn. Alle bekende hydraat- en anhydraatvormen van naltrexon- en naloxonwaterstofchloride kristalliseren in de orthorhombische ruimtgroep $P2_12_12_1$, hoewel de kristalpakkingen duidelijke verschillen vertonen. Dehydratatie veroorzaakt in beide gevallen geen verbreking van de symmetrie maar de verandering in de eenheidscel is voor naltrexon aanmerkelijk anders dan voor naloxon. Dehydratatie van het tetrahydraat van naltrexonwaterstofchloride vindt plaats met verkleining van het volume van de eenheidscel, terwijl dehydratatie van het dihydraat van naloxonwaterstofchloride in uitzetting van de eenheidscel resulteert. De waterstofbrugpatronen behorende bij de twee antagonisten lijken vingerdrukken te zijn voor de kristalstructuren en ook voor hun hydratatie/dehydratatiegedrag. Ondanks dat naltrexon- en naloxonwaterstofchloride chemisch en structureel

verwant zijn en gelijkenissen vertonen in hun biologisch gedrag, is het algehele hydratatie en dehydratatieproces fundamenteel verschillend.

In Hoofdstuk 7 wordt een nieuwe methodologie voor structuurbepaling voorgesteld voor niet-indiceerbare poederpatronen. *FIDDLE* is een methode voor bepaling van kristalstructuren uit poederdiffractiegegevens die problemen die samenhangen met de afzonderlijke indiceringsstap kan omzeilen. Structuurbepaling uit poederdiffractiegegevens kan gezien worden als een proces van globale optimalisering van alle modelparameters, met inbegrip van de parameters van de eenheidscel. Deze strategie wordt toegepast in het *FIDDLE* programma. Voor de gelijktijdige optimalisering van de parameters die een kristalstructuur beschrijven wordt een genetisch algoritme samen met een patroonherkenningsstechniek, gebaseerd op auto- en kruiscorrelatiefuncties, gebruikt. Deze strategie voor simultane indicering en structuurbepaling, zoals in *FIDDLE* wordt toegepast, werd met succes gebruikt voor het bepalen van de onbekende kristalstructuren van ethinylestradiol anhydraat, het monohydraat van naloxon en het anhydraat van creatine, allen gevallen waarbij indicering van de poederpatronen problematisch was.



Acknowledgements

We all have dreams and wishes. Undertaking the Ph.D. in an outstanding research group, in an exceptional university, was one of my dreams. This dream became a reality and from the beginning until the end it was every moment a happy journey.

I would first like to thank the person who made it all possible Dr. René de Gelder. Thank you for your professional and personal support throughout the course of my Ph.D.. I am grateful for all your time and effort in instructing and guiding me during my studies. René thank you for being so easy accessible, giving quick and prompt comments about my (our) work; always diplomatic and always there to help; an outstanding mentor and coach, and a never-ending source of ideas, always with the practical application of research in mind. Thank you very much!

I would like to gratefully acknowledge my promoter Prof. Dr. Elias Vlieg for his many valuable comments concerning my work along the way, for his logical, well-structured and organised approach.

During my Ph.D., I was able to work with many people from whom I've learned a great deal, and many, directly or indirectly, have contributed to my work. I greatly appreciate the opportunity to work with Dr. Hugo Meekes, Peter van Hoof, Anja Stiewe, Leo Woning, Ernst van Eck, Jan Smits, Theo Peters, Jacco van de Streek. Ineke thank you very much for always helping me with NMR, TGA, KF and many other things. Thank you for being so quick in reaction and always there for me, and not only professionally but also personally. You were one of the first persons who helped me to integrate in the Dutch society.

I am also grateful to STW, Schering-Plough Organon, Solvay, DSM, Bruker AXS and CCDC for financially supporting this research and to Edwin Kellenbach, Diederik Ellerbroek, Gert Klein, Peter Vonk and Cristiana Virone for their positive feedback during my research. I would also like to thank John Liebeschuetz, Sam Motherwell, Frank Allen and Edna Pidcock for making my visits to Cambridge pleasant.

My dear colleagues... there are so many things to be said, but I do not know from where to start and in the same time I wish I could be the type of person who could express the feelings in an easier way. Suzanne, Bram, Femke, Onno, Roy... I already miss you, guys! A lot! Thank you all for making my stay in Nijmegen a great journey that I will always remember; thank you for making my days shine! Suzanne and Bram, we were sometimes defining the dress code colours of the department... Shall we make the same with the thesis? ☺ Anyway we definitely have a fire-fighter in common. ☺ Dennis, Jaap, Quinten, Teun, Bas, Peter, Paul, Ingrid, Paula, Alan, Michal, Jan, Erika, Rosalyne, Hans Peter, Kasper, Sander Graswinckel, Menno, Paul P., Maurits, Cristina, Ismail, Jan L., Jan van K., Zjak, Elisabeth, Lucian, Miruna, Jorris thank you all for the nice moments, for your kindness and honesty. Many special thanks also to Fieke, Paul T. and Wim for all the “gezellig” moments in Grenoble and Nijmegen (do you join me in another celebration dance?!). Natasha, my dear friend, thank you for listening to all the stupid things I could think of, thanks for being always there, thanks for all those moments we spent together.

My friends from all over the world: Romania, Spain, Iran, India, Germany, Nicaragua, Chile, Costa Rica, Rwanda, Bolivia, Peru, Ecuador, Guatemala, Japan, Italy, Albania, Colombia, Ghana, Nigeria, Australia and Mexico, thank

you very much for keeping in touch and for your endless help, honesty, kindness and all the crazy moments. Iulia and Cos thanks for all the help with the cover, thanks for being there for me. Thank you Bere, Rober and Sha for being there when we most needed a shoulder to cry, and for sharing so many important moments in life. Gracias de todo corazón! Stef and Sarita, my paranimfen, I do not have words to explain the friendship that we built up in these years. I strongly believe that simple thanks cannot explain my gratitude to you two. You are simply exceptional!

I will never forget all the support given by the Lopez Vazquez family. Muchas gracias por todo su apoyo, estuvieron particularmente cuando más los necesitamos!

Va multumesc scumpii mei parinti pentru tot sprijinul si ajutorul vostru toti acesti ani. Intotdeauna gandindu-va la mine, mi-ati dat energia si spiritul de viata necesar pentru a trece peste fiecare zi petrecuta departe de voi. Intotdeauna cu un sfat bun si un zambet cald care sa-mi dea energia necesara pentru o alta zi. Aceasta teza nu ar fi existat fara voi. Va multumesc ca ati crezut in mine necontenit. Tot ceea ce sunt si ceea ce am realizat in viata va datorez voua. Va multumesc pentru intelegere, incredere si iubirea voastra neconditionata. Tati, I am sure you are now in peace enjoying a very deserved rest. This thesis is for you.

Carlos, mi amor, you are always next to me, supporting me in everything I do... Giving me the best advice at the proper moment... Making me smile when I am crying. Words fail me to express my feelings and a simple “Gracias” cannot be enough. Tu sabes que no soy muy buena para expresar mis

sentimientos, pero te quiero decir que mi corazón esta siempre contigo. Te amo mi amor! Without your encouragement, patience, love and understanding I could not have made it. Solo tu sabes cuanto pasamos para llegar a este momento. Esta tesis es tuya también. Te la mereces. Gracias de todo corazón! Multumesc!

Life is so marvellous, but at the same time so short... with plenty of ups and, unfortunately, also downs... Treasure and enjoy every moment of your life!

Carmen

Delft, March 5th 2009

Curriculum Vitae

Personal Information

- Birth date and place: August 6th, 1979/Constanta, Romania
- Nationality: Romanian

Education

1994 - 1998	High School "Mihai Țămpărescu" Constanta, Romania <i>Diploma in Chemistry and Biology</i>
1998 - 2002	Faculty of Physics, Chemistry and Petroleum Technology Ovidius University Constanta, Romania <i>B.Sc. in Chemistry</i>
2003 - 2004	Faculty of Physics, Chemistry and Petroleum Technology Ovidius University Constanta, Romania <i>and</i> Laboratory for Inorganic Chemistry Delft University of Technology The Netherlands <i>Master in Solid State Physics</i>
2004 - 2008	Institute for Molecules and Materials Molecular Materials and Solid State Chemistry Radboud University Nijmegen, The Netherlands <i>Doctoral studies (PhD)</i>
2009 - present	Jr. Project Leader Pharma, Avantium Technologies The Netherlands

List of Publications

C. Guguta, J.M.M. Smits, R. de Gelder, "*Fiddle. Simultaneous indexing and structure solution from powder diffraction data*", submitted to Journal of Applied Crystallography.

C. Guguta, E.R.H. van Eck, R. de Gelder, "*Structural insight into the dehydration and hydration behavior of naltrexone and naloxone hydrochloride. dehydration-induced expansion vs. contraction*", accepted for publication to Crystal Growth & Design.

C. Guguta, Th.P.J. Peters, R. de Gelder, "*Structural investigations of hydrate, anhydrate, free base and hydrochloride forms of morphine and naloxone*" 2008, Crystal Growth & Design, 8(11), 4150-4158.

C. Guguta, I. Eeuwijk, J.M.M. Smits, R. de Gelder, "*Structural diversity of ethinyl estradiol solvates*", 2008, Crystal Growth & Design, 8(3), 823-831 .

C. Guguta, H. Meekes, R. de Gelder, "*The hydration/dehydration behavior of aspartame revisited*", 2008, Journal of Pharmaceutical and Biomedical Analysis, 46, 617-624.

C. Guguta, H. Meekes, R. de Gelder, "*Crystal Structure of Aspartame Anhydrate from Powder Diffraction Data. Structural Aspects of the Dehydration Process of Aspartame*", 2006, Crystal Growth & Design, 6(12), 2686-2692.

I. Carazeanu, V. Ciupina, **C. Guguta**, G. Prodan, "*Transmission electron microscopy study on the formation of $Al_{18}B_4O_{33}$ whiskers*", 2004, Microchimica Acta, Microchimica Acta, 147(3), 147-150.

V. Ciupina, I. Carazeanu, G. Prodan, **C. Guguta**, "*High – resolution transmission electron microscopy study of $LiNi_xCo_{1-x}O_2$ synthesised by unconventional methods*", 2004, Microchimica Acta, 147(3), 151-155.

I. Carazeanu, E. Chirila, A. Badanoiu, G. Voicu, **C. Guguta**, "*Synthesis of $LiMn_xCo_{1-x}O_2$ by different low temperature techniques*", Annals of Chemistry Ovidius University, 2003, 14, 5-8.

C. Guguta, C. Draghici, E. Chirila, I. Carazeanu, "*Occurrence of some metals in different marine water by FAAS*", Annals of Chemistry Ovidius University, 2003, 14, 39-42.

I. Carazeanu and **C. Guguta**, "*Effect of K_2CO_3 fluxing agent on the $Al_{18}B_4O_{33}$ chemical synthesis*", Annals of Chemistry Ovidius University, 2002, 13,14-17.

I. Carazeanu and **C. Guguta**, "*Characterization of alumina and borated supported catalysts*", Annals of Chemistry Ovidius University, 2002, 13, 18-21.